Aus dem Institut für Prophylaxe und Epidemiologie der Kreislaufkrankheiten
Klinikum der Ludwig-Maximilians-Universität München
München Direktor: Prof. Dr. med. Christian Weber

The role of the transcription factor Nfe2l1 for skeletal muscle metabolism and function

Dissertation
zum Erwerb des Doktorgrades der Naturwissenschaften
an der Medizinischen Fakultät der
Ludwig-Maximilians-Universität zu München

vorgelegt von
Imke Leonie Lemmer

aus
Hannover

Jahr
2023

Mit Genehmigung der Medizinischen Fakultät

der Universität München

Betreuer:	Univ.-Prof. Dr. rer. nat. Alexander Bartelt
Zweitgutachter:	PD Dr. rer. nat. Johann Schredelseker
Dekan:	Prof. Dr. med. Thomas Gudermann
Tag der mündlichen Prüfung:	08. Mai 2024

Table of Contents

Zusammenfassung

Starkes Übergewicht ist eine wachsende Epidemie, die eine große Belastung für die öffentliche Gesundheit darstellt. Durch Fettleibigkeit bedingte Komorbiditäten wie Insulinresistenz, Bluthochdruck, Typ-2-Diabetes und Atherosklerose sind weltweit die häufigsten Todesursachen. In der modernen Gesellschaft führen eine zunehmend sitzende Lebensweise und hochkalorische Lebensmittel zu einer Überernährung, welche die Stoffwechselhomöostase beeinträchtigt. Ein wichtiger Akteur bei der Aufrechterhaltung des Energiestoffwechsels ist die Skelettmuskulatur. Dieses Gewebe macht etwa 40 % des gesamten Körpergewichts aus und ist für etwa ein Drittel des Ruhestoffwechsels verantwortlich, was den Muskel zu einem unverzichtbaren Akteur für den Gesamtenergieverbrauch und die metabolische Gesundheit macht. Externe Einflüsse wie Fettleibigkeit oder körperliche Anstrengung erfordern eine adaptive Erneuerung der Proteinlandschaft und des Stoffwechselprofils des Muskels.

Zentral für die Feinabstimmung der Proteinhomöostase sind einerseits die Synthese neuer Proteine und andererseits die Beseitigung unerwünschter oder fehlgefalteter Proteine. Es ist von großer Bedeutung, dass diese Signalwege streng reguliert werden, da Defizite in diesen Prozessen zu Apoptose führen können. Ein entscheidender Akteur für die Regulierung ist das endoplasmatische Retikulum (ER), da die Faltung der Proteine im ER-Lumen stattfindet. Fehlgefaltete Proteine werden vom ER erkannt und über den ER-assoziierten Abbau (ERAD) entsorgt. Die Abbau-Maschinerie hierfür ist das Ubiquitin-Proteasom-System (UPS), ein hochkonservierter Abbauweg, bei dem fehlgefaltete Proteine mit Ubiquitin markiert und so für den sukzessiven Abbau durch das Proteasom gekennzeichnet werden.

Ein wichtiger Regulator in diesem Prozess ist der Transkriptionsfaktor Nuclear factor erythroid 2-like 1 (Nfe2l1, auch bekannt als Nrf1). Nfe2l1 besitzt einen Rückkopplungsmechanismus, durch welchen er eine Fehlfunktion des Proteasoms erkennt und den Verlust der Proteasom-Aktivität kompensiert, indem er die Transkription neuer proteasomaler Untereinheiten fördert. Diese Rückkopplungsaktivierung zeigt die adaptive Natur von Nfe2l1 und unterstreicht die Bedeutung des Transkriptionsfaktors für die zelluläre Anpassungsfähigkeit. Wie verschiedene Studien bereits belegten, ist Nfe2l1 für die Kälteanpassung im braunen Fettgewebe und für die Aufrechterhaltung des Cholesteringleichgewichts in der Leber unverzichtbar. Über die Rolle von Nfe2l1 in der Skelettmuskulatur ist jedoch nicht viel bekannt, trotz stärkerer Genexpression als in den genannten Geweben.

In der vorliegenden Studie konnte ich zeigen, dass Nfe2l1 in der Skelettmuskulatur eine wichtige Rolle spielt, die über die Steuerung der Proteom- und Ubiquitom-Landschaft in dem UPS hinausgeht. Nfe2l1 definiert den Phänotyp des Muskels *in vivo*, indem der Transkriptionsfaktor den Fasertypen bestimmt und eine Abwesenheit von Nfe2l1 zu einem insgesamt schlankeren Phänotyp der Mäuse führt. Des Weiteren bewirkt das Fehlen von Nfe2l1 eine Umstrukturierung des Energiestoffwechsels und der mitochondrialen Atmung, was eine Resistenz gegen diätetisch induzierte Fettleibigkeit

sowie verbesserte Stoffwechselparameter wie Glukose- und Insulintoleranz zur Folge hat. Interessanterweise beschränkten sich diese positiven Auswirkungen des Verlusts von Nfe2l1 in der Skelettmuskulatur auf die fettleibigen Tiere, die Fitness jedoch konnte dadurch nicht verbessert werden.

Die Daten zeigen die anspruchsvolle Rolle von Nfe2l1 in der Muskulatur für die Aufrechterhaltung des Energiegleichgewichts während der Umgestaltung der Proteinlandschaft und unterstreichen die Bedeutung des Transkriptionsfaktors bei der zellulären Anpassung an metabolische Herausforderungen.

Abstract

Obesity is a rising epidemic, that puts a great burden on public health. Comorbidities arising from overweight, like insulin resistance, hypertension, type 2 diabetes and atherosclerosis are main causes of mortality worldwide. In modern society an increasing sedentary lifestyle and high-calorie foods create a state of constant overnutrition, which leads to an energy imbalance and impairs metabolic homeostasis. A major player in maintaining energy levels is the skeletal muscle. This highly metabolically active tissue composes about 40% of total body weight and accounts for about a third of the resting metabolic rate making it an indispensable player in total energy balance and metabolic health. The muscle controls whole body glucose homeostasis and is thereby responsible for maintaining a healthy energy equilibrium. Facing external stressors like obesity or exercise requires an adaptive remodeling of the protein landscape and metabolic profile.

The two main pillars of fine-tuning these processes are translation of novel proteins on the one hand and disposing of misfolded or obsolete proteins on the other hand. It is of utmost importance that these pathways are tightly regulated, as deficiencies in these processes can lead to apoptosis. A crucial player in these adaptations is the endoplasmic reticulum (ER), as folding of the proteins takes place in the ER lumen. Thus, misfolded proteins are sensed by the ER and disposed of via, e.g., the ER-associated degradation (ERAD). The degradation machinery in this process is the ubiquitin-proteasome system (UPS), a highly conserved degradation pathway in which misfolded proteins are tagged with ubiquitin and thus marked for successive degradation by the proteasome.

An important regulator that emerged in this process is the transcription factor Nuclear factor erythroid 2-like 1 (Nfe2l1, also known as Nrf1). Through its feedback mechanism, it senses proteasomal malfunction and compensates for this loss of activity by promoting the transcription of new proteasomal subunits. This bounce back activation highlights the adaptive nature of Nfe2l1 and stresses its importance for cellular remodeling. Nfe2l1 has been shown to be indispensable for cold adaptation in brown adipose tissue and to maintain cholesterol homeostasis in the liver. However, not much is known about the role of Nfe2l1 in skeletal muscle, even though it is highly expressed in this tissue.

In my study, I demonstrated that Nfe2l1 plays a major role in skeletal muscle physiology. Besides governing the proteomic and ubiquitome landscape, it also defines the muscle phenotype inducing a fiber type switch upon loss of the transcription factor. Absence of Nfe2l1 created a leaner phenotype and led to remodeling of the energy metabolism and mitochondrial respiration. Furthermore, loss of Nfe2l1 resulted in resistance to dietary induced obesity on a high-fat diet, along with improved glucose and insulin tolerance. However, loss of Nfe2l1 did not improved physical fitness of the animals.

The data display a refined role of Nfe2l1 in the skeletal muscle, maintaining energy balance throughout the reshaping process of the protein and ubiquitin landscape and defining the metabolic phenotype. Nfe2l1 emerges as a regulator of muscle fiber type and mitochondrial bioenergetics. This study stresses the importance of myocyte Nfe2l1 in cellular adaptation and homeostasis in response to metabolic challenges.

List of Figures

List of Tables

Abbreviations

a.u.	Arbitrary units
AA	Amino acid
ADP	Adenosine diphosphate
AKT	Protein kinase B (PKB)
AMC	7-Amino-4-Methylcoumarin
AMP	Adenosine monophosphate
AMPK	AMP-activated protein kinase
ANOVA	Analysis of variance
ARE	Antioxidant response element
ATF6	Activating transcription factor 6
ATP	Adenosine triphosphate
BAT	Brown adipose tissue
BiP	Binding immunoglobulin protein
BSA	Bovine serum albumin
bZip	Basic leucine zipper
CAA	Chloroacetamide
CHO	Carbohydrates
CNC	Cap ‘n’ collar
CO_2	Carbon dioxide
CoA	Coenzyme A
CS	Citrate synthase
Ddi2	DNA-damage inducible 1 homolog 2
DiGly	Diglycine
DIO	Diet-induced obesity
DMEM	Dulbecco Modified Eagle Medium
DMSO	Dimethyl Sulfoxide
DNA	Deoxyribonucleic acid
DTNB	5,5′-dithiobis-(2-nitrobenzoic acid)
DTT	Dithiothreitol
e.g.	exempli gratia
ECAR	Extracellular acidification rate
EGTA	Ethylene glycol-bis(2-aminoethylether)-N,N,N′,N′-tetraacetic acid
eIF2α	Eukaryotic translation initiation factor 2 subunit 1
ELISA	Enzyme-linked immunosorbent assay

ER	Endoplasmic reticulum
ERAD	ER-associated protein degradation
et al.	*et alii*
ETC	Electron transport chain
EtOH	Ethanol
FBS	Fetal bovine serum
FCCP	*N*-[4-(Trifluoromethoxy)phenyl]carbonohydrazonoyldicyanide
FFA	Free fatty acid
Fgf21	Fibroblast growth factor-21
Fig.	Figure
G3P	Glyceraldehyde-3-phosphate
GAPDH	Glyceraldehyde-3-phosphate dehydrogenase
Gastroc	Gastrocnemius
GC	Gastrocnemius
Gdf15	Growth differentiation factor-15
GLM	Generalized linear model
GLUT4	Glucose transporter type 4
GO	Gene ontology
GTT	Glucose tolerance test
H&E	Hematoxylin and eosin
HCl	Hydrochloric acid
HDL	High density lipoprotein
HEPES	2-[4-(2-Hydroxyethyl)piperazin-1-yl]ethane-1-sulfonic acid
HFD	High-fat diet
HIF-1α	Hypoxia inducible factor 1-alpha
i.p.	Intraperitoneal
iKO	Inducible mKO
IRE1α	Inositol-requiring enzyme 1 α
ITT	Insulin tolerance test
KD	Knock down
KEGG	Kyoto encyclopedia of genes and genomes
KO	Knockout
LC3	Microtubule-associated proteins 1A/1B light chain 3B
LDH	Lactate dehydrogenase
MAPK	Mitogen activated protein kinases
MeOH	Methanol

MHC	Major histocompatibility complex
mKO	Muscle KO
MRI	Magnetic resonance imaging
mRNA	Messenger RNA
Myh	Myosin heavy chain (referring to the gene)
MyHC	Myosin heavy chain
NaCl	Sodium chloride
NADH	Nicotinamide adenine dinucleotide
NADPH	Nicotinamide adenine dinucleotide phosphate
NaOH	Sodium hydroxide
Nfe2l1 (Nrf1)	Nuclear factor erythroid 2-like 1
Ngly1	N-glycanase 1
NST	Non-shivering thermogenesis
O_2	Oxygen
OCR	Oxygen consumption rate
OXPHOS	Oxidative phosphorylation
P70S6K	Ribosomal protein S6 kinase beta-1
p97	valosin-containing protein (VCP)
PAGE	Polyacrylamid gel electrophoresis
PBS	Phosphate buffered saline
PCA	Principle component analysis
PCR	Polymerase chain reaction
PERK	Protein kinase R-like endoplasmic reticulum kinase
PHD	Prolyl hydroxylase
PI3K	Phosphatidylinositol 3-kinase
PIP3	Phosphatidylinositol 3,4,5-trisphosphate
PKB	Protein kinase B
PMG	Pyruvate, Malate, Glutamate
PPAR-α	peroxisome proliferator-activated receptor alpha
PTM	Post translational modifications
PVDF	Polyvinylidene difluoride
qPCR	quantitative PCR
RER	Respiratory exchange ratio
RMR	Resting metabolic rate
RNA	Ribonucleic acid
RNAseq	RNA sequencing

Rot/AA	Rotenone and Antimycin A
RT	Room temperature
RT-qPCR	Reverse transcriptase qPCR
SDC	Sodium deoxycholate
SDH	Succinate dehydrogenase
SDS	Sodium dodecyl sulfate
SDS-PAGE	Sodium dodecyl sulfate polyacrylamide gel electrophoresis
SEM	Standard error of the mean
siRNA	Small interfering RNA
STAT	Signal transducer and activator of transcription
SUC	Succinate
T2DM	Type 2 diabetes mellitus
TCA	Tricarboxylic acid
TCEP	Tris(2-carboxyethyl)phosphine hydrochloride
TEM	Transmission electron microscopy
TG	Triglycerides
TNF	Tumor necrosis factor
TRIS	Tris(hydroxymethyl)aminomethane
UPR	Unfolded protein response
UPS	Ubiquitin-proteasome system
VCP	valosin-containing protein
WT	Wild-type

1. Introduction

1.1 Obesity and metabolic diseases

Obesity and an overweight population are rising issues worldwide. According to the latest German health reports of 2019/2020 over 50 % of the German population is overweight and 19 % obese[1]. Globally, obesity has almost tripled since 1975 and also in Germany there is an increasing trend of obesity, particularly in the male population[2,3]. Overweight is defined by a body mass index (BMI, kg/m^2) between 25-30 and a person with a BMI ≥30 is considered as obese. Obesity was the 5th most prevalent risk factor for death in 2019 (Fig. 1), responsible for over five million deceases worldwide. Additionally, two other of the top five causes of death, namely high blood pressure and high blood sugar (Fig. 1), are also correlated with overweight. This underscores the urgency of addressing obesity as the global health crisis it is and the demand for efficient treatment.

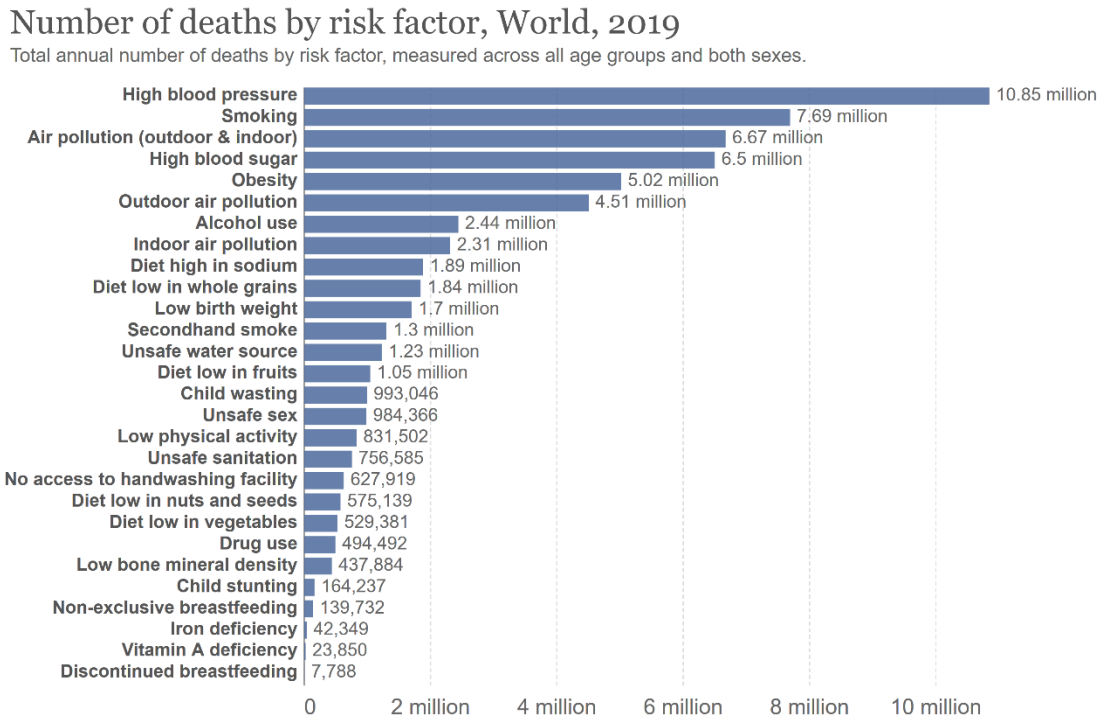

Figure 1: Obesity is among the top 5 risk factors for deaths worldwide (2019). Bar chart showing number of deaths by risk factor globally in 2019. Numbers are total annual deaths across all age groups and both sexes. Data from “https://ourworldindata.org/causes-of-death”.

Furthermore, obesity is associated with chronic, low-grade inflammation, promoting cytokine expansion, which in turn causes obesity-associated diseases[4]. Thus, being overweight or obese is typically not a direct cause of death, but it drastically increases the risk of metabolic diseases and associated comorbidities, as for example hypertension, hypercholesterolemia, coronary artery disease, insulin resistance and type 2 diabetes mellitus (T2DM)[5–7]. Furthermore, diabetes often leads to an aberrant lipid profile characterized by high levels of triglycerides (TGs) and low levels of high-density lipoprotein (HDL) cholesterol. Elevated TG levels are a common feature of diabetic

dyslipidemia, and they are associated with an increased risk of cardiovascular complications in diabetic patients[8].

An additional, yet often less considered burden of obesity, is the reduced quality of life and the accompanying mental health problems of these patients. A study has shown that persons with obesity are five times more likely to experience major episodes of depression[9]. Altogether these consequences and accompanying difficulties of obesity put substantial pressure on the health system, estimating over 10 % of all health care costs in Germany between 2020 and 2050 will account for expenses linked to overweight patients[10]. Thus, it is of utmost importance to understand the underlying causes of obesity, as there are various reasons for the trend we witness and a better understanding of the core principals will help to battle this global concern. Indisputably, there are genetic predispositions and diseases which can cause an accumulation of adipose tissue[11]. However, there are additional factors influencing this development. Modern society has shown a major technical advance by replacing manual labor with machines along with progressing urbanization leading to shorter commutes and improving transportation, all leading to an increasingly sedentary lifestyle[12]. Furthermore, food has become more readily available and the majority is highly processed and nutrient dense, which leads to chronic overnutrition[13,14]. Obesity - formerly a problem of high income states - has now also reached lower income countries, often facing consequences that are more drastic due to a higher susceptibility to low cost highly processed foods and inferior education in the field of nutrition[15]. Nonetheless, for most patients there are simple intervention methods. Often the initial steps to battle overweight are lifestyle changes by an altered meal plan and exercise. For some patients however these mediations are not successful. In more severe cases surgery in form of a gastric bypass or sleeve gastrectomy, where a portion of the stomach is removed, is necessary to decrease food intake, thereby lowering the BMI and improving overall metabolic health[16].

1.1.1 Insulin signaling and glucose metabolism

An important staple of metabolic health are insulin and glucose homeostasis. It is crucial to maintain steady insulin levels and thereby preserve a closely regulated glucose balance. If this delicate system is disturbed the risk of developing insulin resistance or T2DM increases drastically particularly in an obese condition[17].

Insulin is a hormone produced by the beta cells of the pancreas and is secreted upon glucose ingestion. Subsequently, it triggers the transport of glucose into important organs like muscle, liver or adipose tissue, which utilize glucose as fuel for metabolic processes. Glucose uptake is facilitated through the signaling cascade of the insulin receptor. It belongs to the family of tyrosine receptors, meaning that upon binding of insulin the receptor autophosphorylates its tyrosine residues and thereby initiates a complex signaling cascade[18,19]. Initially, Phosphoinositide 3-kinase (PI3K) is activated and via the secondary messenger Phosphatidylinositol 3,4,5-trisphosphate (PIP3) phosphorylates protein kinase B (PKB, better known as Akt). Akt then initiates the transport of vesicles

containing glucose transporter type 4 (GLUT4) to the membrane, thus allowing the uptake of glucose into the cell[20].

By facilitating glucose uptake into the organs blood sugar levels are reduced. Resistance to insulin is often observed in obese patients and pre-diabetic states. A constant exposure to high blood sugar levels by carbohydrate rich diets leads to a persistent high secretion of insulin. Consequently, this triggers an internalization of the insulin receptor and hence leads to a decreased insulin sensitivity. Thus resulting in insulin resistance leading to an insufficient uptake of blood glucose inducing hyperglycemia[21]. A constant exposure of the organs to high glucose levels can cause damage to, e.g., retina of the eyes, kidneys, nerves or the heart[22]. Therefore, maintaining insulin sensitivity in the major organs of glucose uptake like muscle or liver is imperative for metabolic health. Insulin and glucose sensitivity are commonly assessed by performing a glucose or insulin tolerance test (GTT and ITT). In these tests the subject is injected with a high amount of either substrate and the blood glucose levels are measured over time. These tests give a quantitative measure of blood sugar clearance and insulin sensitivity, indicating a subject's metabolic health and giving insights into potential disturbances of this system.

1.1.2 Endocrine fine-tuning in obesity

Insulin is one of the hormones, which is essential for maintaining metabolic homeostasis. However, there are further factors that define metabolic health and also influence insulin sensitivity. Namely, adiponectin is an additional important factor for metabolic homeostasis. Adiponectin is an adipokine, a cytokine predominantly produced and secreted by adipocytes. It increases insulin sensitivity and therefore supports glucose clearance from the blood as well as promoting anti-inflammatory cytokine activation[23]. Moreover, it shows protective characteristics against obesity and T2DM, thus acting as a guardian of adipocyte health[23]. Its protective function or lack thereof becomes increasingly evident in the state of obesity. Circulating adiponectin levels decrease with obesity and metabolic syndrome, therefore diminishing its beneficial effects and fueling insulin resistance[24,25].

Another crucial factor of adipocyte health and whole-body metabolism is leptin. This hormone is likewise produced and secreted by adipose tissue[26]. Leptin blocks the feeling of hunger and regulates the lipid storage of adipocytes. Interestingly, levels of leptin are positively correlated to an increasing BMI. The underlying cause for this phenomenon is a reduced leptin sensitivity with expansion of the adipose tissue[27]. Therefore, despite high levels of circulating leptin, the feeling of hunger cannot be suppressed. However, the reasons accounting for the decreased sensitivity of leptin in obesity are manifold, reaching from genetic dysregulations, to defective signaling cascade or a deficiency in the transport across the blood-brain barrier[28]. This reduction in leptin sensitivity leads to a diminished anorexic effect and in turn increases hunger and fuels the vicious circle of obesity.

1.2 Energy balance and exercise

On a larger scale, not only nutrients and hormones need to be closely regulated to preserve homeostasis, but overall caloric balance has to be maintained. The current development of chronic overnutrition and a predominantly sedentary lifestyle are making it increasingly difficult to sustain a healthy energy balance with the same amount of energy output as calorie intake. Experimentally energy expenditure can be measured via indirect calorimetry by assessing the oxygen consumption rate (OCR)[29]. An essential factor that needs to be taken into account when analyzing the OCR is the body weight of the subject. A larger animal or human being unquestionably has a higher oxygen consumption compared to a small one, hence the energy expenditure is often displayed as a generalized linear model (GLM) plot over body weight[30]. Thereby it becomes apparent that if comparing two groups of different body weights as for example different sexes (Fig. 2a) seemingly different energy outputs lead to a not significantly different GLM. However, if the body weights do not differ between groups indicated differences hold true in the GLM (Fig. 2b). Correspondingly when analyzing data from obese cohorts in comparison to lean controls, the body weight difference needs to be accounted for.

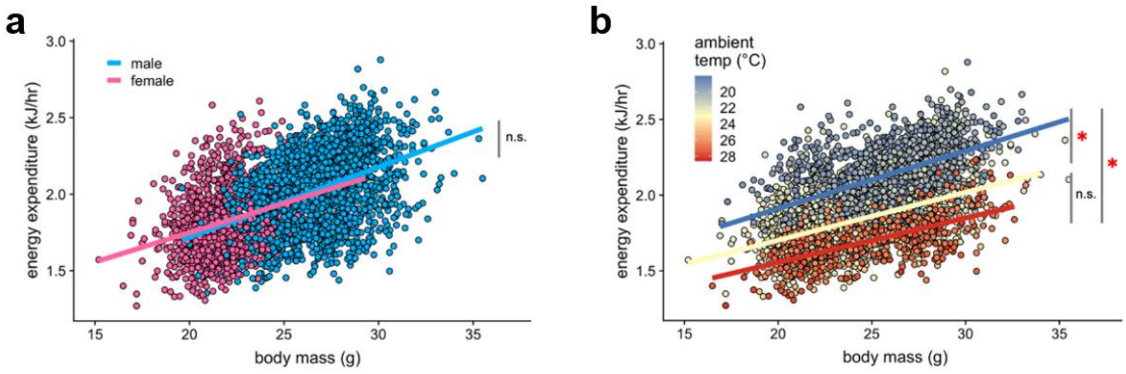

Figure 2: Analyzing energy expenditure data requires consideration of body weight differences. GLM-plots of energy expenditure over body mass of a) male and female mice and b) ambient temperature effects on mice. Adapted from [31].

When further defining the energy expenditure, the calorie utilization can be divided into four different sub-categories. The resting metabolic rate (RMR), thermic effect of food, physical activity and thermogenesis[32]. The latter is facilitated by specific adipose tissue depots consisting of extraordinary adipocytes, capable of creating heat by uncoupling of the electron transport chain (ETC) and using lipids as main fuel source[33]. This adipose tissue is called brown adipose tissue (BAT) due to its darker color, resulting from the higher mitochondria content necessary for the uncoupling, compared to other adipose tissue depots, which are rather white in color. BAT mainly affects energy expenditure in hibernating mammals, but also humans can carry out non-shivering thermogenesis (NST)[34]. Although this ability is widely lost in adults due to the involution of the brown adipose tissue. Recent studies however have shown that BAT can be activated in adult humans by cold plunges which stimulate NST[35]. This proves, that BAT can be activated via a constant mild cold stimulus triggering NST and thereby activating lipolysis, burning

calories and contributing to the energy expenditure, which makes this tissue an interesting therapeutic target.

Another angle to combat the rising obesity epidemic is to increase physical activity[36]. By amplifying the amount of exercise or merely combating the mostly sedentary lifestyle, various metabolic diseases can be prevented or detrimental outcomes ameliorated[37]. These beneficial effects are mostly facilitated by an improvement of energy expenditure through physical activity and thereby restoring caloric balance. An important parameter when measuring metabolic fitness and exercise capacity is the respiratory exchange ratio (RER)[38]. This value defines the ratio of carbon dioxide produced over the oxygen which is consumed. In a resting state, the RER is usually between 0.7 and 1.0. A value closer to 0.7 indicates a metabolic state predominantly utilizing fatty acids as fuel source (Fig. 3). The fatty acid beta-oxidation requires more oxygen than glycolysis and subsequently makes the quotient smaller. The oxygen is supplied in the form of cofactors like NAD^+ or FAD, which in turn are reduced themselves to $NADH+H^+$ and $FADH_2$. On the other hand, a RER close to 1.0 represents a metabolic state predominantly running on carbohydrates, e.g., glucose or glycogen (Fig. 3), using less oxygen.

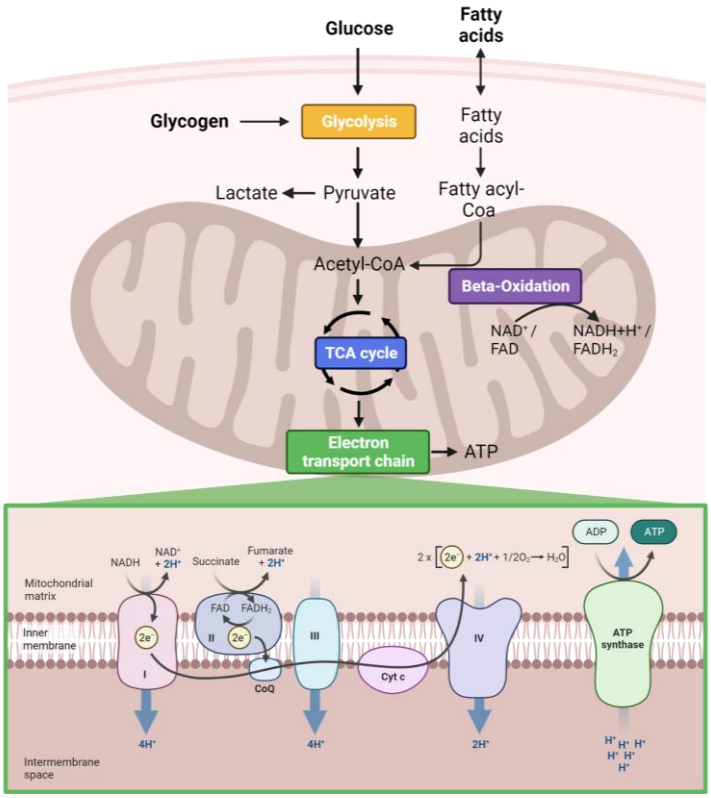

Figure 3: Different nutrients fueling the mitochondrial metabolism. ATP in the mitochondria can be generated from different fuel sources. Glucose or fatty acids can be metabolized and fuel the TCA cycle and subsequently supply the electron transport chain (ETC) with co-factors and electron donors. Created with Biorender.com.

In exercise physiology, the RER is used to calculate the so called “cross-over point”, a measure of metabolic fitness during an exhaustion test[39]. The cross-over point is defined by the point in time where the use of cellular carbohydrate stores in form of glycogen,

exceeds the utilization of fat, due to lack of oxygen uptake. This ratio serves as a measure of exhaustion. Therefore, the later this point is reached during a bout of exercise, the “fitter” the subject is presumed to be[40]. Furthermore, in a physically challenging activity, the RER can also exceed the value of 1.0. This however, is due to the bicarbonate buffering system safeguarding the muscle from acidosis through high amounts of lactate production upon fatigue and not actually giving insight into the specific metabolism any longer[41].

1.3 Skeletal muscle biology

The skeletal muscle makes up about 40% of human body mass. Its proper function is essential for posture, locomotion and physical activity[36]. Beyond that, muscle tissue plays an imperative role in metabolic regulation and energy homeostasis as it is one of the most important deposal sites of glucose and functions as a nutrient and energy storage and sensing site[42]. It thereby contributes largely to total energy expenditure and by regulating blood glucose levels can affect metabolic diseases like cardiovascular diseases, obesity or T2DM. Thus, muscle metabolism greatly contributes to metabolic adaptation and flexibility. Whereas muscle weakness, damage or induced muscle wasting, also known as atrophy, is associated with various metabolic and neurological diseases. Vice versa a sedentary lifestyle, but also aging, with its reduced muscular activity is a main driver for muscle loss and gives rise to cardiometabolic disease and age-related health burdens. In obesity the higher load of circulating free fatty acids (FFA) as well as a chronic low grade of inflammation state[43] leads to a drastically decreased muscular insulin sensitivity[44] and despite a higher demand of weight supporting muscle the skeletal muscle often shows reduced force[45]. Thus, exercising and sustaining muscle mass to increase insulin sensitivity and improve proper glucose homeostasis is imperative for metabolic health and improving longevity[46,47].

Furthermore, muscle is an important player contributing to interorgan cross talk via secretion of cytokines - some of them even muscle specific (myokines)[48]. An emerging player is growth differentiation factor-15 (Gdf15), a cytokine which so far is not very well studied, however it has recently been associated with exercise induced anorexia[49], as well as increasing energy expenditure and thereby promoting weight loss[50]. Neutralizing Gdf15 in a cancer cachexia model however has been shown to improve many metabolic parameters and recover muscle function[51]. Also, recent studies have demonstrated fibroblast growth factor-21 (Fgf21), so far known as a liver cytokine, taking a major role in muscle metabolism[52]. Fgf21 is activated upon ER stress and induces a metabolic shift in the muscle tissue as well as muscle atrophy[53,54]. Somewhat paradoxically secretion of Fgf21 from the muscle has been shown to have beneficial effects, e.g., preventing obesity and insulin resistance[55].

The multiple areas that are impacted by muscle function, signaling and health, resulting in severe effects on whole body metabolism underline the necessity to understand and study muscle biology in respect to health-related disorders and appreciate the muscle as new potential therapeutic target for metabolic diseases.

1.3.1 Muscle fiber types and their metabolic profile

Skeletal muscle cells are formed by proliferation and fusion of several precursor myoblasts, resulting in multinucleated myotubes with centralized nuclei. Consequently, fusion of multiple myotubes, as well as movement of the nuclei to the periphery result in mature muscle fibers[56,57] (Fig. 4). Evenly distributed nuclei on the outside boarder of the myofibers are imperative for the correct function of the muscle[58]. Accordingly, centralized nuclei in mature myofibers are a hallmark of muscle damage or ongoing regeneration and can be observed in multiple myopathies[59]. In these disorders, myosin genes, that are important for development and regeneration after muscle damage, namely *Myh3* and *Myh8*, are activated and therefore can also be seen as surrogate markers of muscle damage[60]. In the process of nuclei movement, the muscle fibers become ordered and build a highly structured entity, called myofibril, consisting of actin and myosin bundles relevant for muscle contraction (Fig. 4).

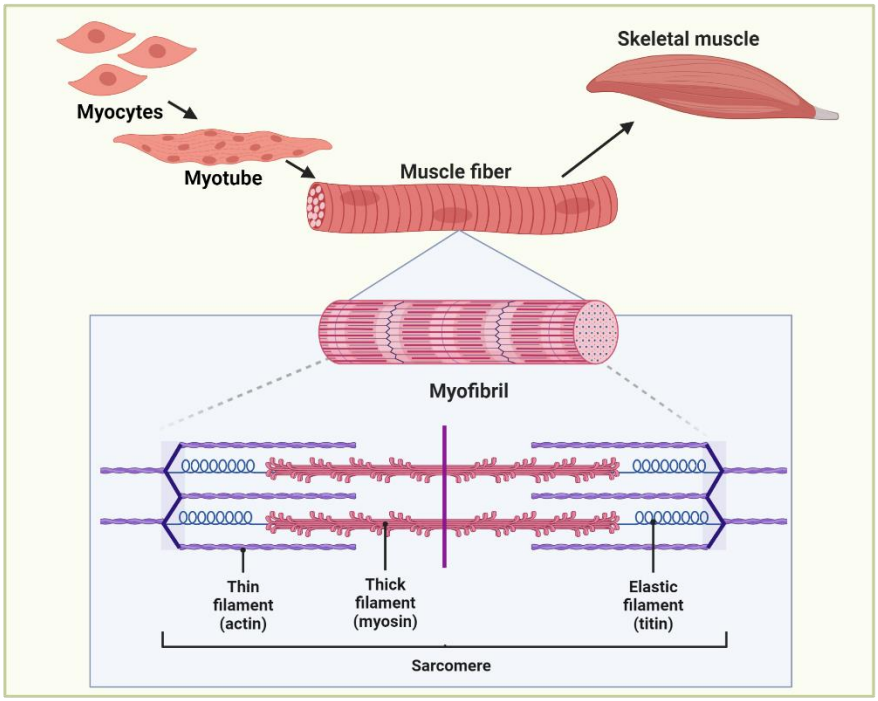

Figure 4: Biogenesis and structure of skeletal muscle tissue. Multiple myocytes fuse into a multinucleated myotubes. Fusion of multiple myotubes and movement of the nuclei to the periphery create highly structured myofibrils giving rise to the muscle fiber. Myofibrils contain the structural proteins titin, actin and myosin. The latter are decisive for contraction speed of the skeletal muscle tissue, which these structures ultimately form. Created with Biorender.com.

The maximal contractile capability subdivides the skeletal muscle in two main groups, defined as slow and fast twitch muscle fibers due to the maximum shortening speed of the myofibril thick filaments (myosin) by the MyHC motor proteins. Consequently, the MyHC type I (encoded by *Myh7*) are called slow twitch and MyHC type IIa and type IIx (encoded by *Myh2* and *Myh1*) are referred to as fast twitch fibers[61].

An essential part of the muscle metabolism and another distinct difference between the two fiber types is the opposing primary fuel usage and metabolic phenotype of the fibers.

The different fiber types show a different abundance of mitochondrial proteins[62,63]. Slow twitch fibers are associated with a higher content of mitochondria and a greater capacity of oxidative phosphorylation compared to fast twitch muscle fibers. Thus, the slow fibers have a higher ATP production and exhaust less easily compared to the fast twitch ones[64]. Therefore, the slow twitch fibers are often referred to as oxidative fiber type. However, the fast twitch muscle can quickly produce ATP by synthesis of lactic acid from pyruvate (Fig. 3), a process that needs less oxygen and therefore is resorted to in a state of high energy demand but insufficient oxygen supply, e.g., during fatigue or maximal capacity exercise. These fibers are also called glycolytic fibers due to their metabolic profile.

Diabetes and obesity are often associated with a shift of muscle fiber towards a more glycolytic profile[65,66]. Obese patients display a lower activity of oxidative enzymes and a higher lipid content in the muscle, contributing to insulin resistance[67]. Mutation models inducing a switch to a MyHC type I fiber can increase energy expenditure in dietary induced obesity and thereby attenuate negative metabolic outcomes[68]. This demonstrates the importance of muscle metabolism and health in metabolic diseases, but also implies a distinction role for the two fiber types under different conditions, presenting the possibility of targeting one or the other fiber specifically and thereby inducing alternate outcomes for whole body metabolism.

1.3.2 Mitochondrial respiration

Mitochondria are highly dynamic and adaptive organelles, maintaining calcium balance, but more importantly, accounting for most of the energy production of a cell. In this process the electron transport chain (ETC) plays an essential role. The ETC is located in the inner mitochondrial membrane and is one of the key factors for maintaining energy homeostasis and the main site of ATP production[69]. The ETC is composed of 4 complexes (I – IV) and the ATP-synthase, while not truly part of the ETC, the ATP-synthase is often referred to as complex V. The complexes create an electrochemical gradient by using redox reactions to pump protons into the intermembrane space using cofactors like NADH and FADH as electron donors and oxygen at the end of the ETC as electron acceptor. The proton gradient is then used to fuel the phosphorylation of ADP to ATP, which is why the entire process is being referred to as oxidative phosphorylation (OXPHOS).

Deficiency of single complexes of the ETC are often detrimental. For example, lack of function of complex III leads to a shift towards a more glycolytic profile[70], and some mutations in the genes responsible for development of complex III are even lethal[71].

Altogether, disruptions in mitochondrial homeostasis can have a large impact on overall cellular energy balance and affect whole body metabolic health. Therefore, it is of the utmost importance to maintain structural and functional integrity of the mitochondria to prevent cell stress and - in the worst case - apoptosis.

1.4 Cell stress pathways and important players

Cellular stress can have many underlying causes. A central pillar of metabolic adaption and cell survival is protein homeostasis, also known as proteostasis. This includes protein synthesis, folding and degradation, which are tightly regulated processes due to the great significance proteins have in regulating various metabolic processes, signaling pathways and enzymatic activities[14]. The proteomic landscape underlies constant remodeling due to the natural half-life of proteins and the continuous pressure of adapting the protein profile according to environmental changes, such as, e.g., nutrient availability or oxygen abundance.

1.4.1 Hypoxia

Hypoxia is a state of low oxygen availability and further characterized by insufficient oxygen supply to tissues or organs. The lack of sufficient oxygen imposes a great amount of stress on the cells. A crucial regulator in the oxygen sensing pathway is the hypoxia inducible factor 1-alpha (HIF-1α), a transcription factor which under normal oxygen conditions is constantly degraded via the ubiquitin-proteasome system. Under low oxygen conditions however, HIF-1α is stabilized and promotes the transcription of its target genes mitigating the pathologies caused by hypoxia[72]. There are different underlying causes of hypoxia. A typical source of low oxygen levels is an impaired blood flow or a reduced oxygen carrying capacity of the blood cells (anemia), to supply the surrounding tissue. Furthermore, hypoxia is a pathology observed in cancer patients. Tumors that grow rapidly often have impaired oxygen supply and consequently display high HIF-1α levels. The transcription factor promotes angiogenesis and erythropoiesis in the tumor tissue and thereby worsens the patients prospects for survival[73,74]. Yet not only cancer is a condition of in which HIF-1α is induced. Further causes of low oxygen supply and activation of the HIF-1α pathway are the following: respiratory diseases, cardiovascular disorders or even sepsis. In general hypoxia induces ER stress by disturbing protein folding through oxidizing disulfide bonds and thereby triggering multiple cellular stress responses, leading to disorders if not addressed in a suitable manner[75].

In summary, this highlights the importance of studying the HIF-1α in basal and pathological conditions. A way to mimic hypoxia experimentally is by treatment with the chemical compound cobalt(II)chloride ($CoCl_2$). It binds the oxygen in the cells and thereby induces hypoxia in vitro[76]. By utilizing this method further important steps to understanding the pathological outcomes and underlying mechanisms of hypoxia can be made.

1.4.2 Mechanistic target of rapamycin (mTOR) signaling

A factor which in recent years has emerged as a chief regulator of metabolism, cell proliferation and protein synthesis is the mechanistic target of rapamycin (mTOR). This highly conserved serine/threonine kinase has first been discovered in *saccharomyces cerevisiae* in the early 1990s[77] and shortly afterwards its mammalian orthologue has been described[78,79]. The protein has its name from the feature that it is bound by the immunosuppressive rapamycin, which consecutively inhibits the mTOR kinase activity. More importantly however, mTOR functions as a sensor for a multitude of environmental stimuli, e.g., nutrient availability, growth factors or cellular stress and adapts cell fate accordingly. The protein mTOR operates as a complex consisting of multiple proteins and has two different manifestations, namely mTOR complex 1 (mTORC1) and mTOR complex 2 (mTORC2). The mTORC1 mainly regulates downstream targets, which control protein translation via the Ribosomal protein S6 kinase beta-1 (p70S6K) (Fig. 5). In a nutrient rich state mTORC1 is active and phosphorylates p70S6K, which in turn initiates protein translation and thereby promotes cell growth and proliferation. Accordingly, degradation pathways like, e.g., autophagy are inhibited by mTORC1 activity. The mTORC2 is less studied, but it is understood, that this complex controls Akt signaling by phosphorylating the serine473 residue. The downstream pathways of Akt then initiate glycolysis and other cell survival signals[80].

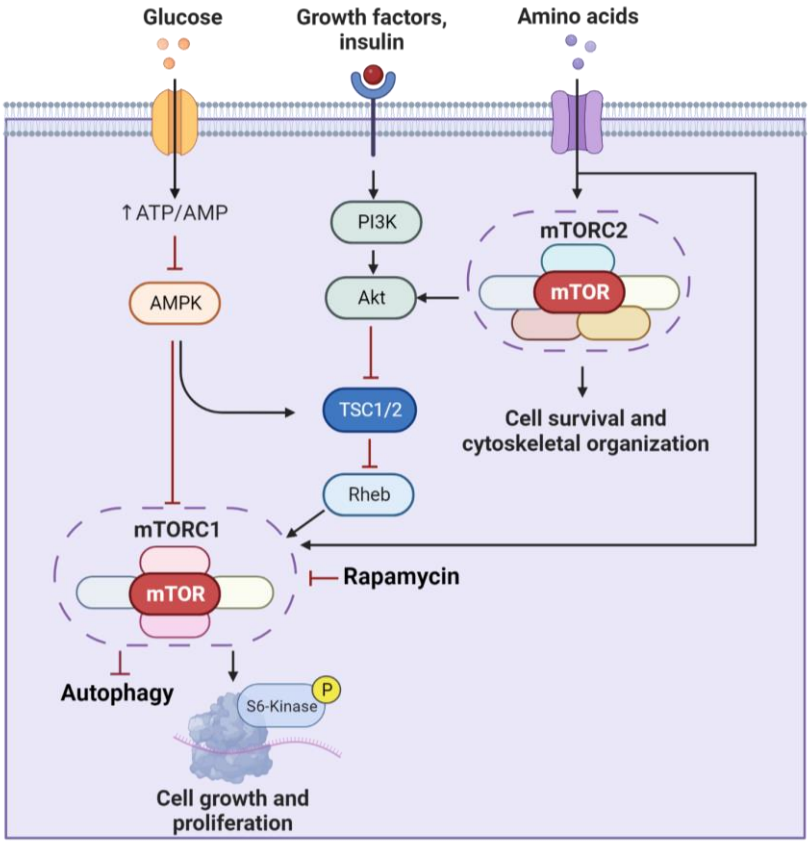

Figure 5: Signaling pathway of the mechanistic target of rapamycin (mTOR). The mTOR complexes 1 and 2 (mTORC1 and mTORC2) are controlled by availability of glucose, growth factors and insulin signaling. An excess of these nutrients initiates a signaling cascade, which activates both mTOR complexes and promotes cell survival, growth and proliferation. Created with Biorender.com.

Dysregulations in the mTOR activities have been associated with multiple diseases like obesity, cancer or also neurodegenerative pathologies. A hyper activation of mTOR has been linked to uncontrollable cell growth in certain cancers. In obesity, overnutrition also leads to a continuously active mTORC1, resulting in excessive adipose tissue growth and insulin resistance, thereby potentially inducing T2DM.

Conclusively, these studies display an essential and intricate role for the two mTOR complexes in various metabolic pathways and a necessity for a closely regulated activation. Their role as crucial nutrient sensors, regulators of many signaling pathways and the implications in numerous globally critical diseases confirm the importance of further study these complexes and potentially target them therapeutically.

1.4.3 Amino acid metabolism

The amino acid metabolism is closely regulated by mTOR activity. Maintaining a carefully managed nutrient pool and constant amino acid availability as well as interorgan flux is crucial for sustaining metabolic homeostasis. Most amino acids can internally be synthesized, while others need to be taken up via food. Amino acids which cannot be synthesized, but need to be taken up via diet are referred to as “essential” amino acids. The remaining “non-essential” amino acids are synthesized either from intermediates of the tricarboxylic acid (TCA) cycle or glycolysis. Subsequently, these can be used as building blocks for proteins or serve as second messengers for interorgan cross talk[81], as well as neurological transmitters[82,83]. Amino acids can also be generated by protein breakdown via the ubiquitin-proteasome system (UPS) or autophagy and consequently recycled and utilized for synthesis of new proteins. Furthermore, amino acids can serve as precursors for glucose synthesis via gluconeogenesis[84] or fuel the TCA cycle producing energy for the cell. However, incorporating them into the TCA entails the release of ammonium, which is potentially toxic for the cells. Hence, the cells dispose of the excess ammonium by incorporating it into the intermediates of the urea cycle and subsequently secrete them as uric acid.

Amino acid metabolism and proteostasis are intricately linked, making the equilibrium of synthesis and breakdown of proteins closely orchestrated by the nutrient sensor mTOR as well as dependent on hormones regulated by underlying total energy levels. If this delicate system is disrupted this leads to multiple metabolic disorders, as for example Phenylketonuria (PKU)[85] or Maple Syrup Urine Disease (MSUD)[86]. Furthermore, faulty catabolism via the urea cycle can lead to an accumulation of ammonium or a rise in pH and thereby induce tissue damage or - in the worst case - organ failure. A maladaptive amino acid metabolism also impacts protein synthesis and thereby secondarily cell growth and regeneration.

Altogether, these examples underline the importance of a closely monitored amino acid metabolism and its greater role in overall metabolism, health and protein homeostasis.

1.5 Endoplasmic reticulum stress responses

Disturbed proteostasis and predominantly an accumulation of misfolded or obsolete proteins is often associated with neurodegenerative diseases like Alzheimer's or Parkinson's disease. However, the phenomenon of accumulating unwanted protein excess also occurs in aging, cancer or metabolic diseases and therefore is a wide-ranging burden that has generated multiple cellular adaptive mechanisms in the course of evolution to cope with different kinds of cell stress. The main pathways safeguarding proteostasis are located in the endoplasmic reticulum (ER), e.g., the unfolded protein response (UPR), autophagy and Endoplasmic-reticulum-associated protein degradation (ERAD) via the ubiquitin-proteasome pathway (UPS). All of these processes are associated with the ER as protein folding takes place in the ER lumen.

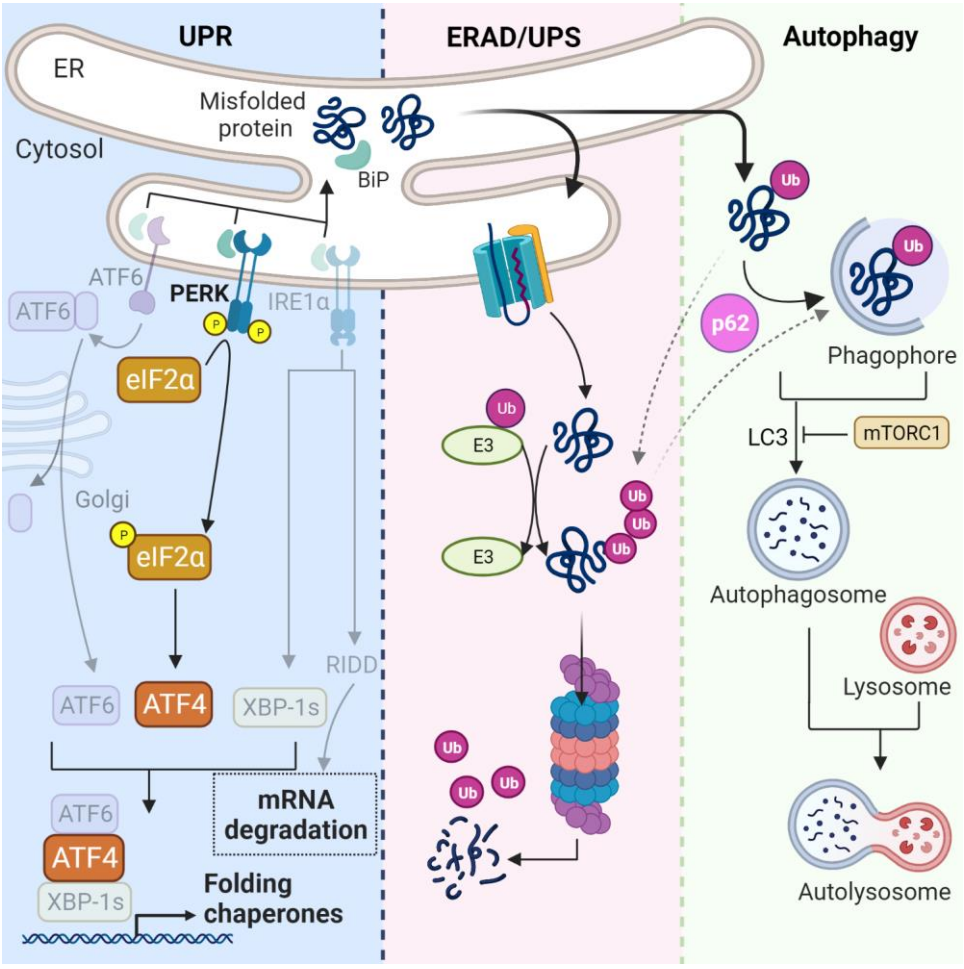

Figure 6: Endoplasmic reticulum (ER) stress response. All three pathways: UPR, ERAD/UPS and autophagy sense misfolded proteins in the ER and help restore cellular proteostasis by degradation or folding assistance. The UPR has three signaling branches, namely ATF6, IRE1α and PERK. The latter activates eIF2α by phosphorylation, consequently recruiting ATF4 and thereby promoting the transcription of folding chaperones. The ERAD/UPS retrotranslocates misfolded proteins to the cytosol, where they are tagged with ubiquitin and subsequently degraded by the proteasome. In autophagy, a mTOR regulated pathway, ubiquitin tagged proteins are shuttled to the phagophore by p62. This adapter protein can also transport misfolded proteins to the proteasome and is therefore a link between these two pathways. Full engulfment then is facilitated by LC3 and the resulting autophagosome fuses with a lysosome for final degradation. Adapted from [87] and created with Biorender.com.

1.5.1 Unfolded Protein Response

The unfolded protein response (UPR) is one branch of the ER stress response. Concisely, the two main functions of the UPR are either to support protein translation by promoting the transcription of folding chaperones or to halt translation by degradation of mRNA[88]. Misfolded proteins are sensed by binding of immunoglobulin protein (BiP, also known as Hspa5). Subsequently BiP binds to one of the three stress receptors on the ER membrane and initiates a signaling cascade to restore proteostasis (Fig. 6). One of these receptors is R-like endoplasmic reticulum kinase (PERK), which upon binding of BiP exerts its kinase activity and phosphorylates eukaryotic translation initiation factor 2-alpha (eIF2α)[89]. Phosphorylated eIF2α terminates all translation processes except for those promoting folding chaperones through activating transcription factor-4 (ATF4). The other two main receptors in the ER membrane binding BiP are activating transcription factor-6 (ATF6) and inositol-requiring enzyme 1-alpha (IRE1α). ATF6 after undergoing splicing in the Golgi also promotes the transcription of folding chaperones. The function of IRE1α is twofold: on the one hand it promotes the decay of mRNA and on the other hand it also promotes the transcription of folding chaperones[90].

The close regulation and homeostasis of folding and translation of proteins is essential to prevent proteotoxic stress. Disorders in the PERK pathway have been associated with multiple diseases like Wolcott-Rallison syndrome, which results from a mutation in the PERK receptor, leading to T2DM and growth retardation of the patients[91]. Furthermore, a hyper activation of PERK is often observed in cancer cells, helping them adapt to, e.g., hypoxia and other stressors during rapid tumor growth[74,92].

1.5.2 Autophagy

Macroautophagy (hereafter referred to as autophagy) is another highly conserved degradation pathway playing a crucial role in maintaining cellular homeostasis. It senses damaged proteins or cell organelles and breaks these down to be recycled or discarded. Autophagy involves multiple autophagy related proteins and uses the ER membrane to engulf the damaged cell fragments[93]. The adapter protein Sequestosome-1 (SQTSM1, or also p62) plays a major role in recognizing and shuttling the cargo to the early structures of autophagic pathway, the phagophore, to initiate engulfment of the damaged cell organelles or proteins. Subsequently, Microtubule-associated proteins 1A/1B light chain 3B (LC3) facilitate the full engulfment and thereby develop the so called autophagosome (Fig. 6). The last step is the fusion of autophagosome and lysosomes to lastly achieve degradation. Autophagy has first been discovered and largely studied in the context of starvation[94,95]. By activating this resourceful pathway, organisms can maintain energy balance throughout starvation, by recycling their own cellular material. Newer studies have also presented a role for mTOR in this process, by negatively regulating autophagy in a nutrient rich state and hereby promoting cell growth[96,97]. Beyond this autophagy has gained importance in numerous additional fields. In obesity and aging autophagy is generally downregulated[98], thus leading to an accumulation of

harmful material in the cell and increasing cellular stress. Moreover, genetic modifications of autophagy genes often lead to neurological damage and impaired function of the immune system[99]. Overall, the involvement of the autophagy pathway in multiple metabolic disorders underlines its significant role in the degradation of damaged organelles or misfolded proteins and maintaining metabolic homeostasis.

1.5.3 The Ubiquitin-Proteasome System

ER-associated protein degradation (ERAD) is another mechanism safeguarding ER homeostasis. In contrast to the UPR, its main focus is not to assist folding but to degrade damaged material, preventing an overflow of misfolded proteins in the ER lumen, as polypeptide chains are translocated into the ER to undergo folding into the final tertiary structure[100]. If errors occur during this process, the unfolded proteins are detected by their exposed hydrophobic fragments[101] and consequently retrotranslocated across the ER membrane into the cytosol for degradation via the ubiquitin-proteasome system[102] (Fig. 6).

The UPS, as a central part of the ERAD machinery, is a multistep process in which damaged, misfolded or obsolete proteins are tagged with ubiquitin and subsequently degraded by the proteasome in an ATP dependent, but lysosome independent manner[103–105]. The first step, the ubiquitylation process is carried out by three different classes of enzymes. The first class are the ubiquitin activating enzymes (E1), which in an ATP dependent manner bind the ubiquitin molecule and transfer it to the next enzyme, the ubiquitin conjugating (E2) enzyme. Lastly, the ubiquitin ligase (E3) recognizes the peptide substrate and binds to it. Simultaneously the E3 also binds the E2 and consequently catalyzes the transferal of the ubiquitin molecule from the E2 enzyme onto the misfolded protein. E3 ligases play a major role in regulating muscle mass. Atrophic muscles display an increased transcription of certain ubiquitin ligases as, e.g., *Trim63* and *Fbxo32*. Furthermore, a study has shown, that loss of these E3 ligases can prevent muscle atrophy[106]. Hence, an increase of these E3 ligase genes are perceived as surrogate markers for muscle wasting.

The tagged protein is then transported to the proteasome. An important player in this process is the p62 adapter protein, which also shuttles ubiquitylated proteins to the autophagy pathway. It thereby emerges as a common player in autophagy and UPS[107]. This link between autophagy and UPS, allows for compensation of the mechanisms between both pathways, adding an extra layer of security to preserve cellular homeostasis[108] (Fig. 6).

The last step of the UPS, the degradation, occurs via the proteasome. This barrel shaped protein complex consists of a core particle, also known as 20S, containing the catalytic activity sites and one or two attached regulatory particles, also referred to as 19S. A proteasome with one regulatory particle is called 26S and with two attached 19S particles results in a 30S proteasome, measures which are named after their sedimentation coefficient[109]. The proteasome occupies a central role in the UPS and in the last decade has emerged as an interesting druggable complex for targeted protein degradation. In

multiple myeloma the proteasome inhibitor bortezomib is used to inhibit cell growth of tumor cells[110]. More recent work is focused on hijacking the cellular UPS system by creating a chimeric molecule, which on one end binds the protein of interest and on the other side recruits E3 ligases, bringing the drug target and UPS pathway in close proximity in order to transfer ubiquitin on the protein of interest and thereby trigger subsequent degradation via the proteasome. These compounds are called PROTACs (Proteolysis Targeting Chimeras) and can be used to specifically target and degrade various proteins, advancing current therapies[111–113]. Moreover, the UPS is an emerging field of interest for multiple diseases acknowledging the importance of proteostasis and identifying a link between decreased function of the proteasome and pathologies such as Parkinson, Alzheimer's[114], muscle atrophy[115] and obesity[116].

1.5.4 Ubiquitin and polyubiquitylation

Ubiquitin is a small, highly conserved protein consisting of 76 amino acids. It is well established, that ubiquitin acts as a marker for degradation in the UPS pathway. Covalently linked to the target protein, it initiates a signaling cascade guiding its substrate to the proteasome for decay. However, there are hypotheses, that the role of ubiquitin goes beyond facilitating degradation. Studies investigating the different subtypes of ubiquitylation have found various types of polyubiquitin chains, multiple ubiquitin molecules connected via one of the seven lysine (K) residues[117] (Fig. 7). These intermolecular linkages make the possibilities of different polyubiquitin chains endless and consecutive plausible biological outcomes are infinite and not well understood[118].

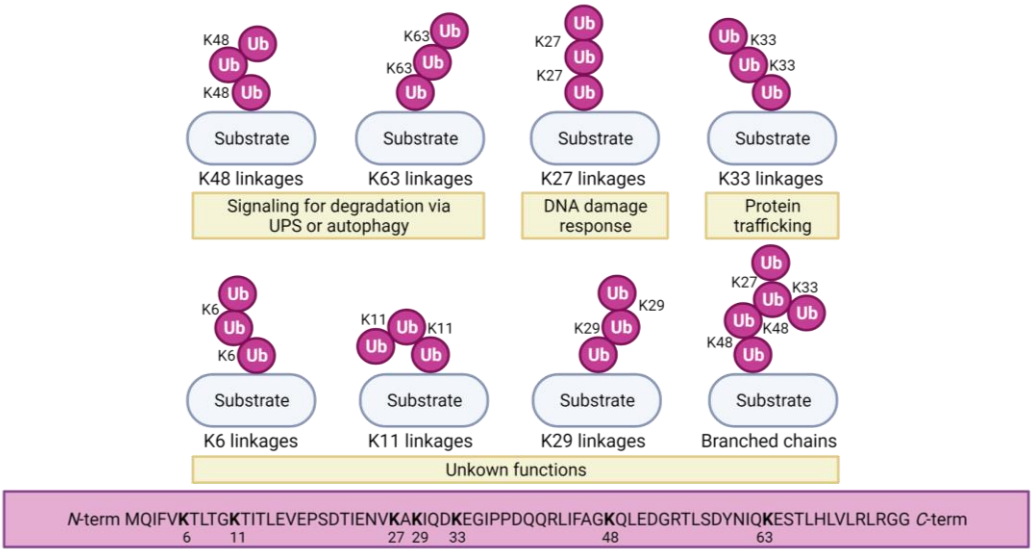

Figure 7: Polyubiquitin chains, different linkages and their functions. Ubiquitin has seven lysine (K) residues, which can form intermolecular linkages. K48 and K63 are main signals for degradation. K27 promotes DNA damage response and K33 is essential for protein trafficking. Other linkages like K6, K11, K29 and branched forms are not well studied thus far. Adapted from [119], created with Biorender.com.

The most studied polyubiquitin linkages are those via K48 and K63 (Fig. 7). Both of these linkage sites are associated with degradation via the UPS and also autophagy, creating a signaling node of these two degradation pathways[118], important for cross-talk or

potential compensatory actions. Furthermore, the polyubiquitylation on K27 plays a role in DNA damage response and K33 in protein trafficking[120]. Also, both are not enriched upon proteasome inhibition underscoring an independent role of these linkages from proteasomal degradation[118]. Regarding the polyubiquitylation chains and their signaling outcomes many aspects are still not well understood and yet to be investigated, making it a very interesting field of study due to the wide-ranging implications the UPS has in many pathologies and cell adaptation[97].

1.6 The Transcription Factor Nfe2l1

Nuclear factor erythroid 2-like 1 (Nfe2l1, or also known as Nrf1 or Tcf11) is a transcription factor regulating the adaptive response of the UPS[121]. Nfe2l1 is tethered to the ER membrane and by trafficking through valosin-containing protein (VCP, also called p97) exposed to the cytoplasm, where it undergoes multiple post translational modifications (PTM), e.g., deglycosylation by N-glycanase 1 (Ngly1)[122] and cleavage by DNA-damage inducible 1 homolog 2 (Ddi2)[123]. Still, the exact mechanism and order of the PTMs remain poorly understood. However, it is acknowledged, that these processing steps release the active form of Nfe2l1, which is constantly degraded by the proteasome under basal conditions (Fig. 8a). This circumstance makes it difficult to detect the cleaved form of the protein (95 kDa) in unstressed conditions.

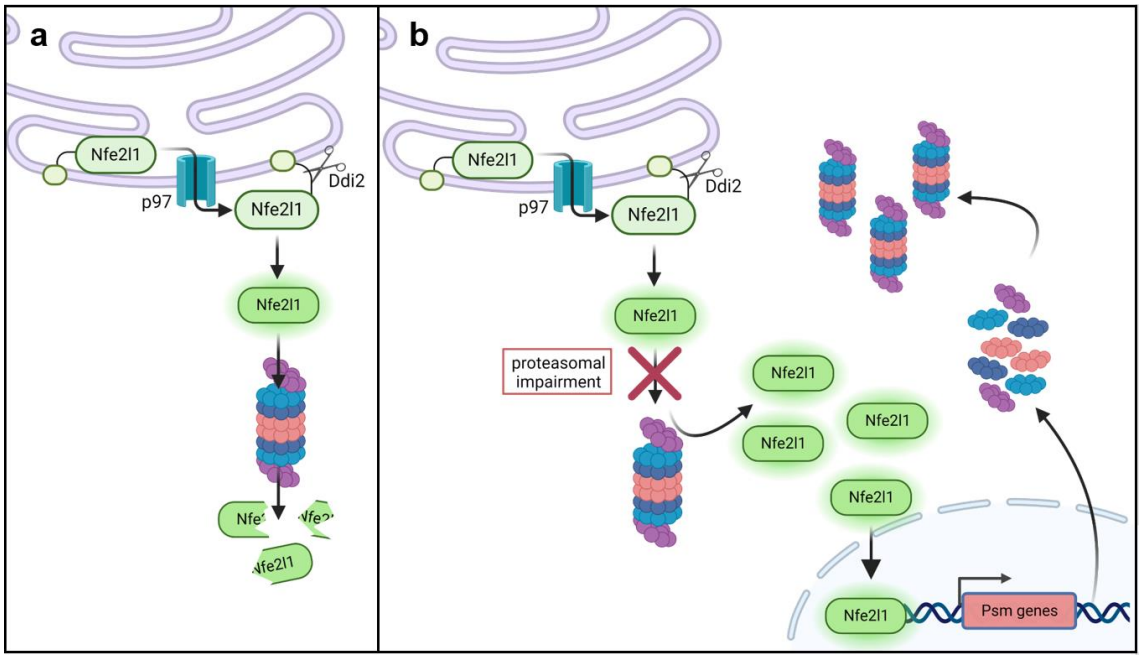

Figure 8: Proposed mechanism for the ER residing transcription factor Nfe2l1. a) Basal conditions: Valosin-containing protein (VCP) or p97 flips Nfe2l1 exposing it to the cytoplasm, where it undergoes cleavage by Ddi2, releasing the active form. In unstressed conditions Nfe2l1 is consequently degraded by the proteasome. b) Upon proteasome inhibition, the active form of Nfe2l1 accumulates in the cytoplasm and translocates into the nucleus, where it binds upstream of proteasomal subunit (Psm) genes and promotes the transcription thereof. The subunits are assembled into new proteasomes and compensate for the loss of proteasome activity. Adapted from [121]. Created with Biorender.com.

Upon chemical inhibition with, e.g., bortezomib or malfunction of the proteasome, Nfe2l1 accumulates in the cytosol and can be detected. Consequently, Nfe2l1 is translocated to the nucleus and binds to the antioxidant response element (ARE) of the promotor region of proteasomal subunit (*Psm*) genes via its basic leucine zipper (bZIP) domain. This initiates the transcription of proteasomal subunits, which in turn can be assembled into new proteasomes and compensate for the initial lack of proteasome function (Fig. 8b). This brilliant bounce-back mechanism emphasizes the importance of Nfe2l1 in the context of proteostasis and cellular stress response.

An important guardian of cellular stress is the ER. The ER stress response and UPS are closely linked and together preserve proteostasis. In the muscle tissue ER stress pathways play a major role in myocyte differentiation and health. Many environmental stimuli, like exercise, starvation, cancer or obesity cause ER stress, making mechanisms that maintain ER homeostasis like UPS an important field of research[124]. A more direct link to myocyte UPS are muscle disorders and atrophy. The wasting of muscle tissue is facilitated by E3 ligases and enhancement of the UPS[106]. Taking this into account, studying a crucial regulator of the ubiquitin-proteasome system like Nfe2l1 in the muscle becomes indispensable to further the understanding of these diseases, particularly since Nfe2l1 has been shown to be a major metabolic player in other tissues.

In brown adipocytes Nfe2l1 is indispensable for thermogenesis[125] and protects the tissue from ferroptosis, a special kind of cell death[126]. In the heart Nfe2l1 has been shown to control regeneration of cardiomyocytes[127] and in the liver the transcription factor safeguards cholesterol homeostasis[128].

Recently Nfe2l1 has been studied in myocytes *in vitro*. These studies imply a positive regulation of Nfe2l1 by mTOR, suggesting a role of Nfe2l1 in this central nutrient sensing pathway and consequent adaptation of the UPS[129,130]. However, not much in known about the role of myocyte Nfe2l1 *in vivo* and how the ubiquitin-proteasome system in the muscle tissue adapts to different environmental stimuli and what role Nfe2l1 plays during these remodeling processes.

1.7 Scientific aims

Obesity is a challenging and growing epidemic. However, not much is known about the underlying biological mechanisms of this condition, giving rise to multiple metabolic diseases. Studying the physiological machineries that lead to energy imbalance and overweight can supposedly help combat this global crisis. One hallmark of obesity is ER stress caused by misfolded proteins and an overwhelmed ubiquitin proteasome system (UPS) leading to proteotoxic stress and apoptosis.

A crucial regulator of the UPS is the transcription factor Nuclear factor erythroid 2-like 1 (Nfe2l1), which controls the adaptive component of the UPS in response to proteasome inhibition and overload. In other tissues, e.g., brown adipose tissue and heart, Nfe2l1 has been shown to be indispensable for metabolic adaptation and tissue regeneration. In skeletal muscle the transcription factor is highly expressed compared to these tissues. Thus, investigating the role of Nfe2l1 in skeletal muscle biology is of great significance.

My aim was to define the role of Nfe2l1 in the skeletal muscle in respect to proteostasis as well as its impact on metabolic adaptation and flexibility *in vivo*. Furthermore, studying the dynamic changes of the muscle protein profile upon loss of Nfe2l1 alongside the specific ubiquitome landscape using mass spectrometry analysis was one key element of my project. Additionally, examining protein fate and the regulation of the UPS in skeletal muscle of obese animals was of particular interest. On the other hand, targeting Nfe2l1 by different interventions *in vitro* as well as inducing the loss of Nfe2l1 in adult animals should elucidate the potential of the transcription factor as novel therapeutic. Additionally, I studied the exercise performance of mice lacking Nfe2l1 in the muscle tissue in comparison to wild type littermate controls.

Overall, this study provides a thorough insight into muscle proteostasis, under different metabolic conditions, highlighting the importance of Nfe2l1 in the UPS pathway, as well as displaying novel consequences of loss of Nfe2l1 on whole body metabolism.

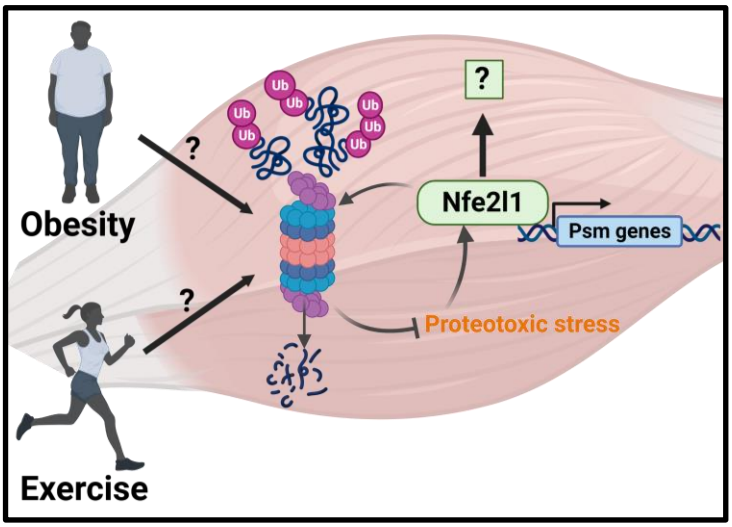

Figure 9: Project overview - Elucidating the role of skeletal muscle Nfe2l1 in the UPS and its impact on metabolism. Studying the impact of exercise and obesity on the UPS with regard to arising proteotoxic stress and the adaptive response of Nfe2l1. Additionally, investigating the metabolic outcome of the Nfe2l1 feedback reaction. Created with Biorender.com.

2. Material and Methods

2.1 Mouse experiments

All mouse experiments and treatments were previously approved by the animal welfare committees of the government of Upper Bavaria, Germany (ROB-55.2-2532.Vet_02-20-32, ROB-55.2-2532.Vet_02-21-56) and the procedures are in line with German Animal Welfare Laws. C57BL/6JRj mice for diet-induced obesity (DIO) study were acquired from Janvier Labs. They were fed a high-fat diet (HFD) over the course of 16 weeks and age-matched to chow controls. The animals with Nfe2l1 floxed were described earlier[125]. These mice crossed with B6.Cg-Tg(ACTA1-cre)79Jme/J (The Jackson Laboratory) stock no. (006149) gave rise to the Nfe2l1 myocyte-specific knockout (mKO) mice. For wild-type (WT) control mice the Nfe2l1 gene remained floxed, however these animals were Cre negative (Cre^-). For the inducible muscle KO (iKO) Nfe2l1 flox-Acta1-CreERT2 mice were injected with 80 mg/kg Tamoxifen (TAM) in Mygliol at d0, d2 and d4. The mice were brought up and housed in standard conditions with individually ventilated cages (IVCs) at room temperature (22 °C), with 12 h light–dark phases, fed ad libitum with either chow or HFD (60 kJ% lard (Sniff, D12492)) as well as water ad libitum. The Sable Systems PromethionCore® was used to determine indirect calorimetry parameters. Body composition was assessed by EchoMRI™ scans in triplicates. The animals were sedated with a mixture of xylazine/ketamine (30/150 mg/kg) (WDT) before blood samples were taken, consequently the animals were perfused with PBS (Thermo Fisher Scientific) containing 50 U/mL heparin. Harvested tissues were snap-frozen in liquid nitrogen and then stored at -80 °C. Plasma parameters such as Leptin (R&D Systems), Adiponectin (R&D Systems) and Insulin (Crystal Chem) were measured with ELISA kits conforming to the instructions of the manufacturer. A Beckman Coulter AU480 Chemistry Analyzer (Beckman Coulter) was used to assess plasma cholesterol and triacylglycerol levels. For insulin and glucose tolerance tests 0.75 U insulin in 0.2% wt/vol BSA dissolved in PBS per kilogram body weight of the animals or 1 mg glucose per gram body weight of the animals was administered intraperitoneal (*i.p.*), consequent to 6 h of fasting. The grip strength testing occurred only on the forelimbs of the animals, which were measured three time consecutively using the Bioseb grip strength test instrument (GS3).

2.2 Cell culture methods and treatments

For in vitro experiments, immortalized C2C12 mouse myoblasts (Sigma-Aldrich, 91031101) were utilized. The C2C12 cells were cultured at 37 °C with 5% CO_2 and maintained in DMEM Glutamax (Thermo) including 10 % FBS (Sigma) as well as 1 % Penicillin/Streptavidin (Sigma) supplementation. The cells were cultured with 40-80 % confluence, and split every two to three days. When the passage number surpassed 40, new cells were thawed and grown. The myocytes were differentiated to myotubes when 95 % confluence was reached and the growth medium was exchanged with DMEM Glutamax enhanced with 2 % horse serum as well as 1 % Penicillin/Streptavidin (Sigma). Old medium was removed and fresh differentiation medium was added to the cells each day for 6 consecutive days. For in vitro treatments, myotubes were treated with DMSO (Sigma) as control or 100 nM bortezomib (SelleckChem), 100 nM epoxomicin, 500 nM MG-132, 200 µM $CoCl_2$ or 20 nM rapamycin before harvest. For silencing of the Nfe2l1 gene, 30 nM SMARTpool silencing RNA (siRNA, Dharmacon) in Lipofectamine

RNAiMAX (Thermo) transfection reagent, was utilized according to the instructions of the manufacturer. Reverse transfection was performed on day two of differentiation. The transfection medium was removed and new differentiation medium was added to the cell 24 h after transfection. Treatment of the C2C12 cells then occurred after 48 h.

2.3 RNA extraction and gene expression measurement

For RNA extraction NucleoSpin RNA kit (Macherey Nagel) was utilized conforming to the manufacturer's protocol. A NanoDrop spectrophotometer (Implen) was used for RNA concentrations measurement. For complementary DNA (cDNA) preparation, 500 ng of isolated RNA were added to 2 µL Maxima H Master Mix (Thermo) and ddH_2O added so the reaction volume was 10 µL. Following the PCR the cDNA was diluted 1:40 with ddH_2O. Subsequently, the RT-qPCR (2 min 50 °C, 10 min 95 °C, 40 cycles of 15 sec 95 °C, 1 min 60 °C) was performed using the Quant-Studio 5 RealTime PCR system (Thermo) to assess relative gene expression. Each reaction contained 4 µL cDNA with 5 µL PowerUp™ SYBR Green Master Mix (Thermo) and 1 µL of 5 µM primer stock (Supplementary Table 1). All cycle thresholds (Cts) of measured genes were normalized to *TATA-box binding protein (Tbp)* measurements by the delta-delta-Ct (ΔΔCt)-calculation. The fold change was used to display the relative gene expression normalized to the appropriate experimental control group. RNA sequencing (RNAseq) was executed by Novogene (UK). For library sequencing they used Illumina NovaSeq platforms, utilizing a paired-end 150 bp sequencing strategy (short-reads).

2.4 Protein isolation for immunoblotting and measurement of citrate synthase activity

Protein isolation for measurement of citrate synthase activity and for immunoblotting were completed as earlier described[131]. In short, tissue or cells were lysed with RIPA buffer (50 mM Tris pH 8 (Merck),150 mM NaCl (Merck), 5 mM EDTA (Merck), 1% IGEPAL® CA-630 (Sigma), 0.5 % sodium deoxycholate (Sigma) supplemented with 0.1% SDS (Roth)). In 10 mL RIPA buffer each one cOmplete mini protease inhibitors (Sigma) and PhosSTOP (Roche Diagnostics) were added fresh every time. Mechanical lysis occurred via a TissueLyser II (3 min, 30 Hz; Qiagen). Subsequently, the lysates were centrifuged for 15 min (21,000 *g*, 4 °C). The supernatant was transferred to a new tube and protein concentrations thereof were measured using a Pierce BCA Protein Assay (Thermo) corresponding to the manufacturer's protocol. Denaturation of 15-35 µg protein occurred via 5% (vol/vol) 2-mercaptoethanol (Sigma) in LDS sample buffer (Thermo) to and boiling samples for 5 min at 95 °C before loading on to Bolt™ 4–12% Bis-Tris (Thermo) or NuPage 12 % (Thermo) gel. SDS-PAGE was performed at a constant voltage with 200 V, 160 mA and 100 W for 40-50 min. Subsequently, blotting of the proteins onto a 0.2 µm PVDF membrane (Bio-Rad) was performed using the Trans-Blot® Turbo™ system (Bio-Rad) with the settings of 25 V, 1.3 A for 15 min. To assess transfer efficiency, the membrane was incubated with Ponceau S (Sigma) for 5 min and subsequently blocked with 1 x Roti-Block (Roth) for 1 h at room temperature. The membrane was incubated rolling overnight at 4°C with primary antibody solution (Supplementary Table 2). Following, the blots were washed with TBS-T (200 mM Tris (Merck), 1.36 mM NaCl (Merck), 0.1% Tween 20 (Sigma)) 3 x for 7 min and membrane incubated in the secondary antibody solutin (Supplementary Table 2) at room

temperature for 1 h. For detection, the blots were washed with TBS-T, developed using SuperSignal West Pico PLUS Chemiluminescent Substrate (Thermo) and scanned in a Chemidoc imager (Bio-Rad) with the appropriate exposure time. Detected protein bands were the normalized to beta-tubulin or Gapdh as a loading control with Image Lab software (Bio-Rad). For measuring the activity of citrate synthase, 15-30 µg protein were added to a reaction buffer (20 mM Tris-HCl, pH 8.0 (Merck), 0.42 mM acetyl-coenzyme A (Sigma), 0.1 mM DTNB (Sigma)). After 5 min of incubation at 37 °C, 0.5 mM Oxaloacetate was supplemented to start the reaction. Following, the emission was measured with a plate reader (Tecan) at 412 nm for 5 min every minute.

2.5 Proteasome activity assay

For Lysis, lysis buffer (40 mM TRIS, pH 7.2 (Merck), 50 nM NaCl (Merck), 5 mM $MgCl_2$ (hexahydrate) (Merck), 2 mM ATP (Sigma), 2 mM β-mercaptoethanol (Sigma), 10 % v/v glycerol (Sigma)) was added to the tissue or cells and mechanical lysis occurred via a TissueLyser II (3 min, 30 Hz; Qiagen). Consequently, the lysates were centrifuged (15 min, 4 °C, 21,000 *g*) and the supernatant was used for further analysis. To assess the three different catalytic activities of the proteasome, the Proteasome Activity Fluorometric Assay II kit (UBPBio) was used in line with the manufacturer's protocol. The excitation wavelength was 360 nm and emission was measured over the course of 15 min in 1 min intervals at 460 nm in a Plate reader (Tecan). The activity was normalized to protein load of each sample, using Bio-Rad Protein Assay Kit II (Bio-Rad) in accordance with the manufacturer's protocol.

2.6 Native PAGE

The native PAGE protocol used to measure proteasome activity in-gel with subsequent immunoblotting was published earlier[132]. In short, lysis occurred using a lysis buffer (50 mM Tris/HCl pH 7.5, 5 mM $MgCl_2$, 2 mM DTT, 2 mM ATP, 10% glycerol (vol/vol), 0.05% Digitonin (v/v)) and phosphatase inhibitor (PhosStop, Roche) and mechanical lysis was performed by a TissueLyser II (3 min, 30 Hz; Qiagen). Subsequently, the samples were incubated on ice for 20 min and then centrifuged (4 °C, 21,000 *g)* for 15 min (2x). The supernatant was transferred into a new tube and used for following analysis. The protein content of the samples was measured with the Bio-Rad Protein Assay Kit II and 15 µg protein was loaded on to a NuPAGE 3-8% Tris-Acetate gel (Thermo). The gel was let run for 4 h at 150 V in the constant voltage setting. Next, the gel was incubated for 30 min at 37 °C in an activity buffer (50 mM Tris, 1 mM DTT, 1 mM $MgCl_2$) with 0.05 mM chymotrypsin-like substrate Suc-Leu-Leu-Val-Tyr-AMC (Bachem). Finally, the fluorescence was detected by a ChemiDoc MP (Bio-Rad). Subsequent immunoblotting of the gel occurred as previously described in chapter 2.4.

2.7 Histology and TEM

After tissue collection, fresh tissues were placed in histology cassettes (Leica), incubated for 24-48 h in 4 % formalin (Sigma) and subsequently dehydrated overnight (70 % EtOH, 96 % EtOH, 100 % EtOH, 100 % Xylene (Sigma)) using an ASP200S (Leica). Next, the tissues were embedded in paraffin (Roth), cut in 4-6 µm sections utilizing a microtome (Leica) and placed on Superfrost™ Plus Adhesion Microscope Slides (Epredia). After

drying the slides overnight, the paraffin was removed and the sections rehydrated by incubating in 100 % Xylene (2 x 5 min), 100% EtOH (2 x 10 dips), 96% EtOH (5 dips), 70 % EtOH (3 dips), ddH_2O (10 dips). Next, the sections were stained using hematoxylin, water and lastly eosin (5 min incubation time each), following dehydration with 70 % EtOH (3 dips), 96 % EtOH (5 dips), 100 % EtOH (2 x 10 dips), Xylene (2 x 2 min). Lastly, the slides were mounted using Histokitt II (Roth) and imaging occurred via a DMi8 (Leica).

Succinate dehydrogenase (SDH) staining was performed with cryosections. To generate cryosections, freshly harvested tissue was dipped in isopentane cooled with liquid nitrogen and consequently stored at -80 °C. These tissues were then cut into 4-6 µm thick sections using a cryotome CM3050S (Leica). Staining occurred for 45 min at 37 °C using nitroblue tetrazolium (1:1000 w/v, Thermo) in SDH stock solution (0.2 M sodium succinate, 0.2 M PBS, Sigma). Next, the samples were rinsed with ddH_2O (3 dips) and dried using an acetone gradient (30 %, 60 %, 30 %, 15 seconds each) and rinsed again with ddH_2O (3 dips). Subsequent dehydration occurred by 2 min incubation each in 70 % EtOH, 90 % EtOH, 100 % EtOH, 50 % EtOH/ 50 % xylene and xylene (2x). Lastly, the slides were mounted using Entellan® (Merck) and imaging occurred via a DMi8 (Leica).

Cryosections were also produced for immunofluorescent staining. The sections were blocked for 1 h at room temperature with 4 % mouse on mouse (MOM) IgG blocking solution (Vector). Next, sections were washed twice for 2 min each with PBS and incubated at 37 °C for 1 h in a mix of primary antibodies (DSHB, University of Iowa) containing: BA-D5 (IgG2b, supernatant, 1:100 dilution) for MyHC-I, SC-71 (IgG1, supernatant, 1:100 dilution) for MyHC-2A and BF-F3 (IgM, purified antibody, 1:100 dilution) for MyHC-2B in PBS with 1 % bovine serum albumin (BSA). Next, sections were washed in PBS (3 x 5 min) and subsequently incubated for 45 min at 37 °C in secondary antibody solution (Jackson ImmunoResearch): goat anti-mouse IgG1, conjugated with DyLight488 fluorophore, goat anti-mouse IgG2b, conjugated with DyLight405 fluorophore, goat anti-mouse IgM, conjugated with DyLight549 fluorophore diluted in PBS with 0.5 % BSA and 5 % goat serum. Images were produced using ZOE™-fluorescent cell imager (Bio-Rad).

For transmission electron microscopy (TEM) sedated mice were perfused with 0.9 % w/v NaCl, following perfusion with electron microscopy grade fixative buffer with: 3 % w/v glutaraldehyde, 3 % w/v paraformaldehyde in phosphate buffer, pH 7.4 (Electron Microscopy Science). Subsequently, tissues were harvested and stored in electron microscopy grade fixative buffer and further treated as described previously[133]. Briefly, fixed tissues were incubated in 2 % osmium tetroxide and subsequently dehydrated by an ethanol gradient series. Clearing of the samples occurred via propylene oxide, and for embedding EPON 812 (Serva Electrophoresis GmbH) was used. Lastly, samples were cured at 45 °C for 20 h, followed by further 24 h at 60 °C. The samples were sectioned into 60 nm thin slices using a Reichert-Jung Ultracut E ultramicrotome with a diamond knife (DiATOME Electron Microscopy Sciences). Silver-looking sections were transferred to a 150 µm mesh copper/rhodium grid (Plano GmbH) and contrasted using alcoholic uranyl acetate and lead citrate. For imaging of the sections, a Libra 120 transmission electron microscope (Carl Zeiss NTS GmbH) equipped with a SSCCD camera system (TRS, Olympus) was used.

2.8 Protein digestion and clean-up for LC-MS/MS

Protein digestion and DiGly peptide enrichment for LC-MS/MS was performed as described previously[134,135]. In short, lysis of the tissue occurred in sodium deoxycholate (SDC) buffer (1 % w/v SDC in 100 mM Tris-HCl, pH 8.5) by homogenizing the tissue in a douncer (Roth) and subsequent boiling at 95 °C for 5 min, shaking at 1000 rpm. Further disruption of the lysates occurred via a Bioruptor (Diagenode, 15 min, cycles of 30 sec). Next, the samples were centrifuged at 10000 *g* for 15 min and the supernatant was used for further analysis. Measuring of the protein concentrations of the samples was performed via the Pierce BCA Protein Assay (Thermo) in accordance with the manufacturer's protocol. Subsequently, 5 mg of protein was reduced and alkylated using 40 mM CAA and 10 mM TCEP and incubated in the dark for 10 min, at 45 °C, shaking at 1000 rpm. Subsequent digestion of the samples occurred overnight at 37 °C while shaking at 1000 rpm, by adding trypsin (1:100 w/w, Sigma) and LysC (1:100 w/w, Wako). For total proteome analysis, aliquots of digested samples (~15 µg) were desalted in self-made 3-layered SDB-RPS StageTips (Empore). In short, samples were diluted to a final volume of 200 µL with 2 % TFA in isopropanol (1:1). After, total proteome samples were transferred onto StageTips and consecutively washed with 1 % TFA in isopropanol and 0.2 % TFA/2 % ACN. Elution of the peptides occurred via 1.25 % ammonium hydroxide (NH_4OH) in 80 % ACN, which was freshly prepared. Peptides were dried for 45 min using a SpeedVac centrifuge (Thermo). Samples were thoroughly resuspended in 2 % ACN/0.1 % TFA and protein concentration determined via a NanoDrop spectrophotometer (Implen). Samples for DiGly enrichment were diluted with 1 % TFA in isopropanol (1:5) and subsequent peptide purification was performed using SDB-RPS cartridges (Strata™-X-C, 200 mg/6 mL, Phenomenex Inc.). Cartridges were equilibrated with 8 bed volumes (BV) of 30 % MeOH/1 % TFA and subsequently washed by adding 8 BV of 0.2 % TFA. Loading of the samples was performed with gravity flow and following washing steps included 8 BV of 1 % TFA in isopropanol and 8 BV of 0.2% TFA/2 % ACN. Elution of the peptides occurred twice with each 4 BV of 1.25 % NH_4OH in 80 % ACN. Subsequently, samples were dried overnight at 45 °C using a SpeedVac centrifuge (Thermo).

2.9 Diglycine (DiGly) remnant immunopurification

The PTMScan® Ubiquitin Remnant Motif (K-ε-GG) (Cell Signaling Technologies) was utilized for DiGly peptide enrichment. The antibody-beads for immunopurification were cross-linked before use, like earlier described[135]. In short, one tube of antibody coupled beads was washed with cold cross-linking wash buffer (100 mM sodium tetraborate decahydrate, pH 9.0). Subsequently, the beads were incubated in cross-linking buffer (20 mM dimethylpimpimidate in cross-linking wash buffer) for 30 min at room temperature whilst mild agitation. Quenching of the reaction occurred by washing twice with cold quenching buffer (200 mM ethanolamine, pH 8.0), following a 2 h incubation at room temperature in quenching buffer under moderate agitation. Finally, the cross-linked antibody beads were washed three time with cold IAP buffer and were ready to use for DiGly peptide enrichment.

The purified and dried peptides were resuspended in immunoaffinity purification (IAP) buffer by 15 min sonification (Bioruptor, Diagenode). Subsequently, the Pierce BCA Protein Assay (Thermo) was used to measure protein concentration of the samples.

3 mg of peptide was added to 1/8 of a tube of cross-linked antibody beads and the final total volume adjusted with IAP buffer to 1 mL. The immunopurification samples were incubated at 4 °C for 2 h whilst mild agitation. Next, the beads were washed twice with cold IAP buffer and twice with ddH_2O. Elution of the peptides from the antibody coupled beads occurred twice by incubation in 200 µL 0.2 % TFA whilst shaking at 1400 rpm for 5 min. The suspension was centrifuged and the supernatant was transferred to the SDB-RPS StageTips. The peptides were washed, eluted, and dried as previously described for total proteome samples (chapter 2.8).

2.10 LC-MS/MS ubiquitome and total proteome measurements

An EASY-nLC™ 1200 (Thermo) was used to perform liquid chromatography of ubiquitome and total proteome samples. The flow rate remained constant at 10 µL/min and 60 °C using a dual buffer system containing buffer A (0.1 % v/v formic acid) and buffer B (80 % v/v acetonitrile, 0.1% v/v formic acid). The in-house made column was 50 cm long, had a 75 µm inner diameter and was packed with C18 ReproSil (Dr. Maisch GmbH, 1.9 µm). For the ubiquitome samples elution started with 5% buffer B, increasing over 73 min to 25 %, 50 % after 105 min and remaining steady at 95 % after a total of 110 min. The gradient for total proteome measurement started at 5 % buffer B and increased to 20 % after 30 min, further increased to 29 % at 39 min, increased to 45 % after 45 min and lastly to 95 % after 50 min. The MS/MS measurement was completed on a Thermo Exploris 480 by injecting 500 ng peptide. For the ubiquitome samples the fragmented ions were detected in Data Independent Acquisition (DIA) mode with 66 isolation windows of variable sizes. The total scan time was 120 min with a scan range of 300–1650 *m/z*. The resolution of the orbitrap was 120,000 by a maximum injection time of 54 ms. MS2 scans were performed with a higher-energy collisional dissociation (HCD) of 30 % at a resolution of 15,000 with a maximum injection time of 22 ms. The MS measurement of the total proteome was performed equivalently, but with High-Field Asymmetric Waveform Ion Mobility (FAIMS) including a correction voltage of -50 V and a total scan time of 60 min. The injection time for the full scan was 45 s and the MS2 had an injection time of 22 s.

2.11 Proteome and Ubiquitome data acquisition and analysis

The directDIA mode in Spectronaut (13.12.200217.43655) was used to analyze DIA raw files. Peptide identification occurred via FASTA files from Uniprot Mus Musculus (10.03.2022) with 21989 entries, Uniprot Mus Musculus isoforms (10.03.2022) with 41771 entries and MaxQuant Contaminants for filtering (245 entries). The total proteome protein groups were measured through label free quantification, following the MaxLFQ algorithm. Further processing and analysis of the raw data was performed using Perseus (version 1.6.2.3) and the Perseus plugin “Peptide Collapse” (version 1.4.2)[136] for creating the site tables for the ubiquitome. For each sample the measured values were log_2-transformed and missing measurements were completed via imputation from normal distribution with a width of 0.3 and downshift 1.8 separately. Hits from the ubiquitome were normalized to number of peptides found in the total proteome. Comparison between conditions of proteome and ubiquitome was performed via Student’s *t*-test in R version 4.2.2 (*P*-value cutoff 0.1 and 0.2 for GO-analysis).

2.12 Untargeted metabolomics, data treating and analysis

Non targeted metabolomics of the muscle tissue was performed by the Metabolomics and Proteomics Core facility (MPC) at Helmholtz Munich (Neuherberg, Germany) as described earlier[137]. In short, the gastrocnemius was homogenized in ddH_2O (5 µL/mg) at 4 °C with 1.4 mm ceramic beads. Precipitation of the metabolites occurred by adding each 500 µL MeOH extraction solvent including recovery standard compounds to 100 µL of tissue homogenate. The supernatant was transferred to a new tube and subsequently dried under constant nitrogen stream (TurboVap 96, Zymark). The dried samples were then stored at −80 °C. For the measurement an ultra-high performance liquid chromatography-tandem mass spectrometry (UPLC-MS/MS) based analytical platform licensed by Metabolon (Durham, NC, USA) using Acquity UPLC (Waters) coupled to a Q Exactive mass spectrometer (Thermo) was utilized. In total UPLC-MS/MS injections occurred three times. The first two injections were utilized for analysis by UPLC-MS/MS positive ionizations, e.g., early, and late eluting compounds, and the last injection for analysis by UPLC-MS/MS negative ionization. Metabolon's proprietary chemical library was used to match the acquired MS/MS data. The library contains retention times, molecular weight (m/z) of metabolites, preferred adducts, in-source fragments, as well as associated MS/MS spectra for all molecules in the library. Median normalization was used on peak area counts and metabolites with over 50 % missing values were excluded. Other missing values were replaced by imputation using the k-nearest-neighbor algorithm. Lastly, values were log10 transformed and further analyzed using the online platform MetaboAnalyst.

2.13 Seahorse assay

Analysis of mitochondrial respiration via seahorse assay was performed as described earlier[138]. In short, the muscle tissue was harvested and lysed with MIBI buffer (210 mM d-Mannitol (Sigma), 70 mM sucrose (Sigma), 5 mM HEPES (Roth), 1 mM EGTA (Roth), 0.5% w/v fatty acid-free BSA (Sigma), pH 7.2) using a tissue homogenizer (Carl Roth). The lysate was centrifuged at 4 °C using 800 *g* for 10 min. The supernatant was then transferred into a new tube and consequently centrifuged at 8000 *g* for 15 min. Following, the supernatant was discarded and the pellet washed twice with MIBI buffer (8000 *g*, 15 min). The washed pellet was suspended shortly in a small volume of PBS to determine the mitochondrial content by using the Pierce BCA Protein Assay (Thermo). Following, the solution was diluted with MASI buffer (220 mM d-Mannitol (Sigma), 70 mM sucrose (Sigma), 10 mM KH_2PO_4 (Sigma), 5 mM $MgCl_2$ (Sigma), 2 mM HEPES (Roth), 1 mM EGTA (Roth), 0.2% w/v fatty acid-free BSA (Sigma), pH 7.2 at 37 °C) with supplementation of 10 mM succinate (Sigma) and 2 mM pyruvate (Agilent). The measurement was performed with 1 µg mitochondria, 16 mM ADP (Sigma), 1 µM Oligomycin (Sigma), 40 µM FCCP (Sigma) and 25 µM Rotenone/AntimycinA (Sigma) using a Seahorse XF24-analyzer (Agilent). The protocol containing exact injection as well as mix and measurement cycles is shown in Supplementary Table 3.

2.14 Oroboros measurement

Measurement of respiration by the mitochondria of permeabilized skeletal muscle fibers was performed via a high resolution respirometer (Oxygraph-2k, Oroboros Instruments)

as earlier described[139]. The measurements were performed in duplicates and to avoid oxygen deficits the assay took place in a hyperoxygenated environment ([O_2], 450-200 nmol/mL). Permeabilization of the gastrocnemius was performed using saponin (50 µg/mL) for 30 min in BIOPS buffer and subsequently two 10 min washes in respiration medium 5 (MiR05)(110 mmol/L sucrose, 60 mmol/L potassium lactobionate, 20 mmol/L Hepes, 10 mmol/L KH_2PO_4, 0.5 mmol/L EGTA, 20 mmol/L taurine, 3 mmol/L $MgCl_2 \cdot 6H_2O$, 1 g/L BSA, pH 7.1) at 37 °C). At first, the leak respiration was measured by addition of 2 mM malate, 10 mM glutamate and 5 mM pyruvate. Subsequently, 5 mM ADP and 3 mM $MgCl_2$ were added to determine NADH-linked respiration. Next, 10 mM Cytochrome C was injected to assess integrity of the outer mitochondrial membrane. 10 mM succinate was used to measure electron input from complexes I and II as well as oxidative phosphorylation. Lastly, 1 mM FCCP was added to assess maximum respiration rate. The respiratory measurements were performed in MiR05 buffer.

2.15 Statistics

Programs and tools that were used for data analysis are GraphPad Prism, Microsoft Excel, ImageLab, MetaboAnalyst and R (4.2.2). Routinely, data are shown as mean ± standard error of the mean (SEM), from all individual measurements. When comparing two groups with one variable the multiple Student's *t*-test was used. All experiments comparing two groups and two variables were analyzed using a two-way ANOVA with Bonferroni post-hoc test. When not indicated otherwise, *p*-values lower than 0.05 between two groups were considered significant and marked with an asterisk, non-significant comparisons have no indication. In ubiquitome and proteome the *p*-value cutoff for the GO analysis was 0.2 and in all further analyses the *p*-value was 0.1. For the analysis of the RNAseq data the R package *limma*[140] was used to calculate the *p*-values and adjust for hypothesis testing using FDR.

3. Results

3.1 Importance of Nfe2l1 in human and murine skeletal muscle

The transcription factor Nfe2l1 has been shown to be a major regulator of the ubiquitin-proteasome system (UPS) in various tissues including brown adipose tissue (BAT), heart and liver[125,127,128]. In human skeletal muscle it is highly expressed in comparison to other important transcription factors in muscle biology (Fig. 10a). Moreover, in our model system *mus musculus,* when comparing expression levels between different tissues, Nfe2l1 displayed the highest mRNA levels in skeletal muscle (Fig. 10b).

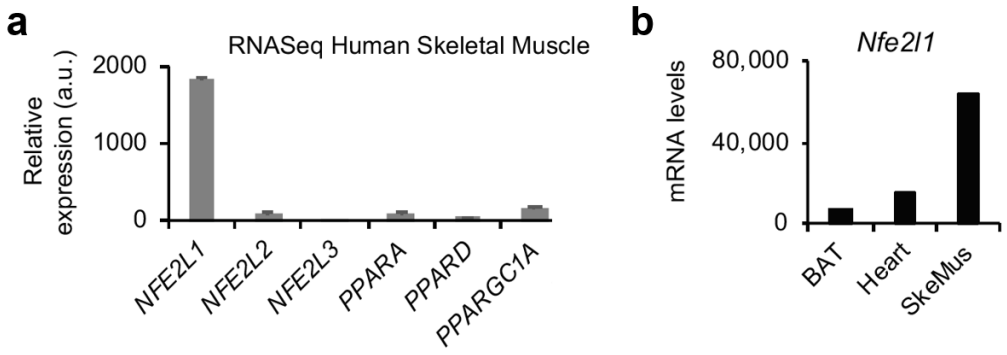

Figure 10: *Nfe2l1* shows significantly higher expression in human muscle compared to other transcription factors and is highly expressed in murine skeletal muscle tissue. a) Gene expression levels of human muscle *Nfe2l1* and other important skeletal muscle transcription factors from RNA sequencing[141]. b) Gene expression levels of *Nfe2l1* per 10^4 copies *Tbp* in mouse tissues[142].

Considering that Nfe2l1 is a crucial factor for thermogenesis in BAT and expression levels in skeletal muscle are thousand folds higher in muscle, these data drove me to investigate the role of Nfe2l1 in skeletal muscle and its impact on skeletal muscle function and effects on whole body metabolism.

3.2 Absence of Nfe2l1 in C2C12 myocytes impacts UPS

Protein levels of the transcription factor Nfe2l1 are virtually absent in normal, unstressed conditions due to it being constantly degraded by the proteasome. Mimicking cellular stress on the UPS by inhibiting the proteasome with different inhibitors initiates the feedback mechanism of Nfe2l1. The protein accumulates and translocates to the nucleus to promote the transcription of proteasomal subunit genes, compensating for the loss of proteasome function[121,143]. Here I show the accumulation of the cleaved and thus activated form of the Nfe2l1 protein upon obstruction of the proteasome with different inhibitors, to determine the appropriate chemical inhibitor for further experiments. The compound MG-132 (Fig. 11a) showed the lowest impact on Nfe2l1 accumulation, while the response on protein level to epoxomicin (Fig. 11b) was higher. The strongest response and buildup of Nfe2l1 was to bortezomib (Fig. 11c).

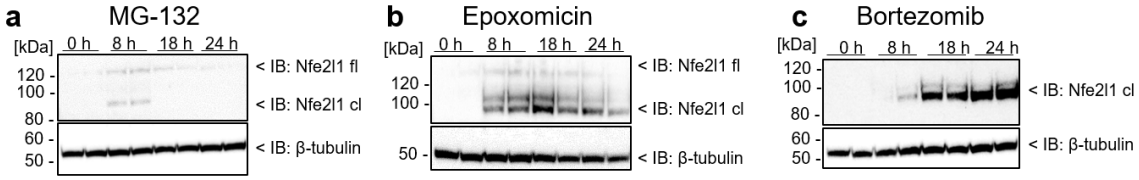

Figure 11: Inhibition of the proteasome leads to an accumulation of cleaved Nfe2l1 in vitro. (a-c) Representative immunoblots of Nfe2l1 full length (Nfe2l1 fl) and cleaved form (Nfe2l1 cl) in C2C12 cells over a 24 h time course treatment with a) MG-132 (500 nM), b) Epoxomicin (100 nM), c) Bortezomib (100 nM).

Knowing the importance of the role of *Nfe2l1* as a regulator of the UPS in different tissues[125,127,128], I here show its crucial role in the skeletal muscle degradation pathway. In the *in vitro* model, using C2C12 myocytes, the knock down (KD) of *Nfe2l1* using small interference RNA (siRNA) showed a consequent decrease of the gene of interest and of downstream targets *Psma1* and *Psmb1* (Fig. 12a). Furthermore, this led to an ablation of Nfe2l1 protein, which upon bortezomib treatment is typically accumulated (Fig. 12b). Looking into proteasomal activity via a fluorometric assay, I could determine a decrease in Chymotrypsin-like activity (Fig. 12c), thus leading to increased ubiquitination of various proteins (Fig. 12d). Interestingly, trypsin-like activity of the proteasome is upregulated upon *Nfe2l1* KD (Fig. 12c).

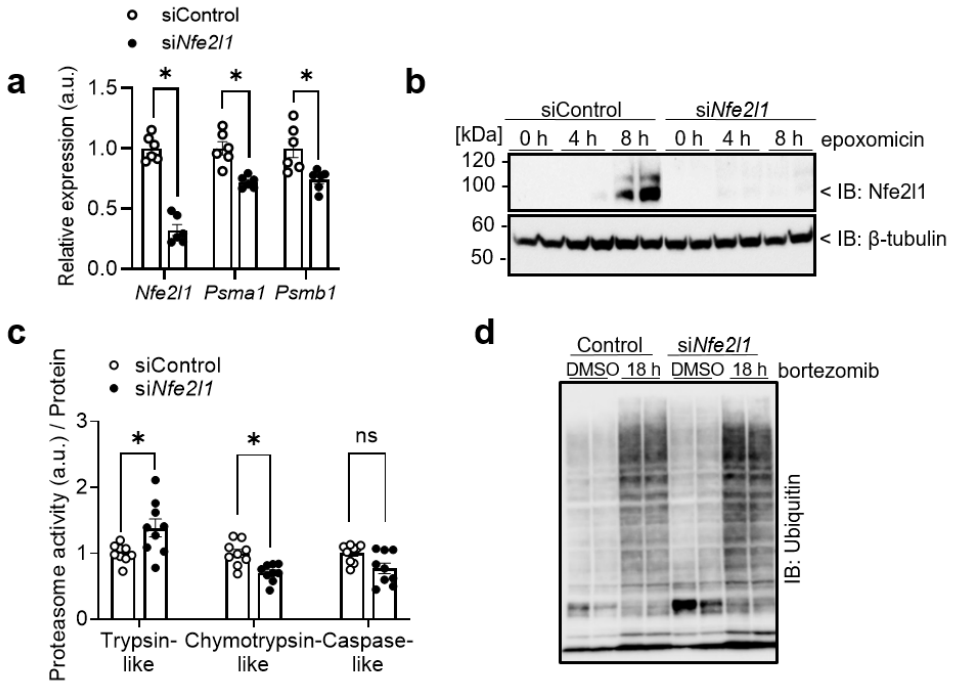

Figure 12: Ubiquitin-proteasome system of C2C12 myocytes depends on *Nfe2l1.* a) mRNA expression levels of *Nfe2l1* and downstream targets *Psma1* and *Psmb1* in *Nfe2l1* KD (si*Nfe2l1*) and control cells (siControl) (two independent experiments with each *n* = 3 technical replicates). b) Protein levels of Nfe2l1 in C2C12 control and *Nfe2l1* KD cells incubated with bortezomib. c) Fluorometric assay of proteasome activity in *Nfe2l1* KD and control cells (three independent experiments with each *n* = 3 technical replicates). d) Immunoblot of proteins with attached ubiquitin after *Nfe2l1* silencing compared to control cells and treatment with proteasome inhibitor bortezomib. The data are mean ±SEM, p<0.05 by two-way analysis of variance (ANOVA) (a, c). Figure adapted from [142].

3.3 Loss of Nfe2l1 *in vivo* leads to reduced UPS activity

In order to study the *in vivo* role of myocyte Nfe2l1 I used a deletion model in which the gene is constitutively knocked out (KO) in the muscle tissue specifically (mKO) via the Cre-Lox-P system. With *Nfe2l1* floxed and the Cre-recombinase under the control of the actin alpha 1 (Acta1) promoter, *Nfe2l1* is solely deleted in tissues expressing skeletal muscle protein Acta1 of Cre-positive (Cre^+) animals. For controls, I used Cre-negative (Cre^-) mice. In line with the in vitro model, I could detect an ablation of *Nfe2l1* gene expression with a significant effect on downstream targets *Psma1* and *Psmb1* (Fig. 13a) in gastrocnemius (GC) tissue of mKO animals compared to wild-type (WT) littermate controls. Subsequently, Nfe2l1 protein was absent in the gastrocnemius tissue of mKO mice (Fig. 13b). Additionally, proteasome activity was decreased in Cre^+ animals, when compared to Cre^-, although interestingly the trypsin-like activity of the proteasome showed an upregulation (Fig. 13c, d). Also, the mKO animals display an upregulation of autophagy (Supplementary Fig. 1a, 2a). The diminished activity of the proteasome resulted in accumulation of ubiquitylated proteins (Fig. 13e), however the hyper ubiquitination pattern of mKO mice was specific for the gastrocnemius, a fast twitch muscle, yet not true for the slow twitch muscle soleus (Fig. 13e).

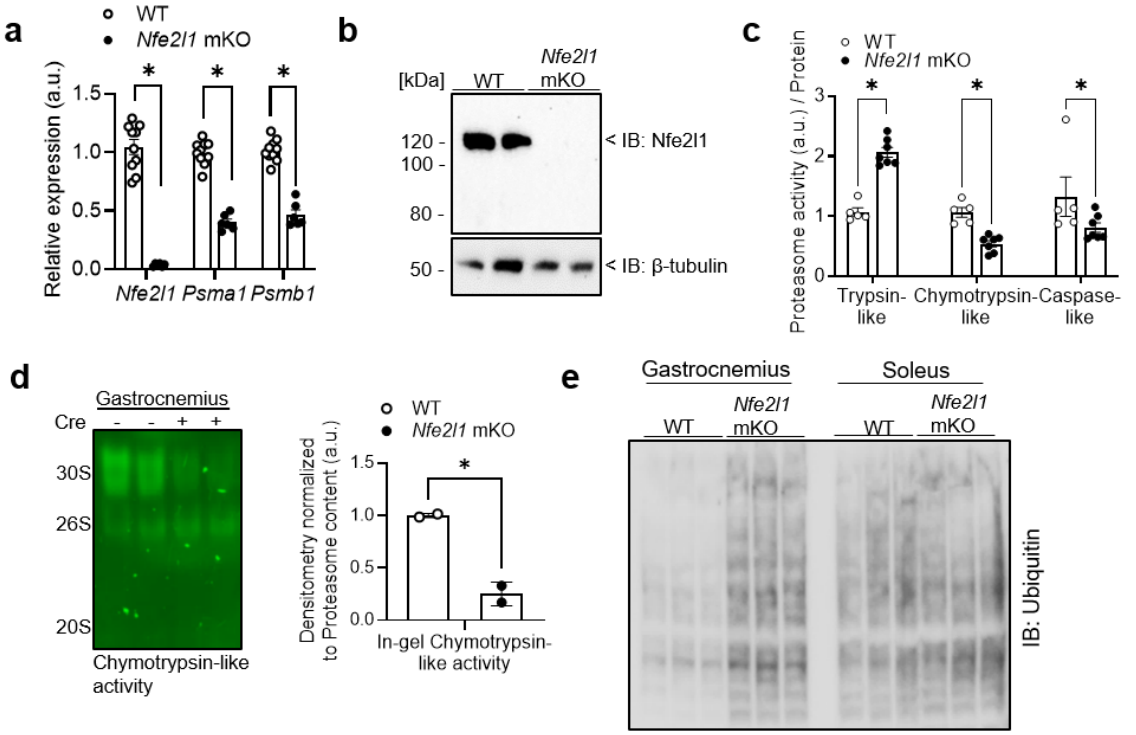

Figure 13: Nfe2l1 is indispensable for the UPS in the gastrocnemius tissue. a) mRNA expression levels of *Nfe2l1* and downstream proteasome subunits *Psma1* and *Psmb1* (*n* = 6-10 mice). b) Western blot of Nfe2l1 in WT and mKO gastrocnemius tissue. c) Cleavage activity of the three proteasome catalytic activity sites assessed via fluorometric assay (*n* = 5-7 mice per group). d) Native-PAGE of in-gel chymotrypsin-like activity of the proteasome and densitometry normalized to total proteasome content. e) Western blot of proteins with attached ubiquitin in gastrocnemius (GC) and soleus tissue from WT controls and *Nfe2l1* mKO mice. The data are mean ±SEM, $p<0.05$ by two-way ANOVA (a, c) or *t*-test (d). Figure adapted from [142].

3.4 Nfe2l1 shapes skeletal muscle ubiquitome

A major denominator of the *Nfe2l1* mKO muscle phenotype is the accumulation of ubiquitylated proteins. In effort to understand which pathways are hampered by the deficient proteasome activity in the mKO mice I performed proteomics and ubiquitomics on the gastrocnemius tissue of these animals and WT controls. The proteome showed 1847 significantly regulated proteins (Fig. 14a) and among the top regulated GO pathways were hits linked to energy metabolism and metabolic processes as well as actin filament organization (Fig. 14b). A KEGG-pathway analysis of the proteasome subunits supported the notion that Nfe2l1 is an imperative part of this catabolic process, as loss of the transcription factor led to a decrease of the majority of proteasomal subunits (Fig. 14c). However, individual, predominantly “Psme” subunits, known to be proteasome activators showed an upregulation (Supplementary Fig. 3a) and could be interesting to further look into.

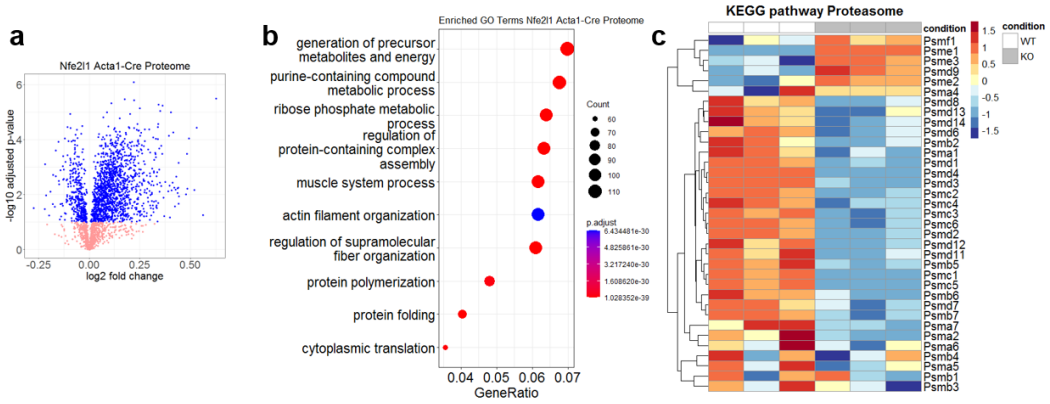

Figure 14: Proteome profile and regulated pathways of *Nfe2l1* mKO and WT animals. a-c) Assessment of the GC proteome of *Nfe2l1* mKO mice and WT littermate controls (*n* = 3 mice per group) using LC-MS/MS. a) Log2 fold changes of identified proteins displayed as volcano plot of hits in proteome (significant hits in blue). b) Gene ontology (GO) analysis of significantly regulated pathways. c) Kyoto Encyclopedia of Genes and Genomes (KEGG)-pathway of regulated proteasome subunits (mmu 3050) of the total proteome. The data are mean ±SEM, p<0.1 by t-test. Figure adapted from[142].

To further study the ubiquitin-proteasome system I wanted to identify ubiquitylated proteins in the gastrocnemius of WT and *Nfe2l1* mKO mice and pinpoint regulated pathways. Therefore, the gastrocnemius was isolated and digested overnight. As a result of the trypsin digestion all post translational modifications (PTM) with ubiquitin were cleaved off and the peptides or ubiquitin itself remained with a diglycine (DiGly) remnant motif, attached to the amino acid lysine (K). Subsequently, the DiGly is pulled down and the peptides analyzed via Mass spectrometry (Fig. 15).

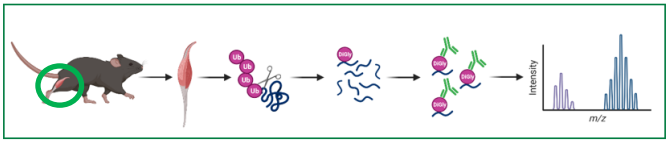

Figure 15: Workflow for ubiquitomics analysis. Gastrocnemius is extracted from the hind limb of the animal and consequently digested via trypsin digest overnight. The remaining DiGly remnant is pulled down and peptides are analyzed via LC-MS/MS.

The PCA analysis showed that the two genotypes cluster well apart from each other (Fig. 16a). Corresponding to previous analyses we detected a substantial increase of ubiquitylated proteins in the *Nfe2l1* mKO gastrocnemius in comparison to WT controls (Fig. 16b). Moreover, GO analysis showed the UPS as one of the top regulated pathways (Fig. 16c), which is in line with earlier assessed *ex vivo* and *in vitro* data. Furthermore, pathways of muscle cell development and morphogenesis as well as response to oxidative stress are present in the top enriched GO terms, which will be further discussed in the following chapters. Lastly, we looked into the polyubiquitylation pattern of the muscle tissue, as different linkages of the 7 lysine residues between ubiquitin molecules themselves, lead to diverse polyubiquitin chains, activating distinct signaling pathways. I therefore checked the abundance of the different lysine residues harboring a DiGly remnant motif of ubiquitin. Notably, the strongest increase in ubiquitylation linkages is on Lysine-(K)-48, which produces polyubiquitin chains, that initiate a signaling cascade for degradation of the tagged protein (Fig. 16d). However, ubiquitin on other Lysine residues such as K27 and K33 were also significantly increased. Not much is known yet about these polyubiquitin patterns, however these indicate a role of Nfe2l1 beyond protein degradation through the UPS.

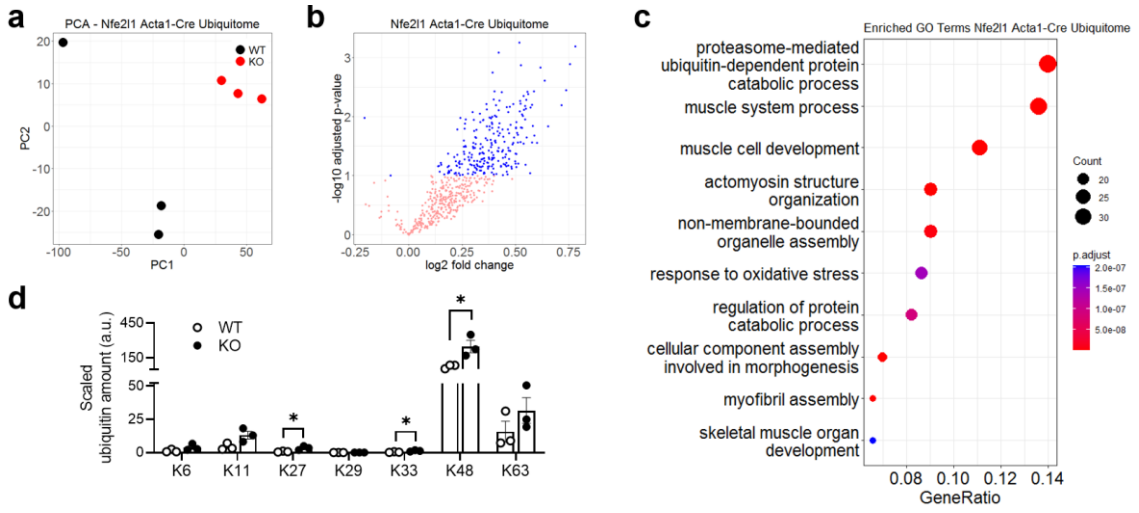

Figure 16: *Nfe2l1* controls the ubiquitin load and profile in gastrocnemius tissue. a-d) Analysis of the ubiquitome of *Nfe2l1* mKO and control mice (*n* = 3 mice per group) in the gastrocnemius tissue. a) Principal component analysis (PCA) of *Nfe2l1* mKO and WT samples in the ubiquitome. b) Volcano plot of the ubiquitome of mKO compared to WT controls. c) Most enriched GO terms in the ubiquitome of the *Nfe2l1* mKO mice. (d) Scaled amount of different lysine (K)-linkages between ubiquitin molecules of WT and mKO mice in gastrocnemius. The data are mean ±SEM, p<0.1 by *t*-test. Figure adapted from[142].

3.5 Gastrocnemius is more affected by the loss of Nfe2l1 than soleus

A distinctive feature to take into account when studying muscle tissue biology are the different fiber types forming diverse and complex muscle tissue. The two main fiber types however, are the slow twitch fiber, with a high abundancy of mitochondria and thereby relying predominantly on oxidative phosphorylation and the fast twitch fiber, largely depending on a glycolytic metabolism for carrying out rapid movement. To get a global understanding the loss of Nfe2l1 has on these different fibers in the *Nfe2l1* mKO model,

muscle tissues samples from the gastrocnemius, representing fast twitch and soleus, defining slow twitch muscle were sent for RNA sequencing. This unbiased approach showed only a small impact on the slow twitch soleus muscle (Fig. 17a, c), however confirmed a stronger phenotypic change in the gastrocnemius muscle upon the loss of Nfe2l1 (Fig. 17b, c). The correlation analysis of the different tissues showed a few hits which are differentially regulated in the two tissues like *Uchl1* (Fig. 17d), which is associated with Parkinson's disease and might be worth further investigations in the future. By clustering the results, the strongest impact of the mKO could be seen on gastrocnemius tissue, where the loss of *Nfe2l1* led to an upregulation of multiple factors (Fig. 17e). Interestingly, the *Nfe2l1* mKO GC cluster was closer to the WT of soleus than to WT of GC itself (Fig. 17e), indicating a phenotypic switch of the fast twitch gastrocnemius tissue in mKO mice, towards a slow twitch fiber. Looking into the gene ontology (GO) pathway of the gastrocnemius the top regulated hit was linked to the UPS (Fig. 17f) verifying the role of Nfe2l1 in this catabolic process in the fast twitch skeletal muscle. Furthermore, pathways linked to muscle cell differentiation and respiration were among the top hits in the GO, indicating a larger impact on the metabolism of these animals.

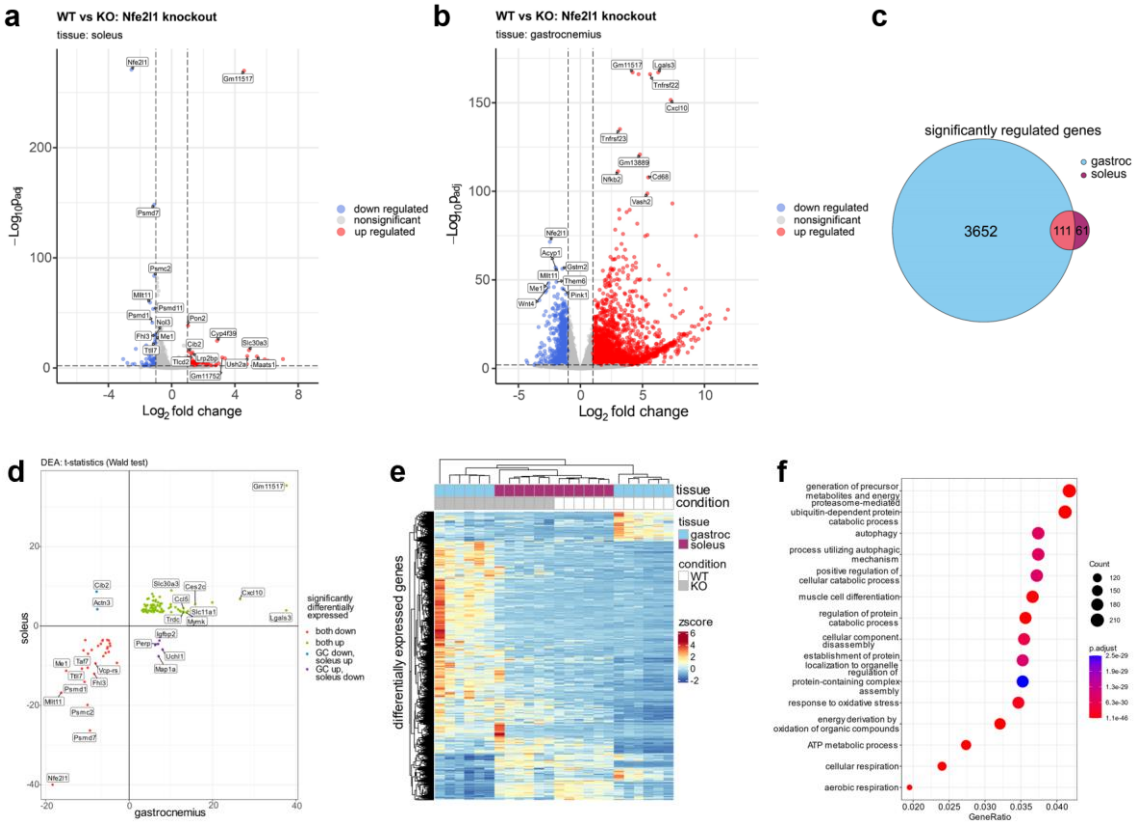

Figure 17: Transcriptome of *Nfe2l1* skeletal muscle knock out shows larger impact on fast twitch muscle fiber type than slow twitch. a) Volcano plot of significantly regulated genes of WT and *Nfe2l1* mKO mice in a) soleus tissue and b) gastrocnemius. c) Venn-Diagram of meaningfully regulated genes in soleus and gastrocnemius (gastroc). d) Differential expression analysis as scatter plot of opposing gene expressions of soleus and gastroc. e) Heat map of significantly impacted genes in gastroc and soleus of mKO mice and WTs. f) Top 15 impacted pathways of GO pathway investigation in gastrocnemius. The data are mean ±SEM, $P < 0.01$ by *t*-test with $n = 6$ per group and tissue. Figures were kindly provided by Nick Diercksen, Phong B.H. Nguyen and Michael P. Menden. Figure adapted from[142].

Overall, these results demonstrated a very interesting effect on the gastrocnemius muscle upon loss of Nfe2l1 and underlined the importance of studying the muscle phenotype and whole body energy metabolism of these mice.

3.6 *Nfe2l1* mKO impacts muscle *in vivo* phenotype

Having gained insight into the transcriptional significance of Nfe2l1, I wanted to investigate the impact *in vivo*. Mice lacking Nfe2l1 in the muscle tissue were smaller (Fig. 18a) and had a significantly lower body weight (Fig. 18b) due to reduced lean mass (Fig. 18c). However, the animals showed no significant difference in fat mass (Fig. 18d).

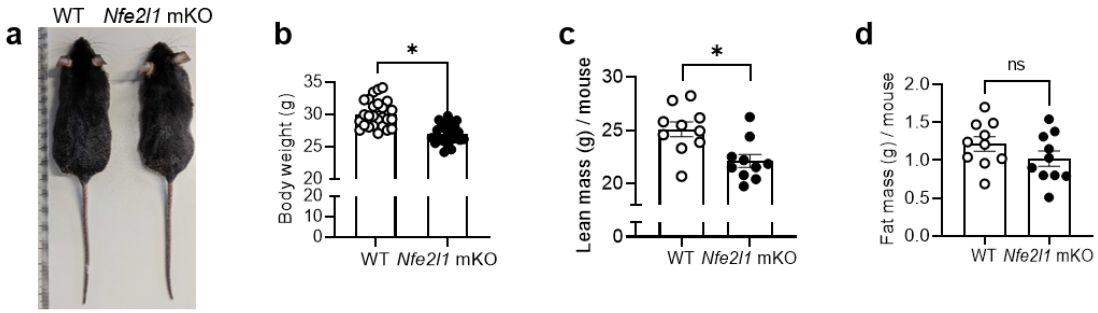

Figure 18: *Nfe2l1* mKO impacts body weight by reduced lean mass of animals. a) Image of WT control and *Nfe2l1* mKO mouse at 3 months of age. b) Body weight of 3 months old WT and *Nfe2l1* mKO mice (n = 26 - 27 per group). c) Lean mass and d) fat mass of WT controls and mKO mice determined by EchoMRI™ (n = 10 mice per group, measured as triplicates). The data are mean ±SEM, p<0.05 by *t*-test (b-d). Figure adapted from[142].

By further investigation of the muscle phenotype I observed a reduced size and a darker red tone of the gastrocnemius of mKO animals in comparison to the WT tissue (Fig. 19a). Moreover, the GC of *Nfe2l1* mKO mice showed a decreased weight compared to WT muscle tissue (Fig. 19b). In addition to reduced muscle size and weight, performance in a forelimb grip strength test was diminished in mice lacking Nfe2l1 in comparison to WT controls (Fig. 19c). However, the soleus showed no difference in tissue weight between wild-type and *Nfe2l1* mKO mice (Fig. 19d). Moreover, these results could indicate an atrophy phenotype, yet markers for muscle wasting were not elevated (Supplementary Fig. 2b).

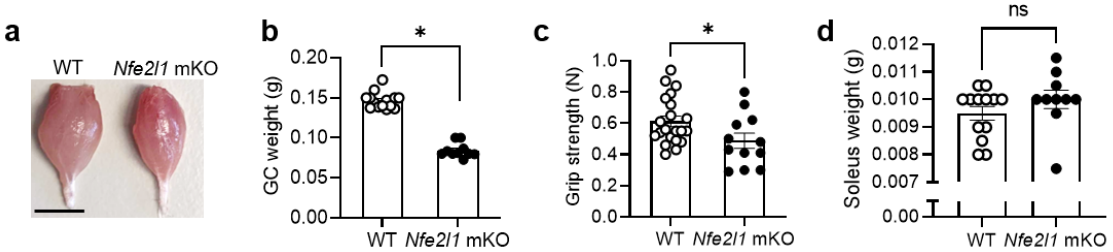

Figure 19: *Nfe2l1* mKO impacts gastrocnemius weight and grip strength performance. a) Representative image of WT and *Nfe2l1* mKO gastrocnemius tissue extracted from the hind limb. Scale bar: 0.5 cm. b) Weights of GC from WTs and mKO mice (n = 10 - 14 mice). c) Grip force of the forelimbs from WT controls and mKO animals (n = 12 - 21 mice). d) Weight of soleus from WT and mKO animals (n = 10 - 13 mice). The data are mean ±SEM, p<0.05 by *t*-test (b-d). Figure adapted from[142].

3.7 The transcription factor Nfe2l1 determines fiber type and mitochondrial respiration

In interest of studying the striking phenotype of the gastrocnemius further, I did a deeper examination of the muscle fibers using the RNAseq data alongside with tissue sections for different histological imaging processes. The relative expression levels of diverse myosin heavy chains (*Myh*) showed a switch in the gastrocnemius of the *Nfe2l1* mKO mice towards a more slow twitch phenotype. *Myh7*, which encodes for the slow twitch fiber type 1 (MHCI) was significantly upregulated (Fig. 20a) along with a down regulation of *Myh4* encoding myosin heavy chain type 2B, a fast twitch fiber (Fig. 20a) in mKO mice. Interestingly, also the expression of markers for perinatal fiber types (*Myh3* and *Myh8*) were significantly increased (Fig. 20a) and suggest a constant remodeling/regeneration of the mKO muscle. The gastrocnemius tissue of the mice lacking Nfe2l1 appears to be more fibrotic and infiltrated by immune cells (Fig. 20b). Also, immunofluorescent staining displays more slow twitch fibers (stained in blue) in the *Nfe2l1* mKO in comparison to WT controls, as well as an increased succinate dehydrogenase (SDH) activity, shown by a stronger staining of the SDH dye (Fig. 20b). The transmission electron microscopy (TEM) of WT and *Nfe2l1* mKO gastrocnemius tissue showed profound differences in mitochondrial morphology, indicated bulging of the mitochondria as well as a decreased fiber bundle size with shorter Z-bands (Fig. 20c).

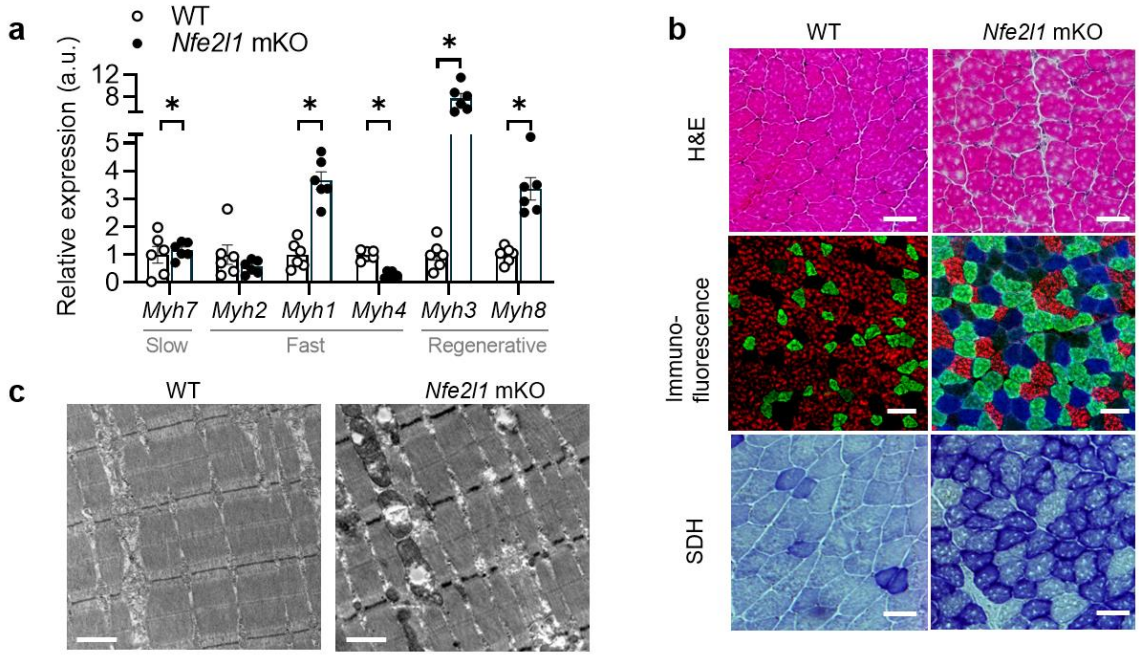

Figure 20: Deletion of Nfe2l1 promotes a fiber type shift in gastrocnemius muscle that impacts the mitochondria phenotype. a) mRNA levels determined by RNAseq and normalized to *Tbp* of different myosin heavy chains in the gastrocnemius from *Nfe2l1* mKO mice and WT controls (n = 6 mice per group). b) Images of hematoxylin & eosin (H&E)-staining, Immunofluorescent staining of fiber types MyHC-2B (red), MyHC-2A (green), MyHC-1 (blue) and succinate dehydrogenase (SDH) staining of complex II as part of the mitochondrial electron transport chain (ETC) in GC tissue sections from WT and *Nfe2l1* mKO mice. All scale bars are 50 µm. c) Images of longitudinal transmission electron microscopy (TEM) sections of GC from WT and *Nfe2l1* mKO mice. Scale bars are 1 µm. The data are mean ±SEM, $p<0.05$ by 2-way ANOVA (a). Figure adapted from[142].

To determine whether the alterations in fiber type and mitochondrial structure translate into functional changes I analyzed the mitochondrial respiratory chain function and complexes. Hereby I could determine a lower amount of complex III in the *Nfe2l1* mKO tissue compared to WTs (Fig. 21a). Furthermore, the oxygen consumption rate (OCR) of isolated muscle fibers was assessed using high-resolution respirometry and normalized to citrate synthase (CS) activity (Fig. 21b). The analysis showed a significantly lower NADH-linked respiration, measured by addition of ADP, of the mKO fibers compared to WT controls. Additionally, oxidative phosphorylation capacity, which is assessed by adding succinate (SUC) as well as maximal respiration, determined by FCCP injection were decreased in fibers lacking Nfe2l1 (Fig. 21b). To verify these results and pin point the OCR to mitochondrial respiration, I performed a seahorse analysis on isolated mitochondria and thereby could confirm a significantly lower maximal respiration upon FCCP addition (Fig. 21c) of the *Nfe2l1* mKO when compared to WT controls.

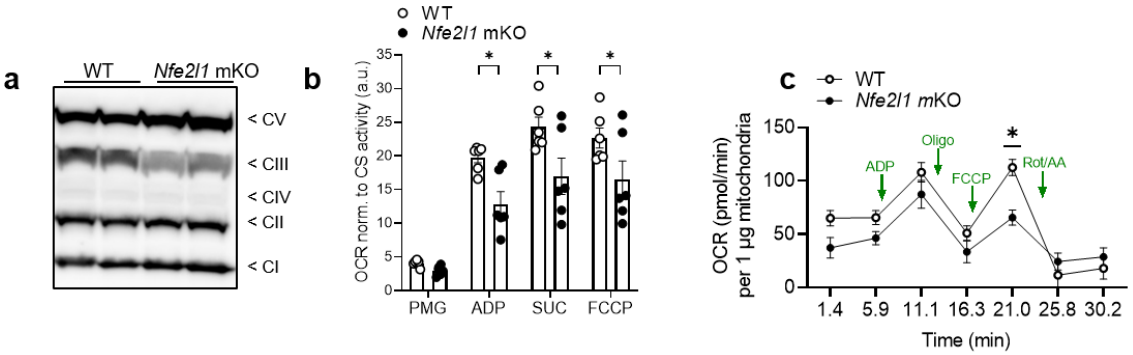

Figure 21: Nfe2l1 is a crucial factor for mitochondrial integrity and respiration. a) Representative western blot of mitochondrial ETC complexes CI-CV in gastrocnemius tissue. b) Oxygen consumption rate (OCR) assed by Oroboros measurement and normalized to citrate synthase (CS) activity of GC muscle fibers from WT and mKO mice after addition of pyruvate, malate, glutamate (PMG), ADP, succinate (SUC) and FCCP (n = 6 mice per group). c) Time course of oxygen consumption of isolated mitochondria from WT control's and *Nfe2l1* mKO mice's GC tissues (n = 4 - 6 mice per group). The data are mean ±SEM, p<0.05 by 2-way ANOVA (b), or t-test (c). Figure adapted from[142].

Altogether, these data demonstrate that loss of *Nfe2l1* in skeletal muscle lead to substantial differences in fiber type, shifting the gastrocnemius towards a slow twitch fiber phenotype. Mitochondrial morphology and function were strongly impacted by the loss of Nfe2l1, showing a decrease in respiratory complex III content and reduced maximal respiration capacity. These data thus underline the crucial role of the transcription factor in muscle tissue morphology and function, showcasing an impact on muscle respiration, which additionally raises the question of the effect on whole body metabolism in animals lacking Nfe2l1.

3.8 Metabolome of *Nfe2l1* mKO mice shifted towards glycolysis

Based on the changes in mitochondrial respiration and fiber type, I then decided to investigate how these alterations impact the metabolic landscape of the muscle. Thus, metabolomics of *Nfe2l1* mKO mice and WT controls was performed. The principal component analysis (PCA) showed a clear clustering of the two genotypes (Fig. 22a).

Generating a heat map of the groups highlights the strongest changes in features regarding the glycolysis and glucose metabolism (Fig. 22b, Supplementary Table 4). Moreover, the greatest increase in metabolite sets in *Nfe2l1* mKO mice is correlated to the methionine metabolism (Fig. 22c). Methionine is an essential amino acid, which can scavenge reactive oxygen species and thereby protect cells from damage or cell death. However, more recent studies on methionine restriction also show beneficial effects thereof[144,145]. Furthermore, the Warburg Effect is among the top 10 hits in the metabolome (Fig. 22c). This pathway is better known from cancer metabolism, where tumor cells in a hypoxic environment bypass the TCA and mitochondrial respiration and primarily generate ATP from glycolysis and lactate production.

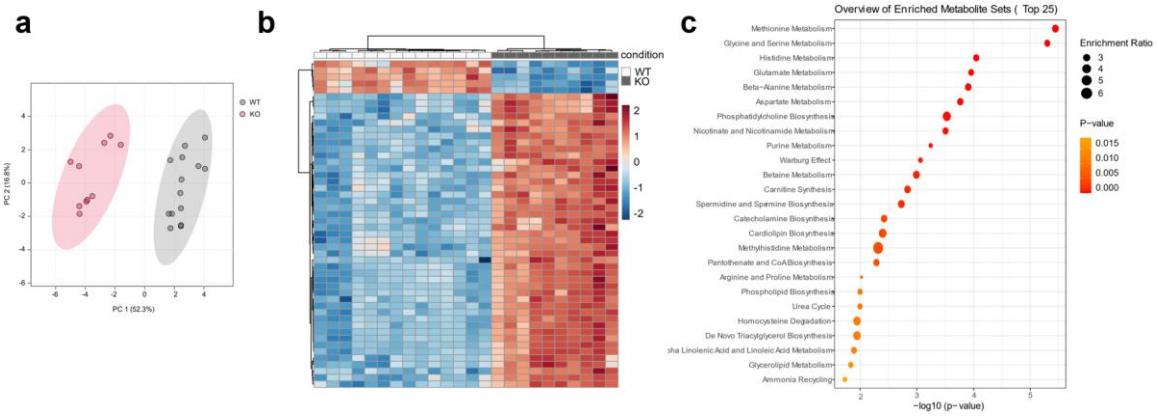

Figure 22: Metabolomics show a shift in fuel usage of gastrocnemius from *Nfe2l1* mKO mice. a) Principal component analysis (PCA) of metabolome from *Nfe2l1* mKO mice and WTs. b) Heatmap of top regulated metabolites in mKO and control mice. c) GO analysis of enriched metabolite sets of the top regulated pathways in WTs and mKO animals. ((a-c) *n* = 10 - 14 mice per group). The data are mean ±SEM, p<0.05 by 2-way ANOVA. Figure adapted from[142].

This unprejudiced approach assessing the muscle metabolome further indicates a strong alteration of the metabolism upon loss of Nfe2l1, emphasizing glycolysis and essential amino acids imperative for antioxidant reactions.

3.9 Lack of myocyte Nfe2l1 increases whole body energy expenditure

A crucial question is how these underlying factors modify the metabolic phenotype of the *Nfe2l1* mKO mice. Thus, I measured various metabolic parameters via indirect calorimetry. Initially, I assessed the respiratory exchange ratio (RER) (Fig. 23a), a factor which provides insight on fuel usage of the animals as well as oxygen consumption (Fig. 23b, c) of the mKO mice and WT controls. No differences in baseline measurements of both metabolic parameters could be detected between the two groups. Considering the bodyweight discrepancy (Fig. 18b) however the *Nfe2l1* mKO animals displayed an increased energy expenditure per gram body weight when compared to WT controls (Fig. 23d) despite a higher food intake of the mKO mice (Fig. 23e) and no difference in activity in the cage (Fig. 23f).

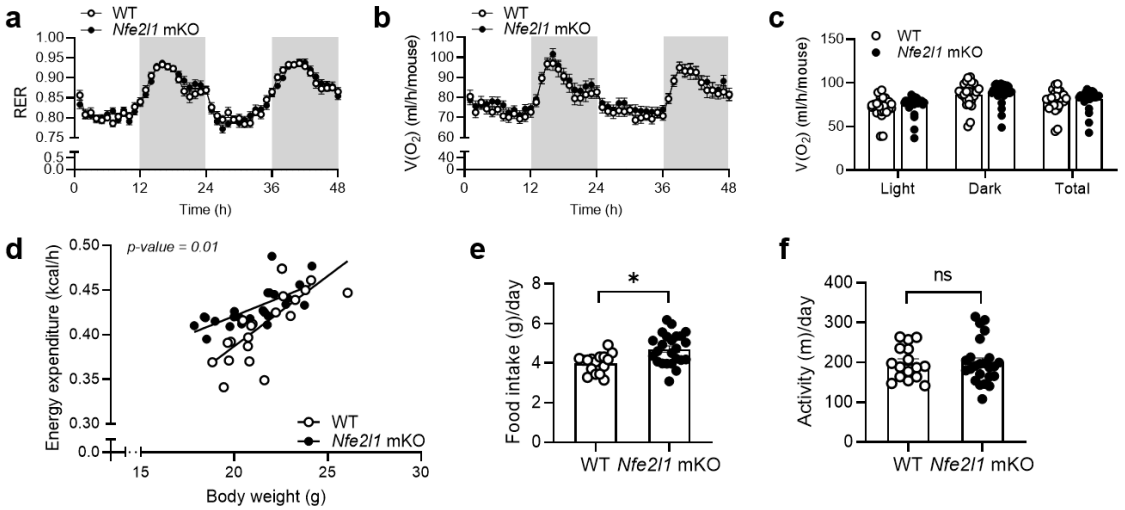

Figure 23: Loss of myocyte *Nfe2l1* impacts energy metabolism. (a-f) Indirect calorimetry of WT controls and *Nfe2l1* mKO mice on chow diet, age: 6 weeks. a) Time course of respiratory exchange ratio (RER). b) Time course and c) Phase-specific and total oxygen consumption ((a-c): *n* = 26 - 28 mice per group). d) GLM-plot of energy expenditure per mouse over body weight (*n* = 22 - 24 mice). e) Food uptake. f) Physical activity ((e-f): *n* = 16 - 24 mice per group). The data are mean ±SEM, p<0.05 by linear modeling (d) or *t*-test (c, e-f). Figure adapted from[142].

These findings point towards an altered energy metabolism upon loss of *Nfe2l1* in skeletal muscle and need additional studies to characterize and highlight differences between WT controls and mKO mice and further determine the underlying causes of these alterations.

3.10 *Nfe2l1* mKO mice show resistance to HFD weight gain

To further elucidate the metabolic differences of the *Nfe2l1* mKO mice compared to WT littermates I performed a high-fat diet (HFD) study. HFD diet experiments in C57BL/6JRj showed a decisive impact of 16 weeks HFD on the UPS. The diet-induced obese (DIO) mice showed an increase in proteasome activity (Fig. 24a, b) in addition to increased proteasome content (Fig. 24c). Interestingly, the expression of *Nfe2l1* was also upregulated after 16 weeks HFD feeding in comparison to chow fed controls (Fig. 24d).

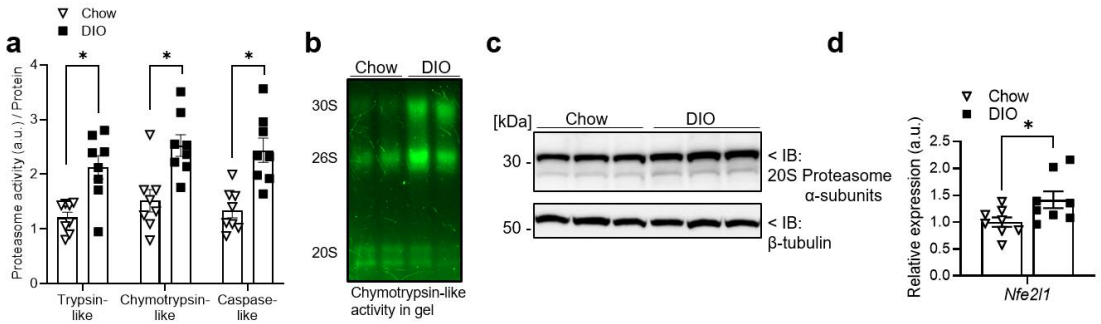

Figure 24: Ubiquitin-proteasome system is upregulated through HFD. (a-d) Analysis of Nfe2l1, proteasome activity and content in GC of chow and diet-induced obesity (DIO) mice after 16 weeks high-fat diet (HFD) feeding: a) Proteasome activity assessed by fluorometric measurement (*n* = 8 mice per group). b) Native-Page of DIO and WT mice. c) Immunoblot of 20S Proteasome subunits. d) Relative expression levels of *Nfe2l1*. The data are mean ±SEM, p<0.05 by 2-way ANOVA (a) or *t*-test (d). Figure adapted from[142].

I therefore decided to investigate the *Nfe2l1* mKO phenotype upon 16 weeks of HFD feeding. Monitoring the body weight development over the course of the diet (Fig. 25a, b) showed substantial differences between the mKO animals and WT controls. Mice lacking *Nfe2l1* were resistant to weight gain on HFD with no significant weight gain over the course of the diet when compared to chow fed mKO animals (Fig. 25a, b). Moreover, comparing energy expenditure in relation to body weight after 8 weeks of diet (Fig. 25c) showed an amplified difference in energy expenditure between genotypes compared to chow controls (Fig. 24d).

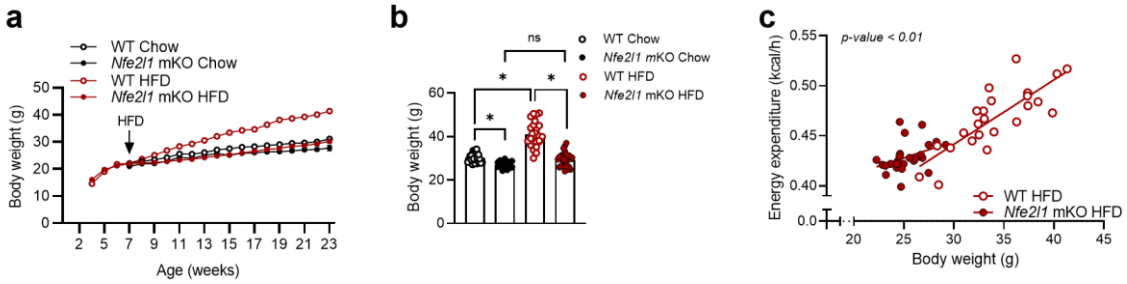

Figure 25: Absence of Nfe2l1 protects animals from HFD weight gain. a) Body weight before and over the course of 16-week diet and b) end-point body weight after diet of WTs and *Nfe2l1* mKO animals. c) GLM-Plot of energy expenditure over body weight per mouse at 8 weeks of HFD. ((a-c): *n* = 24 - 27 mice per group). The data are mean ±SEM, p<0.05 by 2-way ANOVA (b) or linear modeling (c). Figure adapted from[142].

Additional central parameters of metabolic fitness are the ability to maintain glucose and insulin homeostasis. Assessing these via glucose and insulin tolerance tests (GTT and ITT) are pillars of metabolism research. The high fat diet decreased the capability of the animals for glucose clearance in both WT and mKO mice, however the *Nfe2l1* mKO group still performed significantly better than the WT controls on HFD (Fig. 26a). The ITT correspondingly displayed an increased insulin resistance upon HFD, although the mKO mice were significantly more sensitive to insulin injections when compared to WT controls on HFD (Fig. 26b). Furthermore, animals lacking myocyte Nfe2l1 show higher expression levels of Gdf15 and Fgf21 as well as elevated levels of circulating GDF15, both factors which recently have been associated with an increased energy metabolism, a metabolic shift and resistance to obesity[50,53,54] (Supplementary Fig. 4a-d).

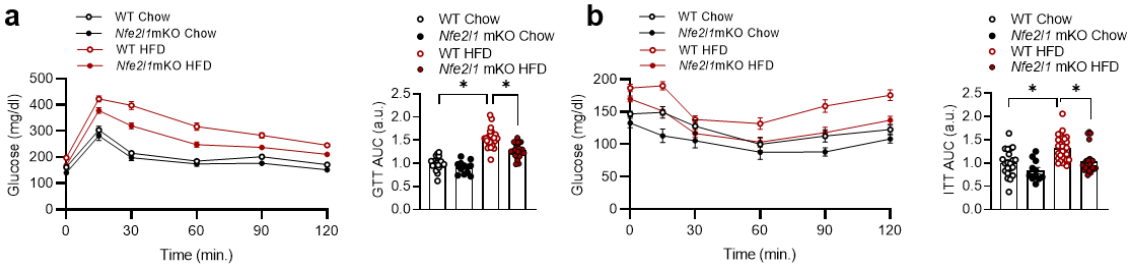

Figure 26: Glucose and Insulin tolerance of *Nfe2l1* mKO mice is improved compared to WT controls when fed with HFD. a) Traces and area under curve (AUC) quantification of intraperitoneal glucose tolerance test (*i.p.* GTT). b) Traces and AUC of intraperitoneal insulin tolerance test (*i.p.* ITT). ((a, b): *n* = 11 - 27 mice per group). The data are mean ±SEM, p<0.05 by 2-way ANOVA of AUC. Figure adapted from[142].

Assessing blood parameters, I detected no difference between WT controls and *Nfe2l1* mKO mice on chow diet. However, after feeding a HFD for 16 weeks the insulin levels significantly increased in the WT controls yet the diet had no effect on insulin levels of *Nfe2l1* mKO mice (Fig. 27a). Adiponectin levels overall decreased on HFD and were lower in *Nfe2l1* mKO mice compared to WT littermates (Fig. 27b). Plasma leptin significantly increased on HFD in both genotypes, but was significantly lower in mKO animals fed with HFD compared to WT controls on HFD (Fig. 27c). Also, plasma cholesterol was increased in mice fed a HFD, however, was significantly lower in mice lacking *Nfe2l1* compared to WTs (Fig. 27d). Finally, circulating triglyceride levels were higher in HFD *Nfe2l1* mKO mice in comparison to controls on the same diet (Fig. 27e).

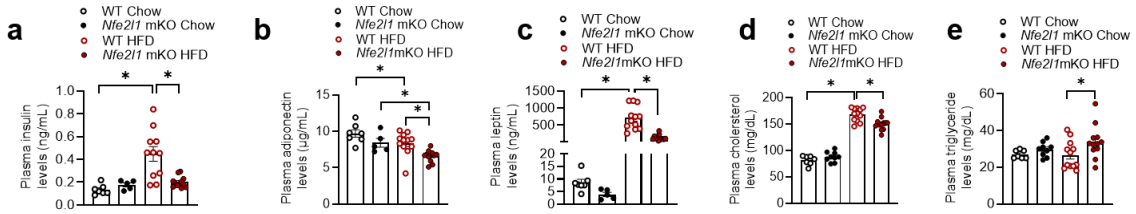

Figure 27: Muscle KO of *Nfe2l1* shows improved plasma parameters on HFD. a-e) Important plasma parameter measurements of WT and *Nfe2l1* mKO animals fed with chow or HFD over the course of 16 weeks. a) Insulin levels, b) Adiponectin levels, c) Leptin levels, determined with respective ELISA kits and d) Cholesterol levels as well as e) Triglycerides levels measured by a Beckman Coulter AU480 Chemistry Analyzer. ((a-e): *n* = 5 - 12 mice per group). The data are mean ±SEM, $p<0.05$ by 2-way ANOVA (a-e). Figure adapted from[142].

3.11 Tamoxifen inducible myocyte Nfe2l1 KO (iKO) effects *in vivo*

The insight, that the constitutive *Nfe2l1* mKO has beneficial effects on metabolic health raises the question if this positive impact can be induced by knockout of the transcription factor in adult animals as well. To investigate this hypothesis an in vivo inducible knockout (iKO) of myocyte Nfe2l1 was created by a tamoxifen (TAM) inducible Cre-recombinase. Nfe2l1 was deleted from Cre-positive animals (iKO) by injection of TAM, Cre-negative animals served as controls (WT). The knockout of *Nfe2l1* after TAM administration could be verified on transcriptional level along with a significant decrease of downstream targets *Psma1* and *Psmb1* (Fig. 28a) in the iKO mice compared to WT controls. The phenotypic effect *in vivo* however were rather mild, as the loss of Nfe2l1 neither impacted the bodyweight (Fig. 28b, c) nor the gastrocnemius weight (Fig. 28d). However, the Nfe2l1 iKO animals showed a reduction in grip strength (Fig. 28e). Lastly, I investigated the energy expenditure as this is the central factor of health benefits seen in the constitutive mKO. However, the energy expenditure remained unchanged after loss of Nfe2l1 6 weeks as well as 10 weeks after TAM injection (Fig. 28f)

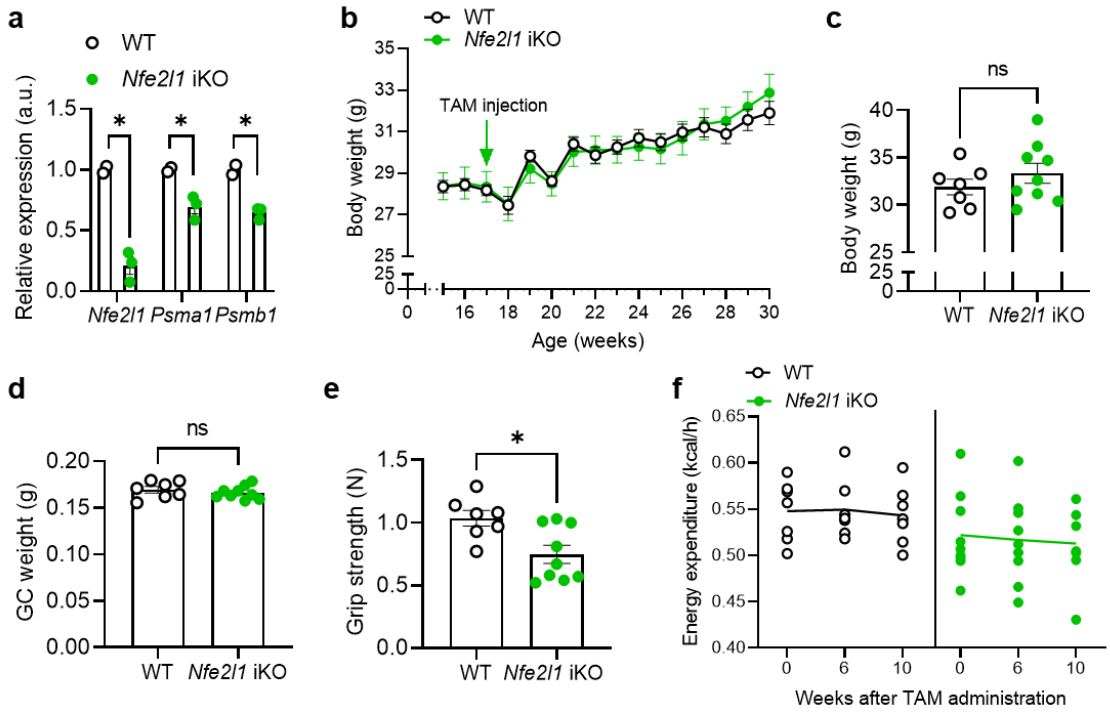

Figure 28: Inducible skeletal muscle Nfe2l1 mKO (iKO) has mild effects on the gastrocnemius and whole body energy metabolism. a) mRNA levels of *Nfe2l1* and downstream targets *Psma1* and *Psmb1* (*n* = 2 - 3 mice per group). b) Body weight before and after *i.p.* tamoxifen (TAM) injection and c) end-point body weight 10 weeks after TAM administration of Nfe2l1 iKO and WT controls. d) Gastrocnemius weight and e) grip strength of the iKO and control animals 10 weeks after TAM. f) GLM-plot of energy expenditure measured by indirect calorimetry before as well as 6 and 10 weeks after TAM injection. ((b-f) *n* = 7 - 9 mice per group). The data are mean ±SEM, p<0.05 by *t*-test (a-f).

3.12 Exercise performance of *Nfe2l1* mKO mice is diminished

Another environmental influence, contrasting a high fat diet, is exercise. The benefits of regular exercise on overall fitness levels, muscle strength as well as health improvements like a reduced risk of cardiovascular diseases and type 2 diabetes are extensively studied. On the other hand, less is known about the remodeling of the muscle tissue after exercise facilitated by an upregulation of the UPS[146]. Considering the major role of Nfe2l1 in regulating the UPS and the strong impact that loss of Nfe2l1 has on the muscle tissue, I was interested in the exercise performance of these animals. An exhaustion test on the treadmill, where after an adaptation phase the speed increases every 2-3 minutes, was used to assess metabolic fitness and fuel usage of the animals. In sport physiology the crossover point, determined by the time point that the animal start relying on carbohydrates (CHO) as main fuel source in contrast to burning lipids, is a major determinant of metabolic fitness. This is assessed by the ratio of produced carbon dioxide and consumption of oxygen. Running on fat requires more oxygen, so during the mild exercise animals mostly run on aerobic metabolism. An increase of intensity and exhaustion push the mice to switch to a more anaerobic metabolism and thereby start utilizing more carbohydrates and glycogen from muscle storage. The further this point is down the line of an exercise session the metabolically fitter the animals are assumed to be. Measuring the fitness and calculating the crossover point of the WT controls showed a switch of fuel utilization at about 22 minutes (Fig. 29a). The animals lacking Nfe2l1 in the muscle tissue however had a shifted cross-over point at 12 minutes into the exercise (Fig. 29b), when undergoing the same test, so 10 minutes earlier than the WT controls. Furthermore, the mKO mice exhausted earlier, at an average of 38 minutes, and the majority could not finish the entire exercise protocol (Fig. 29b).

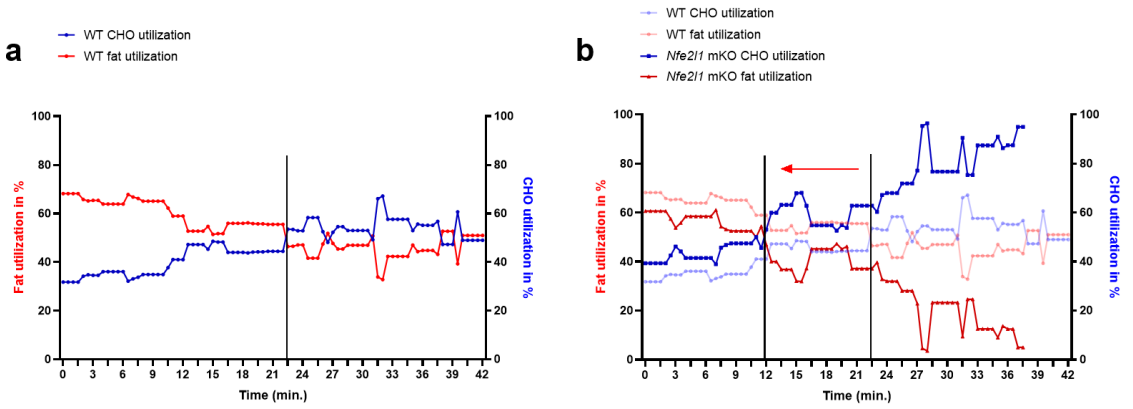

Figure 29: Exercise performance significantly decreased in *Nfe2l1* mKO mice. a) Carbohydrate (CHO) and fat utilization (%) of WT animals in exhaustion test with cross-over point. b) Carbohydrate (CHO) and fat utilization (%) of WT and *Nfe2l1* mKO animals in exhaustion test and shifted cross-over point displayed. (a-b: *n* = 9 - 12 mice per group).

This experiment shows, that the *Nfe2l1* mKO animals, despite being leaner and having a shifted muscle fiber type, fail to perform as well as the WT controls. Conversely, the more slow twitch phenotype of the gastrocnemius in the mKO mice could not translate into enhanced performance.

3.13 Influence of insulin signaling on Nfe2l1

The human body is constantly exposed to different environmental influences and stimuli. To maintain metabolic homoeostasis throughout external influences both anabolic and catabolic pathways have to work together to preserve energy balance. *In vivo* I studied the anabolic signaling pathway by injecting *Nfe2l1* mKO animals and WT controls with 2.0 U/kg insulin or saline as control and subsequently harvested gastrocnemius tissue. The data shows an increase on protein level of *Nfe2l1* following insulin injection (Fig. 30a). Also, interestingly the load of ubiquitylated of proteins is lower in mKO animals injected with insulin, than *Nfe2l1* mKO saline injected mice (Fig. 30b).

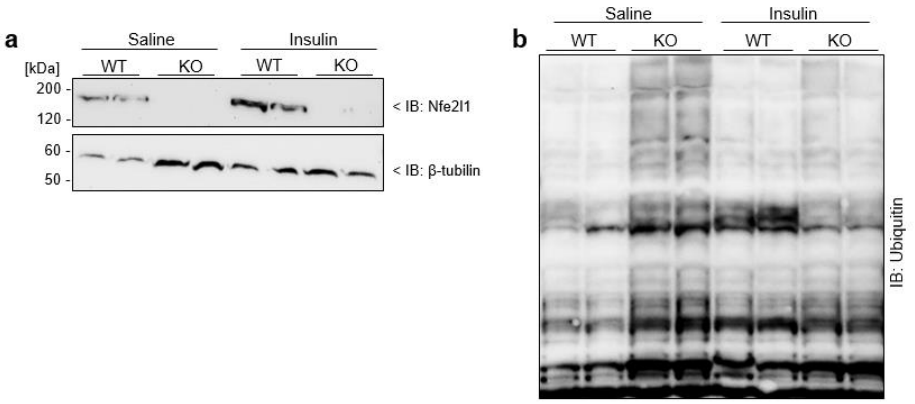

Figure 30: Insulin signaling shows upregulation of *Nfe2l1* levels in vivo. a) Immunoblot of Nfe2l1 and beta-tubulin and b) Ubiquitylated proteins from GC tissue of *Nfe2l1* mKO animals an WT controls after *i.p.* insulin injection, (*n* = 2 mice per group).

This experiment appears very promising in identifying insulin signaling as an upstream regulator of *Nfe2l1* and should definitely be repeated with a higher number of animals.

3.14 Mechanistic target of rapamycin (mTOR) regulation by Nfe2l1

To find a mechanism or an upstream regulatory pathway that controls *Nfe2l1* I did various treatments using C2C12 murine myoblasts as an in vitro model system. In accordance to previously published work, Nfe2l1 was stated to be regulated by the mechanistic target of rapamycin (mTOR) complex 1 (mTORC1)[129,130], a key player in cell growth and survival signaling pathways. To mimic cell starvation and thereby a catabolic state in which mTORC1 is inhibited, I deprived the cells of amino acids over a time course of 48 h. Additionally, the cells were treated with epoxomicin serving as positive control. On transcriptional level (Fig. 31a) no effect of the amino acid starvation could be detected. Solely epoxomicin treatment led to an upregulation of *Psma1*, a downstream target of *Nfe2l1*. The downregulated expression levels of *Ldlr* validate the starvation protocol. Correspondingly, protein levels of Nfe2l1 only changed in the presence of epoxomicin (Fig. 31b), equivalently the ubiquitination was only influenced by proteasome inhibition and not by amino acid availability (Fig. 31c).

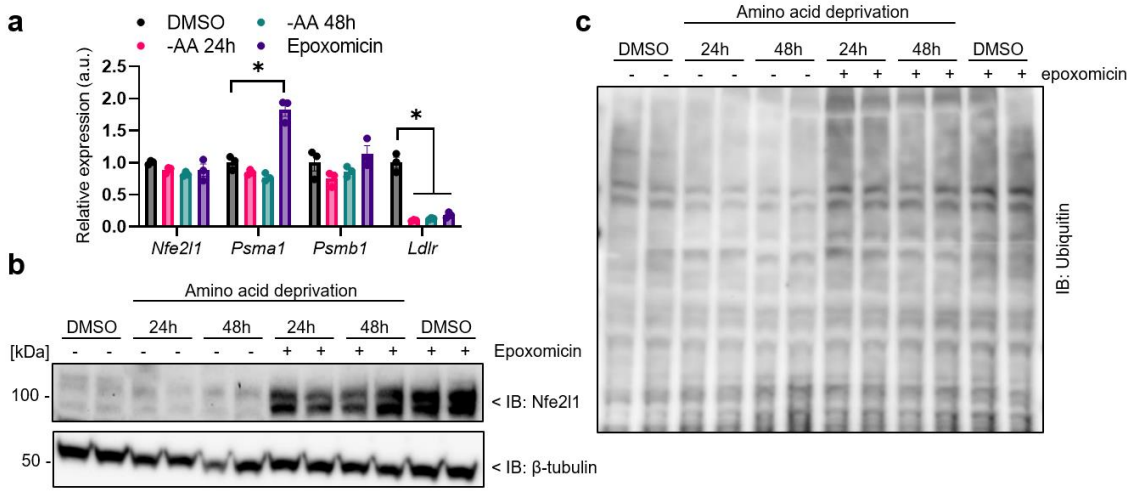

Figure 31: Amino acid deprivation shows now effect on Nfe2l1. a) mRNA levels of *Nfe2l1* and proteasomal subunit genes *Psma1, Psmb1* and *Ldlr* in C2C12 myotubes upon amino acid (AA) starvation and epoxomicin treatment. b) Western blot of Nfe2l1 and beta-tubulin in C2C12 cells after treatment with epoxomicin and amino acid deprivation. c) Western blot of ubiquitylated proteins of C2C12 cells after treatment with epoxomicin and amino acid starvation. (a) Data are mean ±SEM, p<0.05 by 2-way ANOVA.

Next, I used a more unambiguous approach to inhibit mTORC1 by treating C2C12 cells with rapamycin, a well-established mTOR inhibitor. It showed a decrease in expression level of one *Nfe2l1* downstream target *Psma1* (Fig. 32a), however no convincing change was detected on protein level (Fig. 32b). Yet, rapamycin successfully inhibited phosphorylation patterns of mTOR downstream targets (Fig. 32b), which confirms a successful treatment with the inhibitor. Lastly, ubiquitination patterns also did not change upon rapamycin treatment (Fig. 32c).

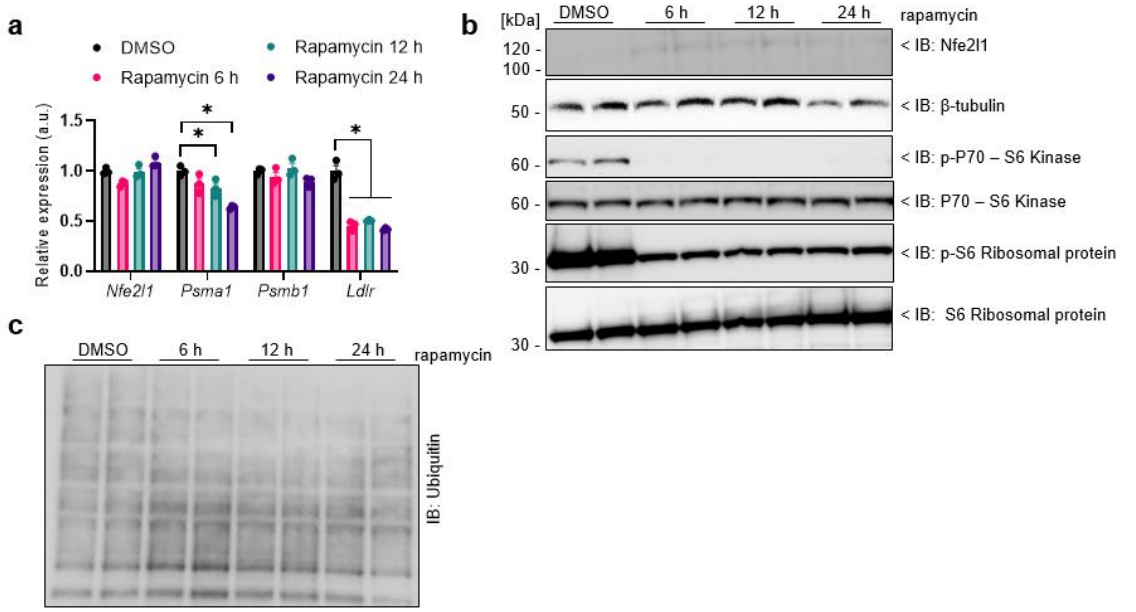

Figure 32: Treatment of C2C12 myotubes with rapamycin had no significant impact on Nfe2l1. a) Relative expression levels of *Nfe2l1, Ldlr* and proteasomal subunit genes *Psma1, Psmb1* in C2C12 myotubes after rapamycin (20 nM) treatment. b) Immunoblot of Nfe2l1, beta-tubulin, (p)-P70-S6 Kinase, (p)-S6 ribosomal protein in C2C12 cells treated with rapamycin. c) Immunoblot of ubiquitylated proteins in C2C12 cells treated with rapamycin (20 nM). (a) Data are mean ±SEM, p<0.05 by 2-way ANOVA.

Finally, I investigated a hypoxia treatment with the aim of mimicking anaerobe conditions during exercise. By incubating the C2C12 cells with $CoCl_2$, a hypoxia mimetic, Nfe2l1 protein levels increased (Fig. 33a). As a control for the treatment itself I determined levels of Hif1α, a transcription factor stabilized in a hypoxic state, which showed a successful treatment (Fig. 33a). Although transcription levels of *Nfe2l1* itself were not influenced by hypoxia, downstream targets of the transcription factor *Psma1* and *Psmb1* showed elevated expression levels (Fig. 33b), which were abrogated by *Nfe2l1* knock down. Interestingly, ubiquitin levels were also increased through this treatment (Fig. 33c).

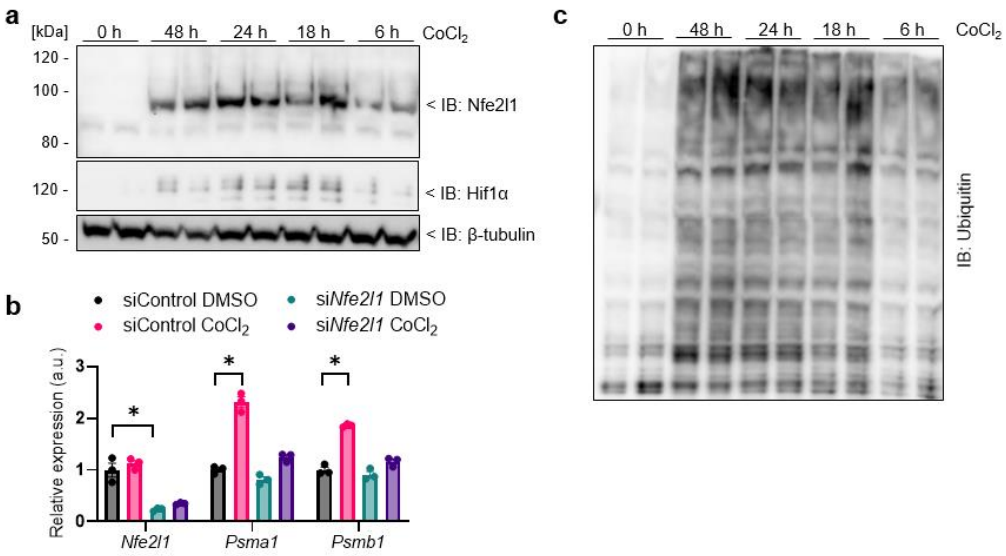

Figure 33: Mimicking hypoxia induces Nfe2l1 accumulation in C2C12 myocytes. a) Immunoblot of Nfe2l1, beta-tubulin and Hif1α in C2C12 cells treated with 200 µM $CoCl_2$. b) Relative expression levels of *Nfe2l1* and proteasomal subunit genes *Psma1, Psmb1* after $CoCl_2$ treatment in C2C12 control (siControl) and *Nfe2l1* KD (si*Nfe2l1*) cells. c) Immunoblot of ubiquitylated proteins in C2C12 cells treated with $CoCl_2$ (200 µM). (b) Data are mean ±SEM, $p<0.05$ by 2-way ANOVA.

In conclusion, these data are indicating that catabolic signaling decreases *Nfe2l1* levels in vitro, whereas anabolic stimuli show an activation of the *Nfe2l1* pathway. Moreover, it is important to point out that experiments should be repeated to evaluate the results and further experiments towards anabolic mTORC1 pathways and insulin signaling are worth additional analyses. As well as the role of Nfe2l1 in hypoxic conditions and determining the cell fate upon loss of the transcription factor to define whether there is a protective role of Nfe2l1 in hypoxia.

4. Discussion

4.1 Protein and ubiquitin landscape is determined by Nfe2l1

Metabolic adaptation requires constant remodeling of the protein landscape, especially in tissues which experience a high metabolic demand, such as skeletal muscle, maintaining protein homeostasis and energy balance is essential for its function[61]. Thus synthesis as degradation of proteins has to occur in a high rate yet still be closely monitored. In my studies I could show that Nfe2l1 is a critical regulator of proteostasis in muscle cells and tissue, by controlling protein recycling through the ubiquitin-proteasome pathway. The transcription factor is imperative for protein turn-over and through the resourceful feedback mechanism demonstrates an adaptive regulation of the UPS in skeletal muscle upon environmental burdens. The ablation of Nfe2l1 in the muscle led to a build-up of ubiquitylated proteins and thereby formed the, for this model characteristic, hyperubiquitylation pattern (Fig. 13e, 16b). Determining the lysine-(K)-linkages of the polyubiquitylation chains and the proteins targeted thereby was presumed to give a deeper understanding of the degradation signaling pathways in the *Nfe2l1* mKO model. As the main degradation pathway in muscle is the UPS[36] K48 is already the predominant polyubiquitylation in control animals. Unsurprisingly, obstructing this pathway in the *Nfe2l1* mKO model showed the highest increase in K48-linkages (Fig. 16d), emphasizing the importance of Nfe2l1 in proper proteasome function and manifesting its imperative role in the UPS pathway. Additionally, other polyubiquitin linkages, like K27 and K33, which are less studied were significantly upregulated in the *Nfe2l1* mKO (Fig. 16d), which indicates a role of the transcription factor beyond proteasomal degradation. For instance, K27 linkage has been demonstrated to be a marker for mitochondrial damage[147] and peptides marked with K33 polyubiquitin have been shown to be shuttled to a component of the autophagy machinery via p62 adapter protein[148]. These associations of the polyubiquitin chains K27 and K33 are in line with other findings in the Nfe2l1 deletion model, as an altered mitochondrial morphology (Fig. 20c, 21a) and function (Fig. 21b, c) can be identified as well as an upregulation of the autophagy and mitophagy pathway (Supplementary Fig. 1a, b, 2a). To make compelling conclusions however, that the polyubiquitin chains formed by K27 and K33 linkages are the underlying causes for the alterations seen upon loss of Nfe2l1, these pathways need to be further investigated, for example by imaging and tracing the different polyubiquitin chains or additionally inhibiting the autophagy system.

Another interesting observation emerged when looking into the KEGG-pathway of the proteasome. Upon the loss of Nfe2l1 I could determine the proteasomal subunits themselves being hyperubiquitylated (Supplementary Fig. 5). This demonstrates that the proteasome is under control of the UPS pathway and is subject to constant degradation and remodeling[149], thus highlighting the metabolic flexibility and adaptive nature of the muscle tissue and the continuous pressure it experiences to meet the proteostatic needs.

Still a question that is difficult to answer is whether Nfe2l1 is solely required to degrade damaged protein or if the role goes beyond the disposal of damaged good towards a

nutrient sensing and amino acid recycling obligation. Here fore, upstream signals and regulators of Nfe2l1 need to be defined, determining the activation of the transcription factor.

4.2 Compensatory mechanisms for lack of proteasome function

The loss of myocyte Nfe2l1 results in a strong phenotype, which shows deficiencies in protein turnover through the UPS and displays a hyperubiquitylation pattern in the muscle. However, the animals are viable and at first sight seem to have no disadvantages compared to WT controls. Thus further investigation of potential compensatory mechanisms and pathways that in myocytes and muscle tissue were indispensable to increase the understanding of this complex phenotype. Strikingly, when determining the different cleavage activities of the proteasome, the chymotrypsin-like protease function, is significantly decreased in the mKO model, however skeletal muscle as well as myocytes showed a very robust and specific upregulation of the trypsin-like proteasome cleavage activity (Fig 12c, 13c). This indicates that the impact of Nfe2l1 is very specific to the chymotrypsin-like function and does not affect the trypsin-like protease activity in skeletal muscle. Underlying reasons for this could be, that the subunits composing the trypsin-like activity are not direct target of Nfe2l1 and therefore not susceptible to the loss of the transcription factor. A promising confirmation for this hypothesis is the transcriptional upregulation of Psmb10 upon loss of Nfe2l1 (Supplementary Fig. 3a). This proteasomal subunit specifically has been shown to code for the trypsin-like activity of the proteasome[109]. Equivalently, Psme2 one of the two known proteasome activators PA28 alpha (Psme1) and beta (Psme2)[125,150] that can increase proteasome activity, are found to be transcriptionally upregulated in the Nfe2l1 muscle deletion model (Supplementary Fig. 3a). Nonetheless, to make reliable statements about Psmb10 and Psme2 regulating proteasome activity, a double knockdown study targeting both Nfe2l1 and Psmb10 or Psme2 would have to be carried out to give valuable insights into the link of the trypsin-like protease activity. Also, an immune blot should be performed to give further insight into upregulation of functional protein of these subunits.

Another plausible pathway that could compensate for the loss of protein degradation by the proteasome is the autophagy pathway. Autophagy is a highly conserved mechanism to dispose of unwanted cellular material and thereby also maintains homeostasis[87]. The UPS and autophagy are the two major degradation pathways in the cell, which hence are closely linked and engage in constant cross-talk. Moreover, there are some nodes in both signaling pathway that are shared and thereby inevitably create junctions between these degradation routes. For instance, autophagic proteins like p62 can also recognize and bind ubiquitin by its ubiquitin binding domain[93]. Generally, the adapter protein p62 is activated upon cellular stress and coordinates the degradation of misfolded proteins by either autophagy or the proteasome[97]. The *Nfe2l1* mKO model shows an upregulation of the autophagy pathway as well as higher levels of p62 (Supplementary Fig. 2a), which could potentially mediate the shuttling of ubiquitin tagged proteins to the autophagophore

and thereby contribute to an increased autophagy. This compensation mechanism for the lack of proteasome function has previously been shown in a Psmd4 deletion model[108]. Moreover, newer studies have shown that proteasomal subunits, like Psma7 and Psmb5 play a role in mitophagy, a more specific form of autophagy, by interacting with autophagy-related gene (ATG) proteins[151]. While not having an upregulation of these subunits, the expression levels are unchanged in the *Nfe2l1* mKO compared to controls (Supplementary Fig. 3b), which could nonetheless play a part in the mitophagy seen in this model.

An additional overlap these two pathways share is the p97/VCP (valosin-containing protein) particle. In the adaptive UPS response, it plays an important role in activating of Nfe2l1, by transporting it across the ER membrane, and thereby exposing it to further posttranslational processing[152]. Also, p97 has recently been associated with initiation of autophagy through Beclin-1 dependent autophagosome biogenesis[153]. Lastly, Mutations in p97 have been linked to myopathies and muscle weakness by giving rise to inclusion bodies. This is in line with our model as we can see similar structures of inclusions in the EM pictures of our gastrocnemius from mKO animals (Fig. 20c) as well as a reduced grip strength (Fig. 19c) upon loss of Nfe2l1[154]. Potentially, the myopathies arising from a p97 mutation are consequences of incorrectly processed or not activated Nfe2l1, which would be an interesting point to investigate in these diseases.

Altogether, most of these characteristics seem to point towards an atrophy phenotype, where muscle mass is diminished through atrogens via autophagy pathways or the UPS[155]. However, interestingly there were no genetic markers indicating a loss of muscle mass through these pathways (Supplementary Fig. 2b). Yet, it is unmistakable that the mKO mice have a lower muscle mass. Another signaling pathway that could account for the loss of muscle mass is the stress response mediated by Fox (Forkhead Box) O transcription factors[155]. Environmental stress and low nutrient availability activate these transcription factors to recycle proteins from large storages like skeletal muscle to prevent amino acid deprivation[156]. In the future it should be determined if the FoxO transcription factors regulate muscle mass upon loss of myocyte Nfe2l1.

Lastly, the reduced muscle mass could be explained by a retardation in development of muscle tissue during adolescence. To investigate this hypothesis am inducible mKO (iKO) of Nfe2l1 was created by a tamoxifen inducible Cre-recombinase. By knocking out Nfe2l1 in adult animals no differences in muscle mass and body weight could be detected (Fig. 28c, d) implying a developmental phenotype of the *Nfe2l1* mKO mice. Similarly, Nfe2l1 has been shown to be imperative for heart development and regeneration after ischemic stroke[127].

In conclusion, the *Nfe2l1* mKO model displays an increase of multiple compensatory pathways to counteract the loss of proteasome activity and restore proteostasis. Some of these pathways are linked to myopathies, which in some parts reflect the phenotypic changes we can determine upon loss of Nfe2l1. However, the notion that these animals experience atrophy and muscle wasting could not be confirmed and may point towards

a developmental phenotype, which preliminary experiments in the inducible knock out of Nfe2l1 in adulthood of the animals underlined.

4.3 Differential impact on the fiber types

The *Nfe2l1* mKO mice show a reduced muscle mass compared to WT controls, yet no loss of muscle through atrophy could be detected. Looking into the muscle tissue it became apparent that there was a muscle fiber type switch towards a slow twitch phenotype in the gastrocnemius muscle (Fig. 20a, b). Differences in fiber type and changes thereof have been largely studied in exercise physiology and neuromuscular disorders. Studies in this field of research are essential to better understand muscle related pathologies and maybe even determine early stage markers for susceptibility or resistance to certain diseases[157]. Muscle composition has been systematically investigated for sport science, injury recovery and prevention as well as many diseases. Beyond the apparent myopathies like muscle atrophy and cancer cachexia that directly impact muscle tissue, there are diseases that affect the muscle concomitantly like chronic obstructive pulmonary disease (COPD)[158] or chronic kidney disease[159,160]. Some of these diseases shift the fiber proportions or have a greater impact on type I fibers and others rather obstruct type II muscle tissue. Expanding knowledge and identifying the underlying causes may not cure the disease itself, but reduce the patients' pain and additional side effects possibly initiating comorbidities. In exercise biology it is well established, that endurance training increases the slow twitch muscle fibers and oxidative phosphorylation by enriching mitochondrial content. This adaptation protects the subjects from muscle fatigue[161]. Interestingly, also damage of muscle tissue shifts the fiber towards a more slow twitch profile[162]. In the *Nfe2l1* mKO exactly this direction of muscle fiber shift can be detected, which underlines the severe impact the loss of the transcription factor has and how the misfolded protein build-up impacts metabolism. Also in some diseases, like Huntington disease the fiber type shifts towards type 1[163] as well as in Thalassemia, which is a genetic disorder leading to improper synthesis of hemoglobin. The emerging muscle phenotype is very similar to the *Nfe2l1* mKO model, as perturbed proteostasis leads to build-up of ubiquitin tagged proteins and a shift in fiber type as well as mitochondrial dysfunction can be seen[164]. However, the question what regulates this shift and why the slow muscle fiber type is preferred in these diseases remains elusive. To the contrary, obesity is often associated with less oxidative fiber and some studies even show that patients with a higher content of glycolytic muscle are more susceptible to developing type 2 diabetes[66,165]. This raises the question if the muscle phenotype shift towards type 1 fibers in the *Nfe2l1* mKO animals safeguards the mice from the broad impact of the high fat diet, like dietary induced obesity (Fig. 25a) as well as glucose and insulin intolerance (Fig. 26a, b). Another characteristic of the *Nfe2l1* mKO that needs further discussion is that the soleus shows no significant metabolic or phenotypic alterations after the loss of Nfe2l1, indicating a lower impact on the oxidative muscle fiber (Fig. 17a, c, e). This could have multiple reasons, such as that the Soleus has a lower protein turn-over than the gastrocnemius or it relies less on the UPS altogether and is therefore less impacted by the loss of Nfe2l1. This also suggests that

the gastrocnemius has a higher pressure of adapting and underlies a more constant and vigorous remodeling than the soleus and that this process is mainly reliant on the adaptive role of Nfe2l1. Unfortunately, there is neither much known about the discrepancies in baseline degradation pathways nor about the rate of the adaptive remodeling concerning the different fiber types. To test this hypothesis, soleus and gastrocnemius should be further investigated with regard to proteasomal content and activity.

4.4 Mitochondrial function and fuel usage

A major denominator of fiber type is the mitochondrial content and activity. Discovery of a shift in the gastrocnemius towards the more oxidative phenotype in the *Nfe2l1* mKO mice, prompted a deeper investigation of the muscle on molecular and functional level. Mitochondria are very dynamic structures with constant remodeling by fission and fusion, consequently disturbances in this structural balance often lead to dysfunction and are associated with various diseases like Huntington, or Alzheimer's disease, myopathies and even diabetes[166–168]. Maintaining structural integrity of the mitochondria therefore is imperative for proper function of the oxidative phosphorylation, as the complexes of the respiratory chain are located in the inner mitochondrial membrane, also known as cristae[69]. The correct assembly and order of the respiratory complexes in the cristae is vital for modeling of the so called supercomplexes, which form the electron transport chain, guiding the electrons across the mitochondrial membrane, and thereby producing ATP. The mitochondria in the *Nfe2l1* mKO muscle look swollen and the cristae shape seems distorted and ruptured in parts (Fig. 20c). Furthermore, less complex III is present in the mKO muscle tissue (Fig. 21a). It would be interesting to investigate whether the impaired cristae structure led to the reduced complex III content or if this has different underlying causes. However, the structural impairment led to a reduction in respiration of the mitochondria in the mKO gastrocnemius muscle (Fig. 21b, c). Additionally, an incorrect translocation of electrons through the cristae by structural disturbances can lead to the production of reactive oxygen species (ROS), which in high doses can damage the cell and lead to apoptosis[169]. Absence of Nfe2l1 led to an increase in autophagy and moreover elevated mitophagy pathways can be determined (Supplementary Fig. 1a, b). To what extent ROS plays a role in cell death in the Nfe2l1 mKO model still needs to be determined, yet the data coherently emphasize the importance of *Nfe2l1* for mitochondrial integrity and function and a loss thereof leads to compromised mitochondrial respiration, despite the relation of loss of the transcription factor and mitochondrial impairment not yet being fully understood. What is known however, is that the *Nfe2l1* mKO is burdened with an overload of ubiquitylated proteins (Fig. 13e, 16b). Studies in the field of protein aggregate overloading show a link to damaged mitochondria and impaired function. These studies are mostly in the field of neurodegenerative diseases like Alzheimer's[170], nevertheless the phenotype of protein overload leading to mitochondrial damage appear very similar to the effects determined in the *Nfe2l1* mKO model. More recently it has been established, that misfolded proteins

of the ER can be transported to mitochondria via contact sites these two organelles build. These protein aggregates subsequently harm the mitochondria and impair function[171]. Another important factor controlling mitochondrial function is calcium load and flux. Mitochondria can take up cytosolic calcium and thereby act as a buffer for intracellular calcium levels. Yet, excessive mitochondrial calcium levels lead to reduced membrane potential and a loss of energy production. Moreover, this leads to swelling and bursting of mitochondria[172], a morphological change also to be observed in the *Nfe2l1* mKO mice (Fig. 20c, Supplementary Fig. 1b). Recently it has also been shown, that calcium levels determine the trophism of the muscle tissue, where a muscle depleted from calcium becomes atrophic and increased calcium influx leads to hypertrophy[173]. Thus it would be interesting to look into the changes in calcium signaling upon loss of Nfe2l1, since an alteration of muscle fiber morphology can be determined however the model lacks elevated atrophy markers, whereby possibly calcium functioning as a second messenger is responsible for the shift in fiber size.

4.5 Energy balance and Organ crosstalk

Unquestionably the *Nfe2l1* mKO model has an altered energy usage compared to WT controls (Fig. 22c, 23d). Interestingly, despite a reduced oxidative phosphorylation capacity of the mitochondria in the *Nfe2l1* mKO animals (Fig. 21b, c), these expend significantly more energy per gram body weight[30]. Looking into the metabolomics dataset a shift towards a more glycolytic metabolism of the gastrocnemius muscle can be detected, as the Warburg effect is one of the top upregulated metabolite pathways (Fig. 22c). This underscores this peculiar phenotype, with a macroscopical shift towards an oxidative fiber (Fig. 20a), yet on molecular level an impaired oxidative phosphorylation alters the metabolism towards a glycolytic signature. Moreover, an impaired electron transport chain (Fig. 21a) along with an upregulation of glycolytic pathways suggest the necessity of an alternative ATP production to maintain cellular energy levels. A straightforward solution would be the upregulation of lactate production to preserve ATP stores. This could also explain the increased energy expenditure as this pathway is much less efficient than the oxidative phosphorylation, yet still significantly contributes to energy expenditure[174]. To address this hypothesis however, performing indirect calorimetry is not sufficient as an increased energy expenditure by lactate production is not measured by indirect calorimetry. The lactate levels of the animals should be measured in plasma and muscle as well as a flux analysis or glucose tracing experiments could be performed in the future to determine the exact pathways through which glucose is metabolized and how ATP is produced. However, the data acquired by indirect calorimetry showed an increased respiration, hence an elevated energy expenditure in the *Nfe2l1* mKO (Fig. 23d, 25c). This increased energy usage along with impaired mitochondrial function, however no detectable change in locomotor activity, could indicate an energy wasting phenotype, where more energy is necessary to maintain basal metabolic rate as well as body temperature upon loss of Nfe2l1. In mammals upholding body temperature is an energy costly process and one of the main contributors

to energy expenditure[175]. Acutely muscle shivering can be used to produce heat, but sustained cold induces non-shivering thermogenesis driven by brown adipose tissue[34,125]. These animals were housed at room temperature, which for mice is below thermoneutrality and therefore mimics mild cold conditions, hence they depend on brown adipose tissue thermogenesis to maintain body temperature. It is known that the thermoneutral zone of mammals is influenced by chemical drugs or pathological conditions[176], thus the temperature for WTs and mKO mice despite being the same, can be experienced differently and lead to increased NST of the mice lacking Nfe2l1 and thereby consuming more energy. This could be verified by housing the animals at 30 °C and monitoring energy expenditure or measuring heat emission by the mice through the tail. Furthermore, since the effect on BAT would be secondary in the mKO model, it is important to study the interorgan crosstalk of muscle and BAT, in particular the axis from skeletal muscle to BAT. A significant upregulation of Fgf21 and Gdf15 in the mKO tissue and also circulating Gdf15 levels could be detected in the mKO model (Supplementary Fig. 4a-d). Both myokines Gdf15 and Fgf21 are known to be induced upon stress and account for loss of muscle mass and function[51,177], attributes well in line with our phenotype. However, focusing on their impact on brown adipose tissue reveals the beneficial impact on whole body metabolism of both myokines[178,179] and adipose tissue browning by Fgf21, by promoting thermogenesis[180]. Additionally, carnosine and anserine were amongst the most abundant metabolites found in the mKO model (Supplementary Table 4). These are also factors known to induce browning[181] and have beneficial effects in metabolic disorders[182].

In conclusion, the increased energy expenditure of the *Nfe2l1* mKO mice could have multiple causes, the most probable ones being either an energy wasting phenotype by an impaired oxidative phosphorylation or a hyper activation of brown adipose tissue due to a shifted thermoneutral zone of the *Nfe2l1* mKO animals. However, as the metabolism is a complex construct, I believe this is not a black or white situation but rather a multifaceted interplay of different factors. Strikingly though, absence of myocyte Nfe2l1 is not detrimental, in fact it rather shows a beneficial impact on metabolism and energy homeostasis.

4.6 Exercise and other environmental influences on Nfe2l1

Maintaining energy balance is essential for cellular homeostasis and metabolic fitness. There are many factors which play a role in upholding and fine-tuning this delicate organization. What needs to be mentioned in this context is the unneglectable impact of environmental influences. Even with decreased proteasomal activity and build-up of ubiquitylated proteins, the loss of myocyte Nfe2l1 showed a predominantly beneficial effect on metabolism. However, the mKO mice also displayed an increase of ER stress markers, e.g., phosphorylated eIF2α (Supplementary Fig. 6a). Furthermore, this does not directly infer a positive consequence under altered environmental conditions. The most prominent and also in this study investigated external influences are exercise and

obesity. Focusing on the latter showed, that the beneficial effect of the absence of Nfe2l1 amplified after 16 weeks of high-fat diet feeding. *Nfe2l1* mKO animals were protected from diet induced obesity and showed improved metabolic parameters (Fig. 25a, 26a, b, 27a-e). The underlying causes remain elusive, however the increased energy expenditure (Fig. 25c) and thereby reduced body weight (Fig. 25a) might account for parts of the improved metabolic parameters. Still, the underlying mechanism that leads to an elevated energy expenditure remains to be determined. On the other hand, exercise capacity of the *Nfe2l1* mKO animals was significantly reduced (Fig. 29a, b), highlighting the metabolic consequence of the impaired oxidative phosphorylation under exercise stress conditions. This can be detected by an earlier onset of the cross-over point, indicating a quicker incapability of the mKOs to use fat as fuel source[39]. This metabolic pathway requires more oxygen and takes place in the mitochondria, which are disrupted in the mKO muscle tissue, so a diminished capability to gain energy from this reaction seems coherent with the phenotype on cellular level. Additionally, to an earlier cross-over point the animals lacking Nfe2l1 often failed to complete the test and exhausted preemptively, indicating a depleted storage or impaired breakdown of glycogen and thereby no energy reserves after glucose is diminished. A similar outcome can for example also be witnessed in Pompe diseases, a glycogen storage disease which shares further similarities with the *Nfe2l1* mKO phenotype. Patients with pompe disease experience muscle weakness caused by glycogen overload in lysosomes. Furthermore, defective autophagy and mitochondrial irregularities contribute to the detrimental outcome of this disease[183]. More generally, storage diseases leading to an accumulation of harmful material encapsulated in inclusion bodies in muscle fiber have been shown to cause myopathies[154]. Underlying reasons often are impaired degradation machineries, emphasizing the importance of proper proteasomal function and adaptation by Nfe2l1 to maintain cellular proteostasis. Moreover, showing that these impairments lead to myopathies and other diseases highlights the significance of studying Nfe2l1 in the context of diseases and affirms the transcription factor as a potential target for therapeutic research.

Understanding the underlying mechanisms is imperative to find solutions and therapies for the certain diseases. In pompe disease for example as well as in nutrient sensing in general the mechanistic target of rapamycin (mTOR) is an indispensable kinase[184,185]. It has also been shown that mTOR regulates Nfe2l1 in MEF cells[130]. Also, in muscle the mTORC1-FoxO pathway has been demonstrated to control muscle growth as well as proteostasis and lies upstream of Nfe2l1[129]. Baseline the mKO mice have elevated levels of phosphorylated Akt and Akt itself in the muscle tissue (Supplementary Fig. 6b), which could imply a regulation of mTORC2 by Nfe2l1 and needs further investigation, since former studies have focused on mTORC1.[129,130] To mimic and activate the Akt-mTOR axis in my studies, *Nfe2l1* mKO and control animals were injected with insulin and the muscle tissue was harvested subsequently. The injection of insulin showed an upregulation of Nfe2l1 and subsequent diminished build-up of ubiquitylated proteins (Fig. 30a, b), which implies a role of Nfe2l1 in the insulin signaling pathway through Akt

in this model as well. However, this is an experiment which should be reproduced with a higher number of animals.

A different angle, was to deprive the cells from amino acids and thereby mimic starvation, supposedly inhibiting mTOR activity. This however showed no impact on Nfe2l1 (Fig. 31a-c). Assuming this treatment was too mild, next I treated with rapamycin, an inhibitor of mTOR. On transcriptional level this showed a decrease in downstream targets of Nfe2l1, however the effects were rather mild (Fig. 32a). In conclusion these experiments linking Nfe2l1 activity to the mTOR pathway look promising and need further investigation, presumably including the TSC loss of function model to genetically inhibit mTOR could give a stronger response and a more clear-cut answer to the regulation of Nfe2l1 through mTOR. Lastly, an upstream regulator of Nfe2l1 could also be hypoxic stress, in line with the altered oxidative phosphorylation due to disrupted mitochondria. Treating C2C12 cells with hypoxia mimetic $CoCl_2$ increased Nfe2l1 and downstream targets on transcriptional level as well as Nfe2l1 protein (Fig. 33a, b). These are promising results that need further investigation.

Taken together the studies investigating mechanisms upstream of Nfe2l1 indicate a role of the transcription factor beyond regulating proteostasis upon proteasome disruption, but raise the question if Nfe2l1 can be seen as a general nutrient and homeostasis sensor activated by different stressors, subsequently remodeling cellular identity through adaptation of the ubiquitin-proteasome system.

References

1. Anja Schienkiewitz, R. K. & Miriam Blume, G. B. M. M. Übergewicht und Adipositas bei Erwachsenen in Deutschland – Ergebnisse der Studie GEDA 2019/2020-EHIS. *J. Heal. Monit.* **7**, (2022).
2. Mensink, G. B. M. *et al.* Übergewicht und Adipositas in Deutschland. *Bundesgesundheitsblatt - Gesundheitsforsch. - Gesundheitsschutz* **56**, 786–794 (2013).
3. WHO. Obesity and overweight. (2021).
4. Hotamisligil, G. S. Inflammatory pathways and insulin action. *Int. J. Obes.* **27**, S53–S55 (2003).
5. Guh, D. P. *et al.* The incidence of co-morbidities related to obesity and overweight: A systematic review and meta-analysis. *BMC Public Health* **9**, 88 (2009).
6. Abdelaal, M., le Roux, C. W. & Docherty, N. G. Morbidity and mortality associated with obesity. *Ann. Transl. Med.* **5**, 161–161 (2017).
7. Kivimäki, M. *et al.* Body-mass index and risk of obesity-related complex multimorbidity: an observational multicohort study. *Lancet Diabetes Endocrinol.* **10**, 253–263 (2022).
8. Klop, B., Elte, J. & Cabezas, M. Dyslipidemia in Obesity: Mechanisms and Potential Targets. *Nutrients* **5**, 1218–1240 (2013).
9. Sarwer, D. B. & Polonsky, H. M. The Psychosocial Burden of Obesity. *Endocrinol. Metab. Clin. North Am.* **45**, 677–688 (2016).
10. OECD. *The Heavy Burden of Obesity*. (OECD, 2019). doi:10.1787/67450d67-en.
11. O'Rahilly, S. & Farooqi, I. S. Genetics of obesity. *Philos. Trans. R. Soc. B Biol. Sci.* **361**, 1095–1105 (2006).
12. Woessner, M. N. *et al.* The Evolution of Technology and Physical Inactivity: The Good, the Bad, and the Way Forward. *Front. Public Heal.* **9**, (2021).
13. Caputo, T., Gilardi, F. & Desvergne, B. From chronic overnutrition to metaflammation and insulin resistance: adipose tissue and liver contributions. *FEBS Lett.* **591**, 3061–3088 (2017).
14. Bartelt, A. & Widenmaier, S. B. Proteostasis in thermogenesis and obesity. *Biol. Chem.* **401**, 1019–1030 (2020).
15. Żukiewicz-Sobczak, W. *et al.* Obesity and poverty paradox in developed countries. *Ann. Agric. Environ. Med.* **21**, 590–594 (2014).
16. Fink, J., Seifert, G., Blüher, M., Fichtner-Feigl, S. & Marjanovic, G. Obesity surgery - weight loss, metabolic changes, oncological effects, and follow-up. *Dtsch. Arztebl. Int.* (2022).
17. Giroud, M., Jodeleit, H., Prentice, K. J. & Bartelt, A. Adipocyte function and the development of cardiometabolic disease. *J. Physiol.* **600**, 1189–1208 (2022).
18. Kasuga, M. *et al.* Insulin stimulation of phosphorylation of the beta subunit of the insulin receptor. Formation of both phosphoserine and phosphotyrosine. *J. Biol. Chem.* **257**, 9891–4 (1982).
19. White, M. F., Maron, R. & Kahn, C. R. Insulin rapidly stimulates tyrosine phosphorylation of a Mr-185,000 protein in intact cells. *Nature* **318**, 183–186 (1985).
20. Cheatham, B. *et al.* Phosphatidylinositol 3-kinase activation is required for insulin stimulation of pp70 S6 kinase, DNA synthesis, and glucose transporter

translocation. *Mol. Cell. Biol.* **14**, 4902–4911 (1994).

21. Lewis, S. T. *et al.* A Receptor Story: Insulin Resistance Pathophysiology and Physiologic Insulin Resensitization's Role as a Treatment Modality. *Int. J. Mol. Sci.* **24**, 10927 (2023).
22. American Diabetes Association. Diagnosis and Classification of Diabetes Mellitus. *Diabetes Care* **32**, S62–S67 (2009).
23. Luo, L. & Liu, M. Adiponectin: friend or foe in obesity and inflammation. *Med. Rev.* **2**, 349–362 (2022).
24. Turer, A. T. & Scherer, P. E. Adiponectin: mechanistic insights and clinical implications. *Diabetologia* **55**, 2319–2326 (2012).
25. Maeda, N. *et al.* Diet-induced insulin resistance in mice lacking adiponectin/ACRP30. *Nat. Med.* **8**, 731–737 (2002).
26. Zhang, Y. *et al.* Positional cloning of the mouse obese gene and its human homologue. *Nature* **372**, 425–432 (1994).
27. Obradovic, M. *et al.* Leptin and Obesity: Role and Clinical Implication. *Front. Endocrinol. (Lausanne).* **12**, (2021).
28. Gruzdeva, O., Borodkina, D., Uchasova, E., Dyleva, Y. & Barbarash, O. Leptin resistance: underlying mechanisms and diagnosis. *Diabetes, Metab. Syndr. Obes. Targets Ther.* **Volume 12**, 191–198 (2019).
29. Delsoglio, M., Achamrah, N., Berger, M. M. & Pichard, C. Indirect Calorimetry in Clinical Practice. *J. Clin. Med.* **8**, 1387 (2019).
30. Tschöp, M. H. *et al.* A guide to analysis of mouse energy metabolism. *Nat. Methods* **9**, 57–63 (2012).
31. Corrigan, J. K. *et al.* A big-data approach to understanding metabolic rate and response to obesity in laboratory mice. *Elife* **9**, (2020).
32. Poehlman, E. T. A review: exercise and its influence on resting energy metabolism in man. *Med. Sci. Sports Exerc.* **21**, 515–25 (1989).
33. Bartelt, A. *et al.* Brown adipose tissue activity controls triglyceride clearance. *Nat. Med.* **17**, 200–205 (2011).
34. CANNON, B. & NEDERGAARD, J. Brown Adipose Tissue: Function and Physiological Significance. *Physiol. Rev.* **84**, 277–359 (2004).
35. Søberg, S. *et al.* Altered brown fat thermoregulation and enhanced cold-induced thermogenesis in young, healthy, winter-swimming men. *Cell Reports Med.* **2**, 100408 (2021).
36. Egan, B. & Zierath, J. R. Exercise Metabolism and the Molecular Regulation of Skeletal Muscle Adaptation. *Cell Metab.* **17**, 162–184 (2013).
37. Garcia, L. *et al.* Non-occupational physical activity and risk of cardiovascular disease, cancer and mortality outcomes: a dose–response meta-analysis of large prospective studies. *Br. J. Sports Med.* **57**, 979–989 (2023).
38. Ramos-Jiménez, A. *et al.* The Respiratory Exchange Ratio is Associated with Fitness Indicators Both in Trained and Untrained Men: A Possible Application for People with Reduced Exercise Tolerance. *Clin. Med. Circ. Respirat. Pulm. Med.* **2**, CCRPM.S449 (2008).
39. Brooks, G. A. IMPORTANCE OF THE 'CROSSOVER' CONCEPT IN EXERCISE METABOLISM. *Clin. Exp. Pharmacol. Physiol.* **24**, 889–895 (1997).
40. Pendergast, D. R., Leddy, J. J. & Venkatraman, J. T. A Perspective on Fat Intake

in Athletes. *J. Am. Coll. Nutr.* **19**, 345–350 (2000).

41. Calvo, J. L., Xu, H., Mon-López, D., Pareja-Galeano, H. & Jiménez, S. L. Effect of sodium bicarbonate contribution on energy metabolism during exercise: a systematic review and meta-analysis. *J. Int. Soc. Sports Nutr.* **18**, (2021).
42. Frontera, W. R. & Ochala, J. Skeletal Muscle: A Brief Review of Structure and Function. *Calcif. Tissue Int.* **96**, 183–195 (2015).
43. Hirosumi, J. *et al.* A central role for JNK in obesity and insulin resistance. *Nature* **420**, 333–6 (2002).
44. Wu, H. & Ballantyne, C. M. Skeletal muscle inflammation and insulin resistance in obesity. *J. Clin. Invest.* **127**, 43–54 (2017).
45. Tallis, J., James, R. S. & Seebacher, F. The effects of obesity on skeletal muscle contractile function. *J. Exp. Biol.* **221**, (2018).
46. VAN DER HEIJDEN, G.-J. *et al.* Strength Exercise Improves Muscle Mass and Hepatic Insulin Sensitivity in Obese Youth. *Med. Sci. Sport. Exerc.* **42**, 1973–1980 (2010).
47. Talar, K. *et al.* Benefits of Resistance Training in Early and Late Stages of Frailty and Sarcopenia: A Systematic Review and Meta-Analysis of Randomized Controlled Studies. *J. Clin. Med.* **10**, 1630 (2021).
48. Mengeste, A. M., Rustan, A. C. & Lund, J. Skeletal muscle energy metabolism in obesity. *Obesity* **29**, 1582–1595 (2021).
49. Klein, A. B. *et al.* Pharmacological but not physiological GDF15 suppresses feeding and the motivation to exercise. *BioRxiv* (2020).
50. Wang, D. *et al.* GDF15 promotes weight loss by enhancing energy expenditure in muscle. *Nature* **619**, 143–150 (2023).
51. Kim-Muller, J. Y. *et al.* GDF15 neutralization restores muscle function and physical performance in a mouse model of cancer cachexia. *Cell Rep.* **42**, 111947 (2023).
52. Keipert, S. *et al.* Skeletal muscle mitochondrial uncoupling drives endocrine cross-talk through the induction of FGF21 as a myokine. *Am. J. Physiol. Metab.* **306**, E469–E482 (2014).
53. Tezze, C. *et al.* Age-Associated Loss of OPA1 in Muscle Impacts Muscle Mass, Metabolic Homeostasis, Systemic Inflammation, and Epithelial Senescence. *Cell Metab.* **25**, 1374-1389.e6 (2017).
54. Romanello, V. & Sandri, M. The connection between the dynamic remodeling of the mitochondrial network and the regulation of muscle mass. *Cell. Mol. Life Sci.* **78**, 1305–1328 (2021).
55. Pereira, R. O. *et al.* OPA1 deficiency promotes secretion of FGF21 from muscle that prevents obesity and insulin resistance. *EMBO J.* **36**, 2126–2145 (2017).
56. Schiaffino, S., Dyar, K. A., Ciciliot, S., Blaauw, B. & Sandri, M. Mechanisms regulating skeletal muscle growth and atrophy. *FEBS J.* **280**, 4294–314 (2013).
57. Liu, J. *et al.* Regulation of myonuclear positioning and muscle function by the skeletal muscle-specific CIP protein. *Proc. Natl. Acad. Sci.* **117**, 19254–19265 (2020).
58. Roman, W. & Gomes, E. R. Nuclear positioning in skeletal muscle. *Semin. Cell Dev. Biol.* **82**, 51–56 (2018).
59. Folker, E. S. & Baylies, M. K. Nuclear positioning in muscle development and disease. *Front. Physiol.* **4**, (2013).

60. Schiaffino, S., Rossi, A. C., Smerdu, V., Leinwand, L. A. & Reggiani, C. Developmental myosins: expression patterns and functional significance. *Skelet. Muscle* **5**, 22 (2015).

61. Smith, J. A. B., Murach, K. A., Dyar, K. A. & Zierath, J. R. Exercise metabolism and adaptation in skeletal muscle. *Nat. Rev. Mol. Cell Biol.* (2023).

62. Murgia, M. *et al.* Protein profile of fiber types in human skeletal muscle: a single-fiber proteomics study. *Skelet. Muscle* **11**, 24 (2021).

63. Deshmukh, A. S. *et al.* Deep muscle-proteomic analysis of freeze-dried human muscle biopsies reveals fiber type-specific adaptations to exercise training. *Nat. Commun.* **12**, 304 (2021).

64. Plotkin, D. L., Roberts, M. D., Haun, C. T. & Schoenfeld, B. J. Muscle Fiber Type Transitions with Exercise Training: Shifting Perspectives. *Sports* **9**, 127 (2021).

65. Tanner, C. J. *et al.* Muscle fiber type is associated with obesity and weight loss. *Am. J. Physiol. Metab.* **282**, E1191–E1196 (2002).

66. Oberbach, A. *et al.* Altered Fiber Distribution and Fiber-Specific Glycolytic and Oxidative Enzyme Activity in Skeletal Muscle of Patients With Type 2 Diabetes. *Diabetes Care* **29**, 895–900 (2006).

67. He, J., Watkins, S. & Kelley, D. E. Skeletal Muscle Lipid Content and Oxidative Enzyme Activity in Relation to Muscle Fiber Type in Type 2 Diabetes and Obesity. *Diabetes* **50**, 817–823 (2001).

68. Kim, A. *et al.* Ablation of USP21 in skeletal muscle promotes oxidative fibre phenotype, inhibiting obesity and type 2 diabetes. *J. Cachexia. Sarcopenia Muscle* **12**, 1669–1689 (2021).

69. Cogliati, S. *et al.* Mitochondrial Cristae Shape Determines Respiratory Chain Supercomplexes Assembly and Respiratory Efficiency. *Cell* **155**, 160–171 (2013).

70. Marín-Buera, L. *et al.* Differential proteomic profiling unveils new molecular mechanisms associated with mitochondrial complex III deficiency. *J. Proteomics* **113**, 38–56 (2015).

71. Visapää, I. *et al.* GRACILE Syndrome, a Lethal Metabolic Disorder with Iron Overload, Is Caused by a Point Mutation in BCS1L. *Am. J. Hum. Genet.* **71**, 863–876 (2002).

72. Egea, V. *et al.* Let-7f miRNA regulates SDF-1α- and hypoxia-promoted migration of mesenchymal stem cells and attenuates mammary tumor growth upon exosomal release. *Cell Death Dis.* **12**, 516 (2021).

73. Semenza, G. L. Targeting HIF-1 for cancer therapy. *Nat. Rev. Cancer* **3**, 721–732 (2003).

74. Harris, A. L. Hypoxia — a key regulatory factor in tumour growth. *Nat. Rev. Cancer* **2**, 38–47 (2002).

75. Rozpedek, W. *et al.* The Role of the PERK/eIF2α/ATF4/CHOP Signaling Pathway in Tumor Progression During Endoplasmic Reticulum Stress. *Curr. Mol. Med.* **16**, 533–544 (2016).

76. Rovetta, F. *et al.* Cobalt triggers necrotic cell death and atrophy in skeletal C2C12 myotubes. *Toxicol. Appl. Pharmacol.* **271**, 196–205 (2013).

77. Heitman, J., Movva, N. R. & Hall, M. N. Targets for Cell Cycle Arrest by the Immunosuppressant Rapamycin in Yeast. *Science (80-.).* **253**, 905–909 (1991).

78. Sabatini, D. M., Erdjument-Bromage, H., Lui, M., Tempst, P. & Snyder, S. H. RAFT1: A mammalian protein that binds to FKBP12 in a rapamycin-dependent

fashion and is homologous to yeast TORs. *Cell* **78**, 35–43 (1994).

79. Brown, E. J. *et al.* A mammalian protein targeted by G1-arresting rapamycin–receptor complex. *Nature* **369**, 756–758 (1994).

80. Sartori, R., Romanello, V. & Sandri, M. Mechanisms of muscle atrophy and hypertrophy: implications in health and disease. *Nat. Commun.* **12**, 330 (2021).

81. Park, G. *et al.* Quantitative analysis of metabolic fluxes in brown fat and skeletal muscle during thermogenesis. *Nat. Metab.* (2023).

82. Zhou, Y. & Danbolt, N. C. Glutamate as a neurotransmitter in the healthy brain. *J. Neural Transm.* **121**, 799–817 (2014).

83. Briguglio, M. *et al.* Dietary Neurotransmitters: A Narrative Review on Current Knowledge. *Nutrients* **10**, 591 (2018).

84. Chandel, N. S. Amino Acid Metabolism. *Cold Spring Harb. Perspect. Biol.* **13**, a040584 (2021).

85. van Spronsen, F. J. *et al.* Phenylketonuria. *Nat. Rev. Dis. Prim.* **7**, 36 (2021).

86. Blackburn, P. *et al.* Maple syrup urine disease: mechanisms and management. *Appl. Clin. Genet.* **Volume 10**, 57–66 (2017).

87. Lemmer, I. L., Willemsen, N., Hilal, N. & Bartelt, A. A guide to understanding endoplasmic reticulum stress in metabolic disorders. *Mol. Metab.* **47**, 101169 (2021).

88. Walter, P. & Ron, D. The Unfolded Protein Response: From Stress Pathway to Homeostatic Regulation. *Science (80-.).* **334**, 1081–1086 (2011).

89. Harding, H. P., Zhang, Y. & Ron, D. Protein translation and folding are coupled by an endoplasmic-reticulum-resident kinase. *Nature* **397**, 271–274 (1999).

90. Shan, B. *et al.* The metabolic ER stress sensor IRE1α suppresses alternative activation of macrophages and impairs energy expenditure in obesity. *Nat. Immunol.* **18**, 519–529 (2017).

91. Zhang, P. *et al.* The PERK eukaryotic initiation factor 2 alpha kinase is required for the development of the skeletal system, postnatal growth, and the function and viability of the pancreas. *Mol. Cell. Biol.* **22**, 3864–74 (2002).

92. Bu, Y. & Diehl, J. A. PERK Integrates Oncogenic Signaling and Cell Survival During Cancer Development. *J. Cell. Physiol.* **231**, 2088–2096 (2016).

93. Pohl, C. & Dikic, I. Cellular quality control by the ubiquitin-proteasome system and autophagy. *Science (80-.).* **366**, 818–822 (2019).

94. Ohsumi, Y. Molecular mechanism of autophagy in yeast, Saccharomyces cerevisiae. *Philos. Trans. R. Soc. London. Ser. B Biol. Sci.* **354**, 1577–1581 (1999).

95. Rabinowitz, J. D. & White, E. Autophagy and Metabolism. *Science (80-.).* **330**, 1344–1348 (2010).

96. Laplante, M. & Sabatini, D. M. mTOR Signaling in Growth Control and Disease. *Cell* **149**, 274–293 (2012).

97. Dikic, I. Proteasomal and Autophagic Degradation Systems. *Annu. Rev. Biochem.* **86**, 193–224 (2017).

98. Kitada, M. & Koya, D. Autophagy in metabolic disease and ageing. *Nat. Rev. Endocrinol.* **17**, 647–661 (2021).

99. Yamamoto, H., Zhang, S. & Mizushima, N. Autophagy genes in biology and disease. *Nat. Rev. Genet.* **24**, 382–400 (2023).

100. Rapoport, T. A. Protein translocation across the eukaryotic endoplasmic reticulum and bacterial plasma membranes. *Nature* **450**, 663–669 (2007).

101. Ruggiano, A., Foresti, O. & Carvalho, P. ER-associated degradation: Protein quality control and beyond. *J. Cell Biol.* **204**, 869–879 (2014).

102. Carvalho, P., Stanley, A. M. & Rapoport, T. A. Retrotranslocation of a Misfolded Luminal ER Protein by the Ubiquitin-Ligase Hrd1p. *Cell* **143**, 579–591 (2010).

103. Waxman, L. & Goldberg, A. L. Selectivity of Intracellular Proteolysis: Protein Substrates Activate the ATP-Dependent Protease (La). *Science (80-.).* **232**, 500–503 (1986).

104. Arrigo, A.-P., Tanaka, K., Goldberg, A. L. & Welch, W. J. Identity of the 19S 'prosome' particle with the large multifunctional protease complex of mammalian cells (the proteasome). *Nature* **331**, 192–194 (1988).

105. Goldberg, A. L. & Dice, J. F. Intracellular Protein Degradation in Mammalian and Bacterial Cells. *Annu. Rev. Biochem.* **43**, 835–869 (1974).

106. Bodine, S. C. Identification of Ubiquitin Ligases Required for Skeletal Muscle Atrophy. *Science (80-.).* **294**, 1704–1708 (2001).

107. Kocaturk, N. M. & Gozuacik, D. Crosstalk Between Mammalian Autophagy and the Ubiquitin-Proteasome System. *Front. Cell Dev. Biol.* **6**, (2018).

108. Demishtein, A. *et al.* SQSTM1/p62-mediated autophagy compensates for loss of proteasome polyubiquitin recruiting capacity. *Autophagy* **13**, 1697–1708 (2017).

109. TANAKA, K. The proteasome: overview of structure and functions. *Proc. Jpn. Acad. Ser. B. Phys. Biol. Sci.* **85**, 12–36 (2009).

110. Goldberg, A. L. Development of proteasome inhibitors as research tools and cancer drugs. *J. Cell Biol.* **199**, 583–588 (2012).

111. Nalawansha, D. A. & Crews, C. M. PROTACs: An Emerging Therapeutic Modality in Precision Medicine. *Cell Chem. Biol.* **27**, 998–1014 (2020).

112. Corson, T. W., Aberle, N. & Crews, C. M. Design and Applications of Bifunctional Small Molecules: Why Two Heads Are Better Than One. *ACS Chem. Biol.* **3**, 677–692 (2008).

113. Churcher, I. Protac-Induced Protein Degradation in Drug Discovery: Breaking the Rules or Just Making New Ones? *J. Med. Chem.* **61**, 444–452 (2018).

114. Thibaudeau, T. A. & Smith, D. M. A Practical Review of Proteasome Pharmacology. *Pharmacol. Rev.* **71**, 170–197 (2019).

115. Goldberg, A. L. Protein turnover in skeletal muscle. II. Effects of denervation and cortisone on protein catabolism in skeletal muscle. *J. Biol. Chem.* **244**, 3223–9 (1969).

116. Díaz-Ruiz, A. *et al.* Proteasome Dysfunction Associated to Oxidative Stress and Proteotoxicity in Adipocytes Compromises Insulin Sensitivity in Human Obesity. *Antioxid. Redox Signal.* **23**, 597–612 (2015).

117. Stringer, D. K. & Piper, R. C. Terminating protein ubiquitination. *Cell Cycle* **10**, 3067–3071 (2011).

118. Kwon, Y. T. & Ciechanover, A. The Ubiquitin Code in the Ubiquitin-Proteasome System and Autophagy. *Trends Biochem. Sci.* **42**, 873–886 (2017).

119. Park, C.-W. & Ryu, K.-Y. Cellular ubiquitin pool dynamics and homeostasis. *BMB Rep.* **47**, 475–482 (2014).

120. Akutsu, M., Dikic, I. & Bremm, A. Ubiquitin chain diversity at a glance. *J. Cell Sci.*

(2016).

121. Steffen, J., Seeger, M., Koch, A. & Krüger, E. Proteasomal Degradation Is Transcriptionally Controlled by TCF11 via an ERAD-Dependent Feedback Loop. *Mol. Cell* **40**, 147–158 (2010).

122. Forcina, G. C. *et al.* Ferroptosis regulation by the NGLY1/NFE2L1 pathway. *Proc. Natl. Acad. Sci.* **119**, (2022).

123. Koizumi, S. *et al.* The aspartyl protease DDI2 activates Nrf1 to compensate for proteasome dysfunction. *Elife* **5**, (2016).

124. Bohnert, K. R., McMillan, J. D. & Kumar, A. Emerging roles of ER stress and unfolded protein response pathways in skeletal muscle health and disease. *J. Cell. Physiol.* **233**, 67–78 (2018).

125. Bartelt, A. *et al.* Brown adipose tissue thermogenic adaptation requires Nrf1-mediated proteasomal activity. *Nat. Med.* **24**, 292–303 (2018).

126. Kotschi, S. *et al.* NFE2L1-mediated proteasome function protects from ferroptosis. *Mol. Metab.* **57**, 101436 (2022).

127. Cui, M. *et al.* Nrf1 promotes heart regeneration and repair by regulating proteostasis and redox balance. *Nat. Commun.* **12**, 5270 (2021).

128. Widenmaier, S. B. *et al.* NRF1 Is an ER Membrane Sensor that Is Central to Cholesterol Homeostasis. *Cell* **171**, 1094-1109.e15 (2017).

129. Kaiser, M. S. *et al.* Dual roles of mTORC1-dependent activation of the ubiquitin-proteasome system in muscle proteostasis. *Commun. Biol.* **5**, 1141 (2022).

130. Zhang, Y. *et al.* Coordinated regulation of protein synthesis and degradation by mTORC1. *Nature* **513**, 440–443 (2014).

131. Muley, C., Kotschi, S. & Bartelt, A. Role of Ubiquilins for Brown Adipocyte Proteostasis and Thermogenesis. *Front. Endocrinol. (Lausanne).* **12**, (2021).

132. Yazgili, A. S. *et al.* In-gel proteasome assay to determine the activity, amount, and composition of proteasome complexes from mammalian cells or tissues. *STAR Protoc.* **2**, 100526 (2021).

133. Egu, D. T., Walter, E., Spindler, V. & Waschke, J. Inhibition of p38MAPK signalling prevents epidermal blistering and alterations of desmosome structure induced by pemphigus autoantibodies in human epidermis. *Br. J. Dermatol.* **177**, 1612–1618 (2017).

134. Hansen, F. M. *et al.* Data-independent acquisition method for ubiquitinome analysis reveals regulation of circadian biology. *Nat. Commun.* **12**, (2021).

135. Udeshi, N. D., Mertins, P., Svinkina, T. & Carr, S. A. Large-scale identification of ubiquitination sites by mass spectrometry. *Nat. Protoc.* **8**, 1950–1960 (2013).

136. Bekker-Jensen, D. B. *et al.* Rapid and site-specific deep phosphoproteome profiling by data-independent acquisition without the need for spectral libraries. *Nat. Commun.* **11**, 787 (2020).

137. Artati, A., Prehn, C., Lutter, D. & Dyar, K. A. Untargeted and Targeted Circadian Metabolomics Using Liquid Chromatography-Tandem Mass Spectrometry (LC-MS/MS) and Flow Injection-Electrospray Ionization-Tandem Mass Spectrometry (FIA-ESI-MS/MS). in 311–327 (2022).

138. Wettmarshausen, J. & Perocchi, F. Isolation of Functional Mitochondria from Cultured Cells and Mouse Tissues. in 15–32 (2017).

139. Pesta, D. & Gnaiger, E. High-Resolution Respirometry: OXPHOS Protocols for Human Cells and Permeabilized Fibers from Small Biopsies of Human Muscle. in

25–58 (2012).

140. Ritchie, M. E. *et al.* limma powers differential expression analyses for RNA-sequencing and microarray studies. *Nucleic Acids Res.* **43**, e47–e47 (2015).

141. Nascimento, E. B. M. *et al.* Comparative transcriptome analysis of human skeletal muscle in response to cold acclimation and exercise training in human volunteers. *BMC Med. Genomics* **13**, 124 (2020).

142. Imke L. Lemmer, Daniel T. Haas, Nienke Willemsen, Stefan Kotschi, Irmak Toksöz, Ejona Gjika, Sajjad Khani, Maria Rohm, Nick Diercksen, Phong B.H. Nguyen, Michael P. Menden, Desalegn T. Egu, Jens Waschke, Steen Larsen, Tao Ma, Zachary Gerhart-Hines, Stepha, A. B. Nfe2l1-mediated proteasome function controls muscle energy metabolism in obesity. *bioRxiv* (2023).

143. Radhakrishnan, S. K. *et al.* Transcription Factor Nrf1 Mediates the Proteasome Recovery Pathway after Proteasome Inhibition in Mammalian Cells. *Mol. Cell* **38**, 17–28 (2010).

144. Ogawa, T. *et al.* S -adenosyl-L-homocysteine extends lifespan through methionine restriction effects. *Aging Cell* **21**, (2022).

145. Wanders, D., Hobson, K. & Ji, X. Methionine Restriction and Cancer Biology. *Nutrients* **12**, 684 (2020).

146. Murton, A. J., Constantin, D. & Greenhaff, P. L. The involvement of the ubiquitin proteasome system in human skeletal muscle remodelling and atrophy. *Biochim. Biophys. Acta - Mol. Basis Dis.* **1782**, 730–743 (2008).

147. Birsa, N. *et al.* Lysine 27 ubiquitination of the mitochondrial transport protein Miro is dependent on serine 65 of the Parkin ubiquitin ligase. *J. Biol. Chem.* **289**, 14569–82 (2014).

148. Nibe, Y. *et al.* Novel polyubiquitin imaging system, PolyUb-FC, reveals that K33-linked polyubiquitin is recruited by SQSTM1/p62. *Autophagy* **14**, 347–358 (2018).

149. Hoeller, D. & Dikic, I. How the proteasome is degraded. *Proc. Natl. Acad. Sci.* **113**, 13266–13268 (2016).

150. Coux, O., Tanaka, K. & Goldberg, A. L. STRUCTURE AND FUNCTIONS OF THE 20S AND 26S PROTEASOMES. *Annu. Rev. Biochem.* **65**, 801–847 (1996).

151. Kocaturk, N. M. *et al.* Novel protein complexes containing autophagy and UPS components regulate proteasome-dependent PARK2 recruitment onto mitochondria and PARK2-PARK6 activity during mitophagy. *Cell Death Dis.* **13**, 947 (2022).

152. Radhakrishnan, S. K., den Besten, W. & Deshaies, R. J. p97-dependent retrotranslocation and proteolytic processing govern formation of active Nrf1 upon proteasome inhibition. *Elife* **3**, (2014).

153. Hill, S. M. *et al.* VCP/p97 regulates Beclin-1-dependent autophagy initiation. *Nat. Chem. Biol.* **17**, 448–455 (2021).

154. Watts, G. *et al.* Novel VCP mutations in inclusion body myopathy associated with Paget disease of bone and frontotemporal dementia. *Clin. Genet.* **72**, 420–426 (2007).

155. Sandri, M. Protein breakdown in muscle wasting: role of autophagy-lysosome and ubiquitin-proteasome. *Int. J. Biochem. Cell Biol.* **45**, 2121–9 (2013).

156. Milan, G. *et al.* Regulation of autophagy and the ubiquitin–proteasome system by the FoxO transcriptional network during muscle atrophy. *Nat. Commun.* **6**, 6670 (2015).

157. Talbot, J. & Maves, L. Skeletal muscle fiber type: using insights from muscle developmental biology to dissect targets for susceptibility and resistance to muscle disease. *WIREs Dev. Biol.* **5**, 518–534 (2016).

158. Maltais, F. *et al.* An Official American Thoracic Society/European Respiratory Society Statement: Update on Limb Muscle Dysfunction in Chronic Obstructive Pulmonary Disease. *Am. J. Respir. Crit. Care Med.* **189**, e15–e62 (2014).

159. Wang, X. H., Mitch, W. E. & Price, S. R. Pathophysiological mechanisms leading to muscle loss in chronic kidney disease. *Nat. Rev. Nephrol.* **18**, 138–152 (2022).

160. Lewis, M. I. *et al.* Metabolic and morphometric profile of muscle fibers in chronic hemodialysis patients. *J. Appl. Physiol.* **112**, 72–78 (2012).

161. Lievens, E., Klass, M., Bex, T. & Derave, W. Muscle fiber typology substantially influences time to recover from high-intensity exercise. *J. Appl. Physiol.* **128**, 648–659 (2020).

162. Shin, J., Nunomiya, A., Gonda, K. & Nagatomi, R. Specification of skeletal muscle fiber-type is determined by the calcineurin/NFATc1 signaling pathway during muscle regeneration. *Biochem. Biophys. Res. Commun.* **659**, 20–28 (2023).

163. Strand, A. D. *et al.* Gene expression in Huntington's disease skeletal muscle: a potential biomarker. *Hum. Mol. Genet.* **14**, 1863–1876 (2005).

164. Reboucas, P. *et al.* Discovery-Based Proteomics Identify Skeletal Muscle Mitochondrial Alterations as an Early Metabolic Defect in a Mouse Model of β-Thalassemia. *Int. J. Mol. Sci.* **24**, 4402 (2023).

165. Hickey, M. S. *et al.* Skeletal muscle fiber composition is related to adiposity and in vitro glucose transport rate in humans. *Am. J. Physiol. Metab.* **268**, E453–E457 (1995).

166. Costa, V. & Scorrano, L. Shaping the role of mitochondria in the pathogenesis of Huntington's disease. *EMBO J.* **31**, 1853–1864 (2012).

167. Eramo, M. J., Lisnyak, V., Formosa, L. E. & Ryan, M. T. The 'mitochondrial contact site and cristae organising system' (MICOS) in health and human disease. *J. Biochem.* **167**, 243–255 (2020).

168. Rajab, B. S. *et al.* Differential remodelling of mitochondrial subpopulations and mitochondrial dysfunction are a feature of early stage diabetes. *Sci. Rep.* **12**, 978 (2022).

169. Ježek, J., Cooper, K. & Strich, R. Reactive Oxygen Species and Mitochondrial Dynamics: The Yin and Yang of Mitochondrial Dysfunction and Cancer Progression. *Antioxidants* **7**, 13 (2018).

170. Abramov, A. Y., Berezhnov, A. V., Fedotova, E. I., Zinchenko, V. P. & Dolgacheva, L. P. Interaction of misfolded proteins and mitochondria in neurodegenerative disorders. *Biochem. Soc. Trans.* **45**, 1025–1033 (2017).

171. Cortés Sanchón, A. *et al.* ER-misfolded proteins become sequestered with mitochondria and impair mitochondrial function. *Commun. Biol.* **4**, 1350 (2021).

172. Vilas-Boas, E. A., Cabral-Costa, J. V., Ramos, V. M., Caldeira da Silva, C. C. & Kowaltowski, A. J. Goldilocks calcium concentrations and the regulation of oxidative phosphorylation: Too much, too little, or just right. *J. Biol. Chem.* **299**, 102904 (2023).

173. Mammucari, C. *et al.* The Mitochondrial Calcium Uniporter Controls Skeletal Muscle Trophism In Vivo. *Cell Rep.* **10**, 1269–1279 (2015).

174. Scott, C. B. Contribution of Blood Lactate to the Energy Expenditure of Weight Training. *J. Strength Cond. Res.* **20**, 404 (2006).

175. Speakman, J. R. Measuring Energy Metabolism in the Mouse – Theoretical, Practical, and Analytical Considerations. *Front. Physiol.* **4**, (2013).

176. Gordon, C. J. Thermal physiology of laboratory mice: Defining thermoneutrality. *J. Therm. Biol.* **37**, 654–685 (2012).

177. Oost, L. J., Kustermann, M., Armani, A., Blaauw, B. & Romanello, V. Fibroblast growth factor 21 controls mitophagy and muscle mass. *J. Cachexia. Sarcopenia Muscle* **10**, 630–642 (2019).

178. Schlein, C. *et al.* FGF21 Lowers Plasma Triglycerides by Accelerating Lipoprotein Catabolism in White and Brown Adipose Tissues. *Cell Metab.* **23**, 441–453 (2016).

179. Laurens, C. *et al.* Growth and differentiation factor 15 is secreted by skeletal muscle during exercise and promotes lipolysis in humans. *JCI Insight* **5**, (2020).

180. Fisher, ffolliott M. *et al.* FGF21 regulates PGC-1α and browning of white adipose tissues in adaptive thermogenesis. *Genes Dev.* **26**, 271–281 (2012).

181. Schaalan, M. F., Ramadan, B. K. & Abd Elwahab, A. H. Synergistic effect of carnosine on browning of adipose tissue in exercised obese rats; a focus on circulating irisin levels. *J. Cell. Physiol.* **233**, 5044–5057 (2018).

182. Anderson, E. J. *et al.* A carnosine analog mitigates metabolic disorders of obesity by reducing carbonyl stress. *J. Clin. Invest.* **128**, 5280–5293 (2018).

183. Kohler, L., Puertollano, R. & Raben, N. Pompe Disease: From Basic Science to Therapy. *Neurotherapeutics* **15**, 928–942 (2018).

184. Meena, N. K. & Raben, N. Pompe Disease: New Developments in an Old Lysosomal Storage Disorder. *Biomolecules* **10**, 1339 (2020).

185. Kim, D.-H. *et al.* mTOR Interacts with Raptor to Form a Nutrient-Sensitive Complex that Signals to the Cell Growth Machinery. *Cell* **110**, 163–175 (2002).

Supplementary figures

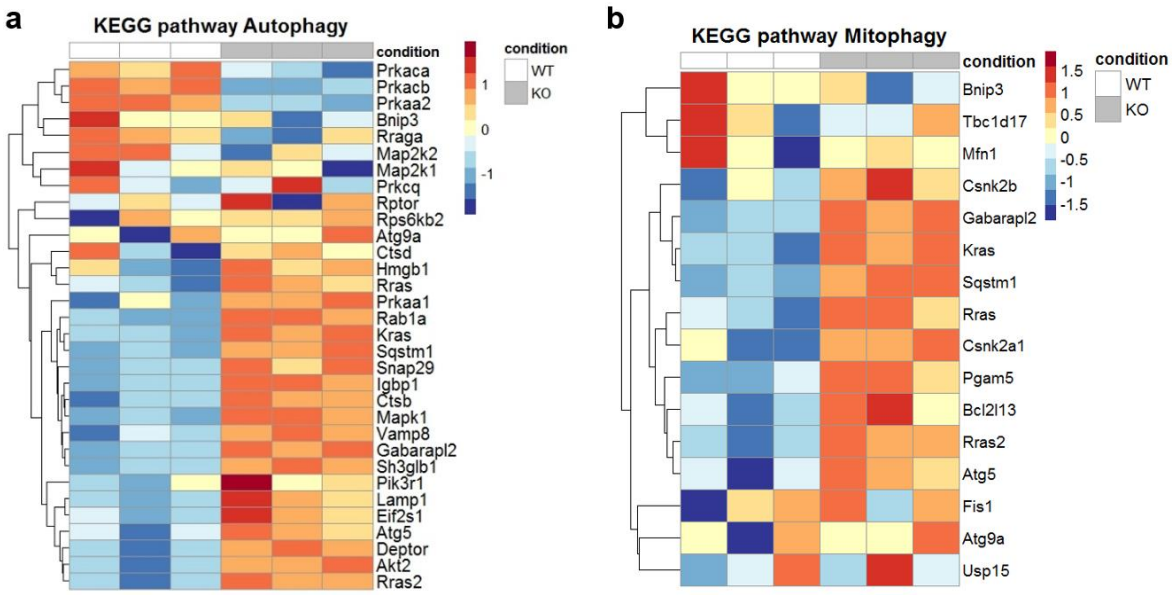

Supplementary Figure 1: Deletion of Nfe2l1 leads to upregulation of autophagy and mitophagy. a, b) KEGG-pathway analysis of proteome from GC tissue from *Nfe2l1* mKO and WTs (n = 3 mice per group). a) Autophagy pathway (mmu 04140) and b) Mitophagy pathway (mmu 04137). Figure adapted from[142].

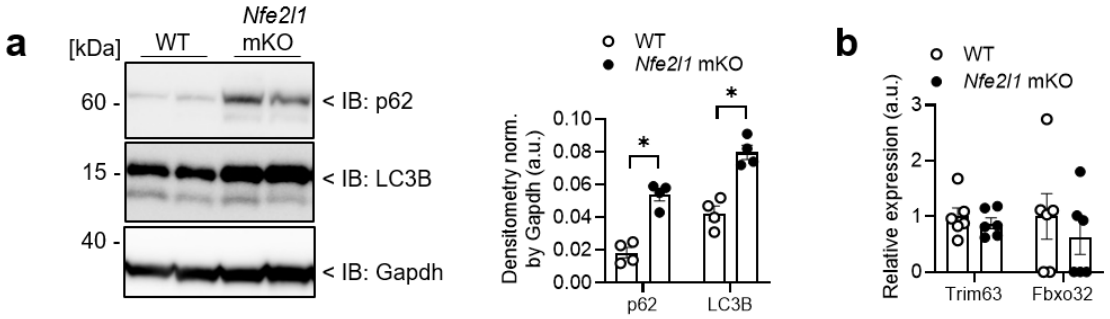

Supplementary Figure 2: Lack of Nfe2l1 leads to elevated autophagy markers but not atrophy in GC. a) Representative immunoblot and corresponding densitometry of p62 and LC3B from GC tissue of WT and *Nfe2l1* mKO mice. b) mRNA expression levels from RNAseq of atrophy markers Trim63 and Fbxo32 in mKO mice and WT controls (n = 6 mice per group). Data are mean ±SEM, p<0.05 by t-test. Figure adapted from[142].

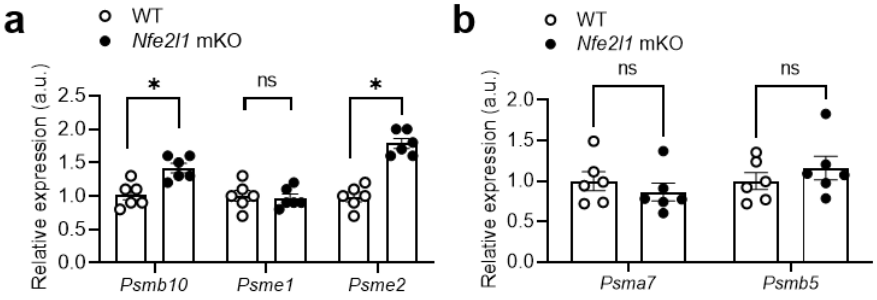

Supplementary Figure 3: Compensating factors for loss of multiple proteasomal subunits. a,b) Relative expression levels from RNAseq of proteasome subunits in WTs and *Nfe2l1* mKO animals (n = 6 mice per group). a) Trypsin-like associated proteasomal subunit *Psmb10* and proteasomal activators *Psme1* and *Psme2*. b) Proteasomal subunits associated with mitophagy *Psma7* and *Psmb5*. Data are mean ±SEM, p<0.05 by 2-way ANOVA.

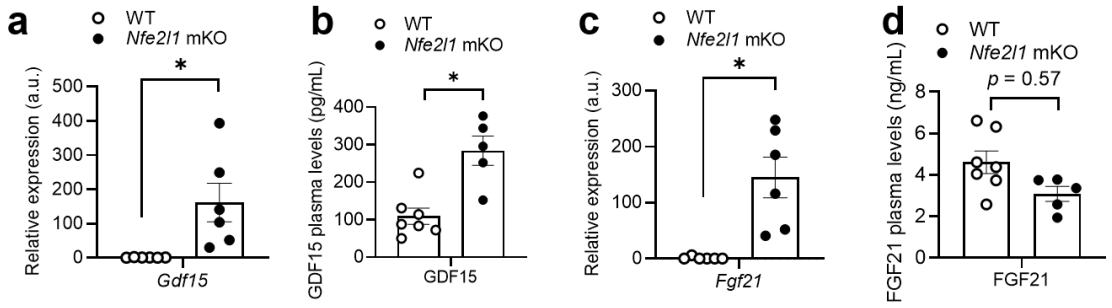

Supplementary Figure 4: Absence of Nfe2l1 leads to elevated mRNA and plasma levels of Gdf15 and Fgf21. a) mRNA levels of Gdf15 and b) circulating plasma levels of GDF15 in *Nfe2l1* mKO and WT mice. c) mRNA Fgf21 levels and d) circulating plasma levels of FGF21 in WT controls and mKO mice. ((a-d) *n*= 5 - 7 mice per group.)) Figure adapted from[142].

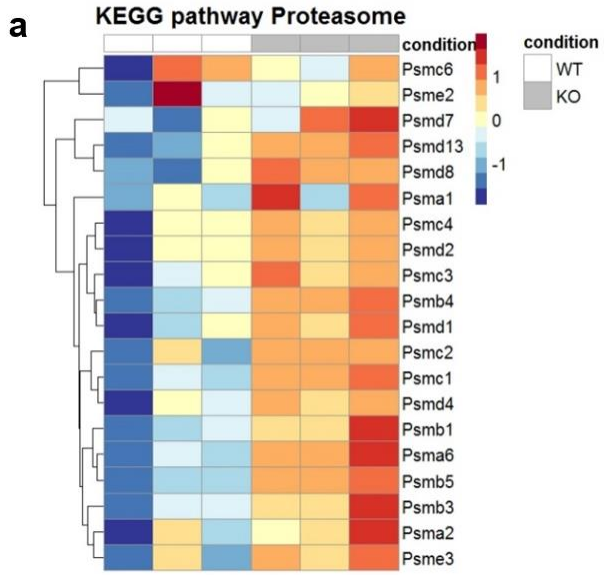

Supplementary Figure 5: Degradation of the proteasome via the UPS. a) KEGG-analysis of the proteasome pathway (mmu 03050) in the ubiquitome of GC muscle tissue (*n* = 3 mice per group). Figure adapted from[142].

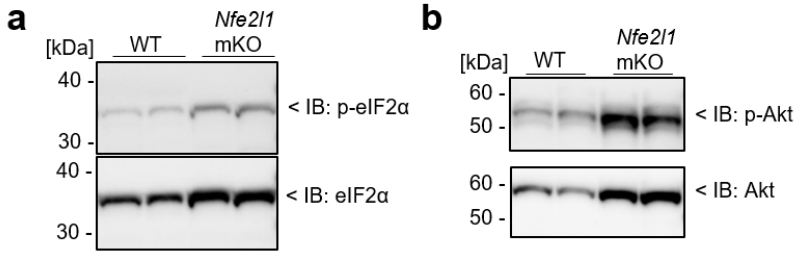

Supplementary Figure 6: Markers of ER stress signaling are elevated in *Nfe2l1* mKO muscle tissue. a,b) Representative immunoblots from WT controls and Nfel21 mKO gastrocnemius tissue of a) (p)-eIF2α and b) (p)-Akt.

Supplementary Tables

Supplementary Table 1: Primers used for RT-qPCR. This table is adapted from Lemmer et al.[142]

Gene	Forward Primer (5')	Reverse Primer (3')
Nfe2l1	GACAAGATCATCAACCTGCCTGTAG	GCTCACTTCCTCCGGTCCTTTG
Psma1	TGCGTGCGTTTTTGATTTTAGAC	CCCTCAGGGCAGGATTCATC
Psmb1	CGTTGAAGGCATAAGGCGAAAA	TTCCACTGCTGCTTACCGAG
Ldlr	CAAGAGGCAGGGTCCAGA	CCAATCTGTCCAGTACATGAAGC
Tbp	AGAACAATCCAGACTAGCAGCA	GGGAACTTCACATCACAGCTC

„**Supplementary Table 2:** Primary and secondary antibodies used for Immunoblotting." This table is from Lemmer et al.[142]

Antibody	Company (Cat. No.)	Dilution
20S Proteasome α subunits	Abcam (ab22674)	1:1000
Akt	Cell signaling technologies (9272)	1:1000
eIF2α	Cell signaling technologies (9733)	1:1000
Gapdh	Cell signaling technologies (5174)	1:1000
LC3B	Cell signaling technologies (2775)	1:1000
Nfe2l1	Cell signaling technologies (D5B10)	1:500
Total OXPHOS rodent	Abcam (ab110413)	1:1000
p62	Abcam (ab155686)	1:1000
p-Akt (Ser)	Cell signaling technologies (4051)	1:1000
p-eIF2α	Cell signaling technologies (3597)	1:1000
Ubiquitin (P4D1)	Cell signaling technologies (3936)	1:1000
β-tubulin	Cell signaling technologies (2146)	1:1000
Anti-rabbit IgG, HRP-linked	Cell signaling technologies (7074)	1:10000
Anti-mouse IgG, HRP-linked	Cell signaling technologies (7076)	1:10000

„**Supplementary Table 3:** Protocol used for isolated mitochondria seahorse.“ This table is from Lemmer et al. [142]

Command	Time
Baseline	Wait: 00:10:00 Mix: 00:01:00 Wait: 00:03:00 Duration: 00:14:00
Measurement Baseline	Mix: 00:01:00 Wait: 00:00:00 Measure: 00:03:00 Cycles: 2 Duration: 00:08:00
ADP (Port A)	Mix: 00:01:00 Wait: 00:00:00 Measure: 00:04:00 Cycles: 1 Duration: 00:05:00
Oligo (Port B)	Mix: 00:01:00 Wait: 00:00:00 Measure: 00:03:00 Cycles: 1 Duration: 00:04:00
FCCP (Port C)	Mix: 00:01:00 Wait: 00:00:00 Measure: 00:03:00 Cycles: 1 Duration: 00:04:00
Rot/AA (Port D)	Mix: 00:01:00 Wait: 00:00:00 Measure: 00:03:00 Cycles: 2 Duration: 00:08:00

„**Supplementary Table 4:** Metabolomics - significantly regulated metabolites in gastrocnemius tissue.“ This table is from Lemmer et al.[142]

Metabolite	t.stat	p.value	-Log10(p)	FDR
glycerophosphorylcholine (GPC)	22.82	8.35E-17	16.078	3.38E-14
1-stearoyl-2-arachidonoyl-GPC (18:0/20:4)	20.74	6.26E-16	15.203	1.04E-13
N-acetylarginine	20.53	7.73E-16	15.112	1.04E-13
1-stearoyl-GPC (18:0)	17.92	1.30E-14	13.885	1.32E-12
palmitoyl sphingomyelin (d18:1/16:0)	17.02	3.75E-14	13.426	2.90E-12
fagomine	-16.91	4.29E-14	13.367	2.90E-12
xanthine	16.55	6.70E-14	13.174	3.77E-12
1-stearoyl-2-arachidonoyl-GPS (18:0/20:4)	16.45	7.56E-14	13.121	3.77E-12
phosphoethanolamine	16.37	8.38E-14	13.077	3.77E-12
valylglycine	15.86	1.59E-13	12.798	6.45E-12
glycerophosphoethanolamine	15.65	2.09E-13	12.681	7.68E-12
deoxycarnitine	15.36	3.04E-13	12.517	1.01E-11
palmitoyl dihydrosphingomyelin (d18:0/16:0)*	15.27	3.45E-13	12.462	1.01E-11
5-(galactosylhydroxy)-lysine	15.26	3.47E-13	12.459	1.01E-11
1-(1-enyl-stearoyl)-2-arachidonoyl-GPE (P-18:0/20:4)*	15.07	4.50E-13	12.347	1.22E-11
ergothioneine	14.22	1.43E-12	11.843	3.63E-11
1-(1-enyl-palmitoyl)-2-arachidonoyl-GPE (P-16:0/20:4)*	14.16	1.56E-12	11.808	3.71E-11
sphingomyelin (d18:2/24:1, d18:1/24:2)*	13.77	2.73E-12	11.564	6.14E-11
adenosine 5'-diphosphoribose (ADP-ribose)	13.65	3.25E-12	11.489	6.92E-11
C-glycosyltryptophan	13.41	4.58E-12	11.339	9.27E-11
1-stearoyl-2-oleoyl-GPC (18:0/18:1)	13.14	6.86E-12	11.164	1.28E-10
1-stearoyl-2-linoleoyl-GPE (18:0/18:2)*	13.13	6.95E-12	11.158	1.28E-10
sphingomyelin (d18:2/23:0, d18:1/23:1, d17:1/24:1)*	12.96	8.92E-12	11.05	1.57E-10
1-palmitoyl-2-stearoyl-GPC (16:0/18:0)	12.61	1.54E-11	10.813	2.60E-10
hydroxy-N6,N6,N6-trimethyllysine*	12.33	2.34E-11	10.631	3.79E-10
sphingomyelin (d18:1/24:1, d18:2/24:0)*	12.00	3.95E-11	10.403	6.16E-10
tricosanoyl sphingomyelin (d18:1/23:0)*	11.91	4.63E-11	10.334	6.94E-10
N-glycolylneuraminate	11.59	7.71E-11	10.113	1.12E-09
serotonin	11.55	8.21E-11	10.085	1.12E-09
linolenate [alpha or gamma; (18:3n3 or 6)]	11.55	8.33E-11	10.08	1.12E-09
dimethylarginine (SDMA + ADMA)	11.43	1.01E-10	9.9955	1.32E-09
histamine	11.26	1.35E-10	9.8713	1.69E-09

guanidinoacetate	11.23	1.40E-10	9.8547	1.69E-09
maltohexaose	11.22	1.42E-10	9.8472	1.69E-09
N-acetylneuraminate	11.01	2.04E-10	9.6914	2.35E-09
uridine	10.93	2.32E-10	9.6338	2.61E-09
tyrosylglycine	10.92	2.39E-10	9.6221	2.61E-09
1-palmitoyl-GPC (16:0)	10.86	2.63E-10	9.5792	2.81E-09
sphingomyelin (d18:2/16:0, d18:1/16:1)*	10.77	3.08E-10	9.5117	3.20E-09
maltotriose	10.62	3.97E-10	9.4008	4.02E-09
trans-4-hydroxyproline	-10.57	4.35E-10	9.3613	4.30E-09
maltotetraose	10.44	5.49E-10	9.2606	5.17E-09
glutathione, oxidized (GSSG)	10.44	5.49E-10	9.2604	5.17E-09
hexadecadienoate (16:2n6)	10.42	5.67E-10	9.2461	5.22E-09
anserine	-10.40	5.91E-10	9.2283	5.27E-09
carnosine	-10.39	5.99E-10	9.2226	5.27E-09
dehydroascorbate	10.23	7.97E-10	9.0985	6.87E-09
cytidine	10.20	8.42E-10	9.0745	7.11E-09
uridine 5'-monophosphate (UMP)	10.17	8.92E-10	9.0496	7.37E-09
3-phosphoglycerate	-10.09	1.04E-09	8.9849	8.39E-09
linoleate (18:2n6)	10.07	1.07E-09	8.9717	8.48E-09
N-palmitoyl-sphingosine (d18:1/16:0)	9.94	1.35E-09	8.8692	1.05E-08
maltopentaose	9.90	1.45E-09	8.838	1.11E-08
sphingomyelin (d18:1/22:1, d18:2/22:0, d16:1/24:1)*	9.88	1.51E-09	8.8209	1.13E-08
behenoyl sphingomyelin (d18:1/22:0)*	9.73	1.97E-09	8.7063	1.43E-08
palmitoleate (16:1n7)	9.73	1.97E-09	8.7053	1.43E-08
1-(1-enyl-palmitoyl)-2-oleoyl-GPC(P-16:0/18:1)*	9.71	2.07E-09	8.6833	1.47E-08
1,2-dilinoleoyl-GPC (18:2/18:2)	9.69	2.15E-09	8.6677	1.50E-08
ceramide (d18:2/24:1, d18:1/24:2)*	9.61	2.49E-09	8.6037	1.71E-08
1-stearoyl-2-oleoyl-GPE (18:0/18:1)	9.58	2.64E-09	8.5778	1.78E-08
glucose	9.53	2.87E-09	8.5416	1.91E-08
1-oleoyl-2-linoleoyl-GPE (18:1/18:2)*	9.44	3.40E-09	8.4685	2.22E-08
sphingomyelin (d18:0/18:0, d19:0/17:0)*	9.40	3.70E-09	8.432	2.35E-08
benzoate	9.39	3.71E-09	8.4304	2.35E-08
phosphoenolpyruvate (PEP)	-9.36	4.00E-09	8.3982	2.49E-08
1-stearoyl-2-linoleoyl-GPS (18:0/18:2)	9.34	4.10E-09	8.3871	2.52E-08
10-heptadecenoate (17:1n7)	9.33	4.19E-09	8.3779	2.53E-08

2-O-methylascorbic acid	9.16	5.76E-09	8.2396	3.43E-08
1-stearoyl-2-linoleoyl-GPC (18:0/18:2)*	9.13	6.19E-09	8.208	3.60E-08
argininate*	9.12	6.25E-09	8.2039	3.60E-08
1-oleoyl-2-linoleoyl-GPC (18:1/18:2)*	9.12	6.30E-09	8.2005	3.60E-08
13-HODE + 9-HODE	9.11	6.43E-09	8.192	3.62E-08
1-stearoyl-2-arachidonoyl-GPE (18:0/20:4)	9.09	6.67E-09	8.176	3.70E-08
1-oleoyl-GPC (18:1)	9.08	6.81E-09	8.1669	3.73E-08
3-indoxyl sulfate	9.04	7.26E-09	8.1388	3.92E-08
urate	8.93	9.06E-09	8.043	4.80E-08
sphingosine	8.93	9.13E-09	8.0394	4.80E-08
oleate/vaccenate (18:1)	8.90	9.61E-09	8.0173	4.94E-08
lignoceroyl sphingomyelin (d18:1/24:0)	8.90	9.64E-09	8.0158	4.94E-08
guanosine	8.78	1.22E-08	7.9154	6.15E-08
spermidine	8.71	1.39E-08	7.8564	6.96E-08
2'-deoxyadenosine 5'-monophosphate	8.67	1.51E-08	7.8208	7.46E-08
1-linoleoyl-GPC (18:2)	8.53	2.00E-08	7.6997	9.74E-08
gamma-glutamyl-epsilon-lysine	8.40	2.61E-08	7.5836	1.26E-07
2-aminoadipate	8.39	2.65E-08	7.576	1.26E-07
1-(1-enyl-palmitoyl)-2-linoleoyl-GPC (P-16:0/18:2)*	8.33	2.99E-08	7.525	1.41E-07
cholesterol	8.20	3.89E-08	7.4106	1.81E-07
leucylglycine	8.18	4.09E-08	7.3882	1.88E-07
indolelactate	8.15	4.36E-08	7.36	1.99E-07
maltose	8.12	4.65E-08	7.3325	2.09E-07
uracil	8.08	4.99E-08	7.3016	2.22E-07
1-palmitoyl-2-linoleoyl-GPC (16:0/18:2)	8.07	5.13E-08	7.2895	2.26E-07
1-palmitoyl-2-docosahexaenoyl-GPE (16:0/22:6)*	-8.06	5.23E-08	7.2814	2.28E-07
arachidonate (20:4n6)	8.04	5.39E-08	7.2682	2.32E-07
sphingomyelin (d17:1/16:0, d18:1/15:0, d16:1/17:0)	8.04	5.47E-08	7.2621	2.33E-07
myristoleate (14:1n5)	7.90	7.23E-08	7.1408	3.05E-07
gamma-glutamylleucine	7.89	7.42E-08	7.1294	3.10E-07
glycylleucine	7.88	7.57E-08	7.1208	3.13E-07
1-palmitoyl-2-palmitoleoyl-GPC (16:0/16:1)*	-7.82	8.54E-08	7.0686	3.47E-07
N-acetylserine	-7.82	8.56E-08	7.0677	3.47E-07
sphingomyelin (d18:1/17:0, d17:1/18:0, d19:1/16:0)	7.79	9.21E-08	7.0356	3.69E-07

kynurenine	7.70	1.10E-07	6.9599	4.35E-07
hypoxanthine	7.70	1.11E-07	6.9535	4.38E-07
N-methyl-GABA	7.69	1.14E-07	6.9426	4.44E-07
sphingomyelin (d18:1/20:0, d16:1/22:0)*	7.64	1.26E-07	6.9007	4.85E-07
inosine	7.61	1.35E-07	6.87	5.15E-07
6-phosphogluconate	7.59	1.39E-07	6.8566	5.27E-07
citrate	7.57	1.46E-07	6.8345	5.49E-07
gamma-glutamylcysteine	7.54	1.54E-07	6.8125	5.67E-07
N,N-dimethyl-pro-pro	7.54	1.54E-07	6.8115	5.67E-07
N-acetylglutamate	7.54	1.56E-07	6.8082	5.67E-07
cytidine 5'-monophosphate (5'-CMP)	7.51	1.66E-07	6.7811	5.99E-07
1-methylhistamine	7.46	1.86E-07	6.7314	6.65E-07
1,2-dilinoleoyl-GPE (18:2/18:2)*	7.41	2.07E-07	6.684	7.36E-07
glycylvaline	7.39	2.16E-07	6.6656	7.61E-07
thioproline	7.38	2.18E-07	6.6616	7.61E-07
1-palmitoyl-2-oleoyl-GPE (16:0/18:1)	7.35	2.33E-07	6.6328	8.06E-07
sedoheptulose-7-phosphate	7.29	2.66E-07	6.5753	9.13E-07
heme	7.17	3.49E-07	6.4576	1.19E-06
dihomo-linoleate (20:2n6)	7.11	3.92E-07	6.4066	1.32E-06
nicotinamide ribonucleotide (NMN)	-7.02	4.84E-07	6.3149	1.62E-06
N-stearoyl-sphingosine (d18:1/18:0)*	-7.00	5.00E-07	6.3014	1.66E-06
1-(1-enyl-palmitoyl)-2-oleoyl-GPE (P-16:0/18:1)*	6.99	5.08E-07	6.2937	1.67E-06
tryptophan	6.88	6.50E-07	6.187	2.12E-06
cysteine-glutathione disulfide	6.88	6.57E-07	6.1822	2.13E-06
eicosenoate (20:1)	6.85	7.04E-07	6.1525	2.26E-06
1-stearoyl-2-docosahexaenoyl-GPC (18:0/22:6)	6.77	8.34E-07	6.0791	2.66E-06
glycerate	-6.74	9.01E-07	6.0454	2.85E-06
dihydroxyacetone phosphate (DHAP)	6.59	1.26E-06	5.898	3.97E-06
1-(1-enyl-palmitoyl)-2-linoleoyl-GPE (P-16:0/18:2)*	6.54	1.42E-06	5.8479	4.42E-06
adenosine 3',5'-diphosphate	6.50	1.55E-06	5.8083	4.81E-06
adenosine	-6.46	1.70E-06	5.7688	5.22E-06
1-palmitoyl-2-linoleoyl-GPE (16:0/18:2)	6.45	1.72E-06	5.7644	5.24E-06
tetradecadienoate (14:2)*	6.39	1.97E-06	5.7064	5.94E-06
1-palmitoyl-2-oleoyl-GPG (16:0/18:1)	6.34	2.25E-06	5.6486	6.74E-06
phenylalanine	6.33	2.28E-06	5.6418	6.79E-06

sphinganine	6.28	2.53E-06	5.5964	7.49E-06
inosine 5'-monophosphate (IMP)	-6.18	3.21E-06	5.4941	9.41E-06
1-stearoyl-2-oleoyl-GPS (18:0/18:1)	6.15	3.48E-06	5.4588	1.01E-05
CoA-glutathione*	6.14	3.51E-06	5.4547	1.02E-05
1-palmitoyl-GPE (16:0)	6.12	3.71E-06	5.4304	1.07E-05
glycerol 3-phosphate	-6.10	3.82E-06	5.4175	1.09E-05
methylphosphate	-5.95	5.44E-06	5.2644	1.54E-05
dihomo-linolenate (20:3n3 or n6)	5.94	5.56E-06	5.2545	1.57E-05
ascorbate (vitamin C)	5.93	5.68E-06	5.246	1.59E-05
phosphopantetheine	5.93	5.78E-06	5.2381	1.60E-05
sphingomyelin (d18:1/21:0, d17:1/22:0, d16:1/23:0)	5.92	5.94E-06	5.226	1.64E-05
N6-carboxymethyllysine	5.88	6.52E-06	5.1857	1.78E-05
2-methylcitrate/homocitrate	5.81	7.55E-06	5.1218	2.05E-05
pipecolate	5.80	7.87E-06	5.1042	2.12E-05
nicotinamide adenine dinucleotide (NAD+)	-5.79	7.99E-06	5.0976	2.14E-05
aconitate [cis or trans]	5.79	8.03E-06	5.0954	2.14E-05
flavin adenine dinucleotide (FAD)	5.77	8.26E-06	5.083	2.19E-05
choline phosphate	5.74	8.87E-06	5.0519	2.33E-05
coenzyme A	5.72	9.44E-06	5.0249	2.47E-05
alpha-tocopherol	5.66	1.07E-05	4.9699	2.78E-05
guanosine 5'-monophosphate (5'-GMP)	5.65	1.12E-05	4.9527	2.88E-05
docosahexaenoate (DHA; 22:6n3)	5.50	1.58E-05	4.8006	4.06E-05
N,N,N-trimethyl-alanylproline betaine (TMAP)	5.50	1.60E-05	4.7966	4.07E-05
pyridoxal phosphate	5.47	1.69E-05	4.7714	4.28E-05
cytidine-5'-diphosphoethanolamine	5.42	1.90E-05	4.7216	4.78E-05
S-lactoylglutathione	5.42	1.91E-05	4.7184	4.78E-05
choline	5.40	1.99E-05	4.7011	4.94E-05
phosphate	-5.40	2.03E-05	4.6935	5.00E-05
N-acetylaspartate (NAA)	5.33	2.37E-05	4.6257	5.81E-05
N-acetyltaurine	-5.31	2.52E-05	4.5989	6.14E-05
glutamine	5.30	2.56E-05	4.5926	6.20E-05
glutamate	5.17	3.49E-05	4.4575	8.41E-05
glycerophosphoinositol*	-5.09	4.24E-05	4.3729	0.0001015
1-(1-enyl-palmitoyl)-GPE (P-16:0)*	5.05	4.64E-05	4.3339	0.0001104
(N(1) + N(8))-acetylspermidine	5.04	4.76E-05	4.3226	0.0001127
argininosuccinate	5.01	5.12E-05	4.291	0.0001205

fructosyllysine	4.95	5.92E-05	4.2277	0.0001386
1-palmitoyl-2-oleoyl-GPC (16:0/18:1)	4.94	6.14E-05	4.2116	0.000143
1-methyl-4-imidazoleacetate	4.93	6.20E-05	4.2079	0.0001434
1-stearoyl-GPS (18:0)*	4.92	6.39E-05	4.1942	0.0001471
glutathione, reduced (GSH)	4.89	6.83E-05	4.1657	0.0001562
putrescine	4.84	7.82E-05	4.1068	0.0001779
phenylalanylglycine	4.83	7.87E-05	4.1042	0.000178
2,6-dihydroxybenzoic acid	4.79	8.69E-05	4.0611	0.0001955
N-acetylglutamine	4.65	0.0001233	3.9091	0.0002729
methyl-4-hydroxybenzoate sulfate	4.65	0.0001238	3.9074	0.0002729
1-methyl-5-imidazoleacetate	4.65	0.0001239	3.907	0.0002729
beta-citrylglutamate	4.65	0.000124	3.9067	0.0002729
palmitoyl ethanolamide	4.64	0.0001259	3.8998	0.0002757
1-myristoyl-2-palmitoyl-GPC (14:0/16:0)	-4.62	0.0001329	3.8765	0.0002894
N-acetylalanine	4.61	0.0001358	3.867	0.0002942
2-hydroxyglutarate	4.56	0.0001521	3.8179	0.0003277
N6-methyllysine	4.55	0.0001562	3.8062	0.0003348
malate	4.49	0.0001819	3.7403	0.0003876
carnitine	4.46	0.0001955	3.7089	0.0004145
cystathionine	4.44	0.0002066	3.6849	0.0004357
valylglutamine	4.37	0.0002455	3.61	0.0005152
glycosyl-N-stearoyl-sphingosine (d18:1/18:0)	4.35	0.0002548	3.5938	0.0005319
gamma-glutamylglutamine	4.32	0.0002747	3.5612	0.0005705
2'-deoxycytidine	4.32	0.0002768	3.5578	0.000572
adenosine 5'-monophosphate (AMP)	4.31	0.0002864	3.5431	0.0005887
behenoyl dihydrosphingomyelin (d18:0/22:0)*	4.29	0.0002983	3.5253	0.0006102
1-(1-enyl-oleoyl)-GPE (P-18:1)*	4.28	0.0003081	3.5113	0.0006271
N-delta-acetylornithine	4.24	0.0003376	3.4717	0.0006836
glycosyl ceramide (d18:2/24:1, d18:1/24:2)*	4.21	0.0003577	3.4465	0.0007207
1-stearoyl-GPE (18:0)	4.19	0.0003782	3.4223	0.0007574
fructose 1,6-diphosphate/glucose 1,6-diphosphate/myo-inositol diphosphates	4.19	0.0003796	3.4207	0.0007574
cysteinylglycine	4.17	0.0003947	3.4037	0.0007836
5-hydroxylysine	4.17	0.0004019	3.3959	0.000794
N-acetylhistidine	4.15	0.0004145	3.3825	0.0008148
1-myristoyl-2-arachidonoyl-GPC (14:0/20:4)*	-4.12	0.0004479	3.3488	0.0008763
3-(3-hydroxyphenyl)propionate sulfate	4.12	0.0004506	3.3462	0.0008774

glycosyl ceramide (d18:1/20:0, d16:1/22:0)*	4.10	0.0004715	3.3266	0.0009136
2-methylmalonylcarnitine (C4-DC)	4.07	0.0005059	3.296	0.0009756
1-(1-enyl-oleoyl)-2-oleoyl-GPE (P-18:1/18:1)*	4.03	0.0005618	3.2504	0.0010784
pantetheine	4.02	0.0005718	3.2428	0.0010923
10-nonadecenoate (19:1n9)	4.02	0.000581	3.2359	0.0011046
succinylcarnitine (C4-DC)	4.00	0.0006013	3.2209	0.001138
prolylglycine	4.00	0.0006085	3.2158	0.0011462
hydroxypalmitoyl sphingomyelin (d18:1/16:0(OH))**	3.97	0.0006452	3.1903	0.0012098
pantothenate	3.93	0.0007124	3.1473	0.0013296
pyridoxamine phosphate	3.91	0.0007513	3.1242	0.0013957
4-guanidinobutanoate	3.90	0.0007709	3.113	0.0014256
gamma-glutamylthreonine	3.89	0.0007805	3.1076	0.0014369
1-(1-enyl-stearoyl)-2-oleoyl-GPE (P-18:0/18:1)	3.88	0.0008082	3.0925	0.0014811
sphingomyelin (d18:0/20:0, d16:0/22:0)*	3.88	0.0008124	3.0902	0.0014821
2-hydroxy-3-methylvalerate	3.87	0.0008288	3.0815	0.0015053
5-phosphoribosyl diphosphate (PRPP)	3.83	0.0009079	3.0419	0.0016416
glycerophosphoglycerol	3.82	0.0009327	3.0303	0.0016788
3-hydroxydecanoate	3.80	0.0009865	3.0059	0.0017678
1-oleoyl-GPE (18:1)	3.76	0.0010767	2.9679	0.001921
N6,N6,N6-trimethyllysine	-3.76	0.0010832	2.9653	0.0019241
homocysteine	3.75	0.0010949	2.9606	0.0019365
propionylcarnitine (C3)	3.57	0.0016923	2.7715	0.00298
2-oxoarginine*	3.56	0.0017555	2.7556	0.0030778
allantoin	3.55	0.0017952	2.7459	0.0031338
1-stearoyl-GPI (18:0)	3.52	0.0019391	2.7124	0.0033706
imidazole lactate	3.50	0.0020327	2.6919	0.0035182
5-methylthioadenosine (MTA)	3.49	0.00207	2.684	0.0035675
alpha-ketoglutarate	3.42	0.0024389	2.6128	0.0041854
leucine	3.42	0.0024514	2.6106	0.0041891
pterin	3.40	0.0025809	2.5882	0.0043919
1-palmitoyl-2-docosahexaenoyl-GPC (16:0/22:6)	-3.39	0.0026309	2.5799	0.0044583
sphingomyelin (d18:1/18:1, d18:2/18:0)	3.33	0.0030379	2.5174	0.0051264
S-adenosylmethionine (SAM)	3.32	0.0031397	2.5031	0.0052762
N-acetylmethionine	3.26	0.0035636	2.4481	0.0059638
N1-methyl-2-pyridone-5-carboxamide	3.25	0.0036529	2.4374	0.0060881

hypotaurine	3.24	0.0037368	2.4275	0.0062025
docosapentaenoate (n3 DPA; 22:5n3)	3.24	0.0037853	2.4219	0.0062573
nicotinamide	3.22	0.0039375	2.4048	0.0064825
1-oleoyl-2-docosahexaenoyl-GPE (18:1/22:6)*	3.20	0.0041062	2.3866	0.0067329
(16 or 17)-methylstearate (a19:0 or i19:0)	3.18	0.0042855	2.368	0.0069985
N-acetylcarnosine	-3.16	0.0045454	2.3424	0.0073931
4-hydroxyhippurate	3.13	0.0049113	2.3088	0.0079563
cytosine	3.12	0.0049567	2.3048	0.0079978
1-stearoyl-2-linoleoyl-GPI (18:0/18:2)	3.08	0.0054167	2.2663	0.0087054
oleoylcholine	3.07	0.0055468	2.256	0.0088792
glycosyl-N-(2-hydroxynervonoyl)-sphingosine (d18:1/24:1(2OH))*	3.06	0.0057021	2.244	0.0090919
2-methylbutyrylcarnitine (C5)	-3.06	0.0057401	2.2411	0.0091166
betaine	3.06	0.0057957	2.2369	0.009169
4-imidazoleacetate	3.04	0.005969	2.2241	0.0094065
malonylcarnitine	3.00	0.0065374	2.1846	0.010262
2-palmitoyl-GPC (16:0)*	2.97	0.0071389	2.1464	0.011163
1-methylguanidine	2.91	0.0081404	2.0894	0.01268
gamma-glutamylvaline	2.91	0.0081892	2.0868	0.012707
alpha-hydroxyisovalerate	2.84	0.0094311	2.0254	0.014579
N-acetylthreonine	-2.84	0.0095149	2.0216	0.014652
S-adenosylhomocysteine (SAH)	2.79	0.010584	1.9754	0.016236
1-stearoyl-2-arachidonoyl-GPI (18:0/20:4)	2.75	0.011681	1.9325	0.017832
valine	2.75	0.011712	1.9314	0.017832
N-acetyl-aspartyl-glutamate (NAAG)	2.74	0.01191	1.9241	0.018055
1-palmitoyl-2-dihomo-linolenoyl-GPC (16:0/20:3n3 or 6)*	-2.74	0.011947	1.9227	0.018055
arginine	2.71	0.012693	1.8964	0.01905
N-acetylglucosaminylasparagine	2.71	0.0127	1.8962	0.01905
1-linoleoyl-2-linolenoyl-GPC (18:2/18:3)*	2.71	0.012894	1.8896	0.019268
isovalerylcarnitine (C5)	2.70	0.012941	1.888	0.019268
oxindolylalanine	2.69	0.013316	1.8756	0.019755
mead acid (20:3n9)	2.66	0.014308	1.8444	0.021148
3-hydroxyoctanoylcarnitine (1)	-2.63	0.015218	1.8176	0.022413
sarcosine	2.62	0.015623	1.8062	0.022925
taurocyamine	2.61	0.016122	1.7926	0.023572
3-ureidopropionate	2.60	0.016386	1.7855	0.023872

adenine	2.58	0.017071	1.7678	0.02478
S-nitrosoglutathione (GSNO)	2.57	0.017339	1.761	0.025079
4-methyl-2-oxopentanoate	2.57	0.017459	1.758	0.025163
3-methylhistidine	2.55	0.018258	1.7386	0.026221
spermine	-2.54	0.018772	1.7265	0.026865
cysteine	2.44	0.023054	1.6373	0.032877
homostachydrine*	2.43	0.023632	1.6265	0.033583
isoleucylglycine	2.41	0.024833	1.605	0.035165
tyrosine	2.41	0.024922	1.6034	0.035168
3-amino-2-piperidone	2.39	0.026006	1.5849	0.03657
asparagine	2.35	0.028438	1.5461	0.039852
docosapentaenoate (n6 DPA; 22:5n6)	2.34	0.028541	1.5445	0.039859
1-linoleoyl-2-arachidonoyl-GPC (18:2/20:4n6)*	-2.27	0.033202	1.4788	0.046209
acetyl CoA	2.25	0.034902	1.4572	0.048408

Acknowledgements

First and foremost, I want to thank my professor Alexander Bartelt for giving me the chance to purse my PhD in his lab and for the scientific guidance during the last 4 years. It has been a great experience, with opportunities I could have never imagined and giving me a framework in which I could grow not just as a scientist, but also as a person.

Also, I want to thank my colleagues and peers who made the time in the lab and all the conferences such enjoyable experiences and creating a pleasant atmosphere in the lab. Thinking of my name-twin Nienke, how we started together and every now and then merged into one entity: “Nimke”, thanks for always being around and the emotional support. Thanks to Stefan (Esteban) for always helping with everything: mice, cell treatments, coding and getting mad if not asked to help out. Thanks to Anahita for all the more or less voluntary laughter you brought us. And thanks to Caro for always helping out whenever, wherever! Thanks to Henrika for showing me all the animal handling. Thanks to Joel for always being in a good mood and also being a great help with experiments and an incredible reference finder. Also, I am very happy about our new PhDs Alba and Anna, bringing fresh energy to the team! I am grateful for the students, I had that helped me with my projects and made endless Nfe2l1 blots without complaining. Thanks to Leo for always being helpful and kind hearted and having goat cheese 3 times. Thank you to Virginia for always cheering me on and being such a kind spirit. Furthermore, I am grateful for our past members, Dr. Honey and Dr. Maude Maude, for guidance in the beginning of my PhD and Janina for getting me accommodated in the lab. Last, but not least thank you to our technicians, Silvia and Thomas for the assistance and help with whatever I needed.

I also want to thank my “foster” lab from the Helmholtz Center, namely Natalie Kramer’s group for taking good care of me, especially Natalie herself for helping with our wild undertaking of establishing Ubiquitomics. Foremost, also thanks to Daniel for the support and enduring long hours in the lab with me, it has always been fun. Furthermore, I want to thank the other collaborators from the Helmholtz Center Munich; Kenneth Dyar, Maria Rohm and Stefan Herzig for providing me with the tools, insights and knowledge to further my project. Also, thanks to Nick Diercksen, Phong Nguyen, Michael Menden for providing me with beautiful RNAseq figures. Furthermore, I want to extend my gratitude to Zachary Gerhart-Hines, Tao Ma and Steen Larson for assistance with the respiratory measurements. Also, thanks to Desalegn Egu and Jens Waschke for helping with the TEM microscopy.

Additionally, I would like to thank my friends for cheering me on and having faith in me and especially the Jiu-Jitsu community for keeping me sane and grounded.

I also want to express my deepest appreciation to my family and especially my parents for always supporting and believing in me. Without them this all would not have been possible and I wouldn’t be where I am today.

Last but not least, thank you Alex for enduring me, constantly building me up and bringing so much joy and happiness in my life!

Affidavit

Eidesstattliche Versicherung

Lemmer, Imke Leonie

Name, Vorname

Ich erkläre hiermit an Eides statt, dass ich die vorliegende Dissertation mit dem Titel:

The role of the transcription factor Nfe2l1
for skeletal muscle metabolism and function

selbständig verfasst, mich außer der angegebenen keiner weiteren Hilfsmittel bedient und alle Erkenntnisse, die aus dem Schrifttum ganz oder annähernd übernommen sind, als solche kenntlich gemacht und nach ihrer Herkunft unter Bezeichnung der Fundstelle einzeln nachgewiesen habe.

Ich erkläre des Weiteren, dass die hier vorgelegte Dissertation nicht in gleicher oder in ähnlicher Form bei einer anderen Stelle zur Erlangung eines akademischen Grades eingereicht wurde.

München, 04.06.2024 Imke Leonie Lemmer

Ort, Datum Unterschrift Doktorandin bzw. Doktorand

List of publications

Lemmer IL, Daniel T. Haas, Nienke Willemsen, Stefan Kotschi, Irmak Toksöz, Ejona Gjika, Sajjad Khani, Maria Rohm, Nick Diercksen, Phong B.H. Nguyen, Michael P. Menden, Desalegn T. Egu, Jens Waschke, Steen Larsen, Tao Ma, Zachary Gerhart-Hines, Stephan Herzig, Kenneth Dyar, Natalie Krahmer, Alexander Bartelt. Nfe2l1-mediated proteasome function controls muscle energy metabolism in obesity. b*ioRxiv*, May 2023, doi: 10.1101/2023.04.20.537611 and under revision at *Nature Metabolism* as of August 2023.

Anahita Ofoghi, Stefan Kotschi, **Imke L. Lemmer**, Daniel T. Haas, Nienke Willemsen, Batoul Bayer, Sophie Möller, Stefanie Haberecht-Müller, Elke Krüger, Natalie Krahmer, Alexander Bartelt. Activating the NFE2L1-ubiquitin-proteasome system by DDI2 protects from ferroptosis. *bioRxiv,* July 2023 and under revision at Cell death and differentiation as of July 2023.

Lemmer IL, Bartelt A. Brown fat has a sweet tooth. Nat Metab. 2023 Jul;5(7):1080-1081. doi: 10.1038/s42255-023-00824-9.

Lemmer IL, Willemsen N, Hilal N, Bartelt A. A guide to understanding endoplasmic reticulum stress in metabolic disorders. Mol Metab. 2021 May; 47:101169. doi: 10.1016/j.molmet.2021.101169.

Talks:

- *Myocyte Nfe2l1-mediated proteasome function controls energy metabolism in obesity*. **Imke Lemmer**, Daniel T. Haas, Nienke Willemsen, Stefan Kotschi, Irmak Toksöz, Ejona Gjika, Sajjad Khani, Maria Rohm, Nick Diercksen, Phong B.H. Nguyen, Michael P. Menden, Desalegn T. Egu, Jens Waschke, Steen Larsen, Tao Ma, Zachary Gerhart-Hines, Stephan Herzig, Kenneth Dyar, Natalie Krahmer, Alexander Bartelt. FAPESP-BayLat workshop, May 2023.
- *Nfe2l1 shapes the muscle ubiquitome to regulate fiber type and metabolic fitness*. **Imke Lemmer**, Daniel T. Haas, Nienke Willemsen, Stefan Kotschi, Irmak Toksöz, Ejona Gjika, Sajjad Khani, Maria Rohm, Nick Diercksen, Phong B.H. Nguyen, Michael P. Menden, Desalegn T. Egu, Jens Waschke, Steen Larsen, Tao Ma, Zachary Gerhart-Hines, Stephan Herzig, Kenneth Dyar, Natalie Krahmer, Alexander Bartelt. Keystone Symposium for Ubiquitin Biology, November 2022.
- *Ferroptosis: From Molecular Basics to Clinical Applications.* Anahita Ofoghi, Stefan Kotschi, **Imke Lemmer**, Daniel Haas, Nienke Willemsen, Batoul Bayer, Sophie Möller, Stefanie Haberecht-Müller, Elke Krüger, Natalie Krahmer, Alexander Bartelt. SPP2306, Dresden Germany, November 2022.
- *Nfe2l1 drives proteostasis in myocytes and skeletal muscle.* **Imke Lemmer**, Sajjad Khani, Henrika Jodeleit, Alexander Bartelt, ELC Tutzing, Germany, 2020

Poster:

- *Ferroptosis: When metabolism meets cell death.* Anahita Ofoghi, Stefan Kotschi, **Imke Lemmer**, Daniel Haas, Nienke Willemsen, Batoul Bayer, Sophie Möller, Stefanie Haberecht-Müller, Elke Krüger, Natalie Krahmer, Alexander Bartelt. EMBO Workshop, Seeon, Germany, 2023
- *Myf5^{+} stem cells require calibration of proteasome activity to develop into healthy brown adipose tissue and skeletal muscle.* Nienke Willemsen, Carolin Muley, **Imke Lemmer**, Stefan Kotschi, Henrika Jodeleit, and Alexander Bartelt. Translational metabolism Wageningen, Netherlands, 2023
- *Nfe2l1 in muscle proteostasis and energy metabolism.* **Imke Lemmer**, Daniel Haas, Nienke Willemsen, Sajjad Khani, Kenneth Dyar, Zach Gerhart-Hines, Natalie Krahmer, Alexander Bartelt. ELC Tutzing, Germany, 2022.
- *Nfe2l1 shapes the skeletal muscle ubiquitome to regulate fiber type and metabolic fitness.* **Imke Lemmer**, Daniel Haas, Nienke Willemsen, Sajjad Khani, Kenneth Dyar, Zach Gerhart-Hines, Natalie Krahmer, Alexander Bartelt. Understanding Ubiquitylation: From Molecular Mechanisms to Disease, Würzburg, Germany 2022
- *Nfe2l1 in muscle proteostasis and energy metabolism.* **Imke Lemmer**, Daniel Haas, Nienke Willemsen, Sajjad Khani, Kenneth Dyar, Zach Gerhart-Hines, Natalie Krahmer, Alexander Bartelt. Ubiquitin and friends, Vienna, Austria 2022
- *Myocyte Nfe2l1 promotes proteasome function and regulates energy expenditure in obesity.* **Imke Lemmer**, Daniel Haas, Nienke Willemsen, Sajjad Khani, Kenneth Dyar, Zach Gerhart-Hines, Natalie Krahmer, Alexander Bartelt. Keystone Symposium for adipose tissue and metabolism, Whistler, Canada, 2022
- *Myf5^{+} stem cells require calibration of proteasome activity to develop into healthy brown adipose tissue and skeletal muscle.* Nienke Willemsen, **Imke Lemmer**, Carolin Muley, Stefan Kotschi, Henrika Jodeleit, and Alexander Bartelt. Keystone Symposium for adipose tissue and metabolism, Whistler, Canada, 2022
- *Adaptive proteasome function in Myf5+ progenitors affect energy homeostasis and thermogenesis.* Nienke Willemsen, Shan Jiang, **Imke Lemmer**, Anke Baronowsky, Johannes Keller, and Alexander Bartelt. ELC Tutzing, Germany, 2022
- *Nfe2l1 in muscle proteostasis and energy metabolism.* **Imke Lemmer**, Sajjad Khani, Henrika Jodeleit, Alexander Bartelt, ELC Tutzing, Germany, 2021